CFD Modelling of Turbulent Flow in Open-Channel Expansions

Sahar Najmeddin

A Thesis

in

The Department

of

Building, Civil, and Environmental Engineering

Presented in Partial Fulfillment of the Requirements

for the Degree of Master of Applied Science in Civil Engineering at

Concordia University

Montreal, Quebec, Canada

May 2012

CONCORDIA UNIVERSITY
School of Graduate Studies

This is to certify that the thesis prepared

By: Sahar Najmeddin

Entitled: CFD Modelling of Turbulent Flow in Open-Channel Expansions

and submitted in partial fulfillment of the requirements for the degree of

Master of Applied Science (Civil Engineering)

complies with the regulations of the University and meets the accepted standards with respect to originality and quality.

Signed by the final examining committee:

Dr. A. Zsaki Chair

Dr. M. Paraschivoiu, MIE, External-to-Program Examiner

Dr. L. Wang Examiner

Dr. S. Li Supervisor

Approved by _____
Chair of Department or Graduate Program Director

_____
Dean of Faculty

Date _____

ABSTRACT

CFD Modelling of Turbulent Flow in Open-Channel Expansions

Sahar Najmeddin, M. A. Sc.

Concordia University, 2012

Channel expansions provide a transition from a narrow to a relatively wide channel-section, which is necessary in many hydraulic structures. In the transition, flow tends to separate from its diverging sidewalls and create turbulent eddies, if the angle of divergence exceeds a threshold value. This phenomenon can cause undesirable flow energy losses and erosion to the sidewalls locally and even further downstream. Previously, researchers have tried to optimise the transition's horizontal shape in order to reduce flow separation; the results are inconclusive. The purpose of this study is to extend earlier investigations about fitting a hump in the vertical to eliminate flow separation. This study uses the CFD modelling approach. This approach permits an efficient and systematic exploration of the effects of different angles of divergence, crest height of the hump and the Froude number of subcritical flow. The model results are validated using existent analytical solutions under simplified conditions and available experimental data for a limited number of cases. Flow quantities presented in this thesis include details of the velocity, vorticity, eddy structure, and cross-sectional area of flow reversal; these quantities are distributed at selected vertical and horizontal planes, and are available for the cases of with and without a hump. It is shown that the use of a hump effectively reduces flow separation and eddy motion in the transition. This is because the flow is forced to accelerate over the hump, and as a result, the otherwise adverse pressure gradient, which is known to be responsible for flow separation, diminishes. A hump in the vertical can easily be incorporated into the bed of existent channel expansions, and would be less expensive to construct than to modify the horizontal shape (or the sidewalls) of existent expansions. The results presented in this thesis are of practical values for the optimal design of humps.

ACKNOWLEDGEMENT

First of all, I would like to thank my supervisor, Dr Samuel Li, for his guidance and supervision that helped me throughout this research. His support and guidance in completing every step of this research is greatly appreciated. It has been a privilege working under the supervision of Dr. Li for the past two years and I take this opportunity to express my gratitude for his support.

Also, I would like to thank the examiners Dr**.** M. Paraschivoiu and Dr. L. Wang as well as the thesis committee chair Dr. A. Zsaki, for their comments and suggestions that helped prepare the version of this thesis.

Last but not least, I would like to thank my dear parents and my dear sister for their endless love and support through the whole duration of my studies. Also, these achievements would not be possible without my beloved husband's unconditional love and support.

TABLE of CONTENTS

LIST OF FIGURES

LIST OF TABLES

LIST OF SYMBOLS

A= Area $\left(m^2\right)$

b_1 = upstream channel width at CS1 (m)

b_2 = channel width at the entrance to an expansion, CS 2 (m)

b_3 = channel width at the exit of an expansion, CS 3(m)

C = log- layer constant (-)

c_f = wall shear stress coefficient (-)

E_1 = specific energy at CS 1(m)

$E_{d/s}$ = percentage in area occupied by eddies between the downstream end of an expansion and the downstream end of a model channel (%)

E_{ex} = percentage in area occupied by eddies in an expansion (%)

E_l = percentage in area occupied by eddies to the left sidewall (to an observer facing downstream) (%)

E_r = percentage in area occupied by eddies to the right sidewall (to an observer facing downstream) (%)

F = volume fraction (-)

f_a = volume of fraction for air (-)

F_r = Froude number (-)

h = vertical distance between the water surface and the point of interest (m)

h_e = energy loss due to flow separation and eddy motion (m)

h_f = energy loss caused by friction (m)

h_L = energy loss in the expansion (m)

k = turbulence kinetic energy (m^2 / s^2)

k_E = energy loss coefficient (-)

L = characteristic length (m)

L_1 = upstream channel section length (m)

L_2 = expansion length (m)

L_3 = downstream channel section length (m)

P = Reynolds-averaged pressure (N/m^2)

p = instantaneous pressure (N/m^2)

P_r = turbulence production term

Q = total discharge (m^3 / s)

q = discharge per unit width (m^2 / s)

R_e = Reynolds number (-)

r = width ratio (-)

S_{ij} = mean flow strain rate ($\frac{1}{s}$)

t = time (s)

u = flow velocity (m / s)

U = Reynolds averaged velocity component (m / s)

u' = velocity fluctuation component (m / s)

u^+ = near wall velocity (m / s)

U_t =velocity tangent to the wall at a distance of Δy from the wall (m/s)

u_τ = friction velocity (m/s)

U_0 = characteristic velocity (m/s)

y^+ = dimensionless distance from the wall (-)

v_1 = cross sectional mean flow velocity at CS1 (m/s)

v_2 = cross sectional mean flow velocity at CS2 (m/s)

$\overline{V}_a$ = average velocity after the entrance to an expansion (m/s)

$\overline{V}_b$ = average velocity before the entrance to an expansion (m/s)

$V_{\min,a}$ = minimum velocity after the entrance to an expansion (m/s)

$V_{\min,b}$ = minimum velocity before the entrance to an expansion (m/s)

Vor_{high} = percentage in area of high-vorticity region at the entrance to an expansion (%)

Vor_{left} =percentage in area of high-vorticity region to the left of an expansion (to an observer facing downstream) (%)

Vor_{right} = percentage in area of high-vorticity region to the right of an expansion (to an observer facing downstream) (%)

y = depth of flow (m)

y_1 = depth of flow upstream of an expansion or at CS 1 (m)

y_2 = depth of flow at the entrance to an expansion or at CS 2 (m)

Δy = distance from the wall (m)

$\Delta z_{\max}$ = maximum allowable elevation difference (m)

α = angle of divergence (^{o})

δ = boundary layer thickness (m)

ε = turbulent dissipation (m^2 / s^3)

η_1 = elevation above the channel bed (m)

κ = Karman constant (-)

μ = dynamic viscosity of water (Ns / m^2)

ν_t =kinematic eddy viscosity (m^2 / s)

ρ_a = density of air (kg / m^3)

ρ_w = density of water (kg / m^3)

τ_{ij} = shear stress tensor (N / m^2)

τ_w = wall shear stress (N / m^2)

ω = specific dissipation, parameter in the $k - \omega$ turbulence model ($\frac{1}{s}$)

Chapter One Introduction

1.1 Background

In general, channel transitions are defined as changes in cross-sectional area in the direction of open channel flow. Transitions can also include changes in bed level. A channel expansion is a transition that connects a relatively narrow upstream channel-section to a wide downstream channel-section. Such a transition is an important component of many hydraulic structures. Due to an increase in cross-sectional area, channel expansions cause flowing water to decelerate. Under steady flow conditions, flow deceleration will lead to an increase in water pressure that in turn triggers flow separation and creates turbulent eddy motions. These turbulent eddy motions can exist over a long distance downstream of the transition. They cause undesirable energy losses and sidewall erosion.

In order to control energy losses and erosion, we need to improve our understanding of the problem of flow in a channel expansion. This problem has not been thoroughly investigated in the past. A lack of thorough knowledge about the problem has motivated this study. From the energy conservation perspective, it is particularly important to be able to reduce or even eliminate areas of turbulent eddy motions in the expansion.

The problem of turbulent flow in an open channel expansion is very complicated, with turbulent eddy motions, flow separation and so on. It is difficult to use the analytical approach to obtain solutions to the problem even under highly simplified conditions. The experimental approach may be taken to tackle the problem, but experiments are very expensive to carry out. Therefore, it may not be feasible to experimentally investigate the effects of many factors that potentially control the behaviour of flow in a channel expansion. In this study, the CFD

modelling approach is taken. This approach permits an efficient and systematic exploration of the effects of such factors as the angle of divergence, the crest height of a hump fitted at the channel bed and the Froude number on the flow in an expansion. The idea of using a hump in the vertical to reduce eddy motions and flow separation in expansions is interesting, because it is an easier and more economic solution compared to optimising the horizontal shape (or the sidewalls) of existing expansions.

This study focuses on subcritical flows (with the Froude number less than unity) as they prevail in open channels. A number of important questions need to be answered. How does the flow field, in particular the distribution of eddy motions, vary with the angle of divergence? How does the velocity field change with elevation above the channel bed? In what way we can evaluate flow reversal in the expansion? Qualitatively, the use of a hump fitted at the channel bed is known to help reduce flow reversal and eddy motions, but quantitatively, how efficient is the use of it? Will answers to the above questions be different at different Froude numbers?

1.2 Specific objectives

The objectives of this study are

- to numerically simulate subcritical flow in channel expansions with different angles of divergence. We will consider an angle of divergence equal to 10.34º, 7.54º and 5.04º in order to match experimental conditions. This will allow data comparison.
- to quantify areas of eddy motions and flow reversal in expansions (at different cross-sections and longitudinal planes).
- to investigate the effects of the Froude number.

- to determine the effectiveness of fitting a hump at the channel bed to suppress eddy motions and flow separation. We will consider two simple humps: one with a crest height of 1/4″ (or 0.00635 m, with $\Delta z / y = 2.54\%$), and the other with a crest height of 1/2″ (or 0.0127 m, with $\Delta z / y = 5.08\%$). These selections are consistent with experimental setup used in previous studies.

1.3 Scope of the work

To achieve the above-mentioned objectives, the rest of this thesis is organized as follows. Chapter 2 gives a summary of previous studies on the topic of flow in expansions, including experimental and analytical studies on flow separation and the formation of turbulent eddies. Previous works on other established facts concerning the design of hydraulically efficient channel expansions are reviewed in this chapter. This chapter also summarises previous studies about the effects of a hump in the vertical on the reduction of eddy motions and flow reversal.

Chapter 3 describes the modelling methodologies used in this study. This chapter provides the theoretical background and fundamental concepts of CFD modelling of free surface flow. The k-ω turbulence model is explained in details, and reasons for choosing this model are discussed. Details of the boundary conditions, including conditions at inlet, outlet, bottom and sidewalls of the model channel are discussed. Also, the choice of meshes, including volume mesh and inflations (near bottom and sidewalls) for accuracy improvement is discussed in this chapter.

In Chapter 4, the energy principle and the concept of specific energy for flow in channel expansions are discussed, together with the concept of E-y curve. The expected behaviour of flow in channel expansions and over a hump is also explained.

Chapter 5 presents the numerical results of the flow field in a flat-bottom expansion and expansions with a 1/4″ (or 0.00635 m, with $\Delta z / y = 2.54\%$) or 1/2″ (or 0.0127 m, with $\Delta z / y = 5.08\%$) hump. The results include velocity, flow streamlines, vorticity contours, and along-channel velocity contours at different cross-sections along the length of expansions. In longitudinal planes at different elevations above the channel bed, areas of eddy motions are determined. In cross-sections, eddy motions are evaluated as regions where flow reversal occurs. Percentages in area of low-velocities and high-vorticity areas are evaluated. A comparison of the percentages between a flat-bottom expansion and expansions with a 1/4″ (or 0.00635 m, with $\Delta z / y = 2.54\%$) or 1/2″ (or 0.0127 m, with $\Delta z / y = 5.08\%$), are made. Percentages in area of backward flow (flow reversal) at different cross-sections are evaluated and compared. This chapter also discusses the effects of the Froude number, ranging from 0.3 to 0.7.

In chapter 6, we draw conclusions and make suggestions for future work.

Chapter Two Literature Review

2.1 Experimental studies of subcritical flow in expansions

Previously, a number of researchers have experimentally studied the problem of subcritical flow in expansions. Alauddin and Basak (2006) took the experimental approach to study flow separation in an expanding transition and further downstream. The purpose was to design an expanding transition with minimum flow separation and hence small energy head losses. The authors made measurements of velocity profiles at the inlet, in the expansion, and at the outlet of a sudden expansion, and determined a transition profile closely matching to the shape of separating streamlines in the expansion. Presumably, using the transition profile to build an expanding transition diminishes the energy-dissipating effects of eddies associated with flow separation.

Alauddin and Basak (2006) reported that such an expanding transition gave an overall efficiency of 80.3%, representing an improvement from previous work. The overall efficiency is defined as the ratio of the potential-energy gain to the kinetic-energy loss as water flows through the transition. A higher efficiency means less energy head losses. Alauddin and Basak (2006) suggested that all other existent transitions had a lower efficiency because of their abrupt ending at the downstream end. They concluded that the provision of a smooth outlet by their transition profile was the key to virtually eliminate flow separation and eddy formation.

2.2 Channel expansions fitted with a local hump

Ramamurthy and Basak (1970) conducted an experimental study of flow separation in an expanding transition and the suppression of flow separation by fitting a simple hump at the

channel bottom. Flow through expansions would encounter an adverse pressure gradient, decelerate, and therefore separate from the sidewalls. As a result, turbulent eddies form along the sidewalls and cause flow energy dissipations. Ramamurthy and Basak (1970) showed that both the angle of divergence and the length of transition relative to the inlet dimension have effects on flow separation. They also showed that inserting a hump in the bottom profile could suppress flow separation. As they explained, the specific energy head remains the same before and after a horizontal transition, if the energy losses due to friction are negligible. In the presence of a hump, there is a loss of velocity head up to the crest of the hump, and a gain of velocity head after passing the crest.

The results of Ramamurthy and Basak (1970) were based on measurements of depth and velocity at a number of selected sections including the entrance and exit sections of the transition. Without a hump, the flow became more turbulent and asymmetric at a larger Reynolds number, and even with a hump, the same asymmetry appeared at large Reynolds numbers, as revealed by velocity contours. Flow separation was reduced or eliminated after inserting a hump. In conclusion, expanding transitions fitted with a hump perform well in terms of flow energy conservation. The experimental investigation of Ramamurthy and Basak (1970) was limited to a couple of humps with specific crest heights.

2.3 Flow patterns in a channel expansion

2.3.1 Asymmetric behaviour of flow in symmetric expansion

Some previous researchers of fluid flow in expansions have dealt with the case of sudden expansions (see e.g. Mehta 1979, 1981; Graber 1982; Nashta and Garde 1988; Manica and Bortoli 2003). The results reported in their studies highlighted the effects of different expansion

ratios on mean flow velocities, fluid pressure distributions and turbulence characteristics. Specially, the asymmetric behaviour of the flow field in perfectly symmetric expansions is very important. First, Abbott and Kline (1962) observed asymmetric flow patterns in their experimental investigations. They also found that the Reynolds numbers and turbulence intensities have no effect on flow pattern. Filetti and Kays (1967) found that the flow in rectangular channel with expansion ratios of 2.125 and 3.1 is asymmetric.

Also, Mehta (1979) conducted an experiment with a two-dimensional rectangular channel and found that the flow is symmetric at an expansion ratio of 1.25 and asymmetric at expansion ratios of 2.0, 2.5 and 3.0. He also found that the expansion ratio has an important effect on asymmetrical behaviour of channel expansions. According to Graber (1982), flows are symmetric in symmetric, two-dimensional rectangular channels with the expansion ratio of less than 1.5. He presented the cause of the asymmetric behaviour of the flow is a static instability of the flow system.

The stability of the system depends on the forces acting on the system and their variation as the system undergoes a small deflection. If the change in stabilizing momentum reaction exceeds the change in the destabilizing pressure force, the system is stable. If not, the asymmetric behaviour of the flow would be expected. The results of the stability analysis of Graber (1982) show that channels have the limitation that the maximum Froude number is less than 0.2. The result also predicts instability for expansion ratios greater than 1.5 that is in good agreement with experimental observations.

Manica and Bortoli (2003) considered laminar flow with low Reynolds number in a symmetric sudden expansion (Figure 2.1). Their numerical results show that below a certain critical Reynolds number (about 50), the flow pattern is symmetric about the channel central

line; the two vortices in the expansion corners are more or less of the same size. The symmetric flow pattern becomes unstable at Reynolds number above the critical value. Pair of steady asymmetrical vortices appears as one recirculation region grows at the expense of the other.

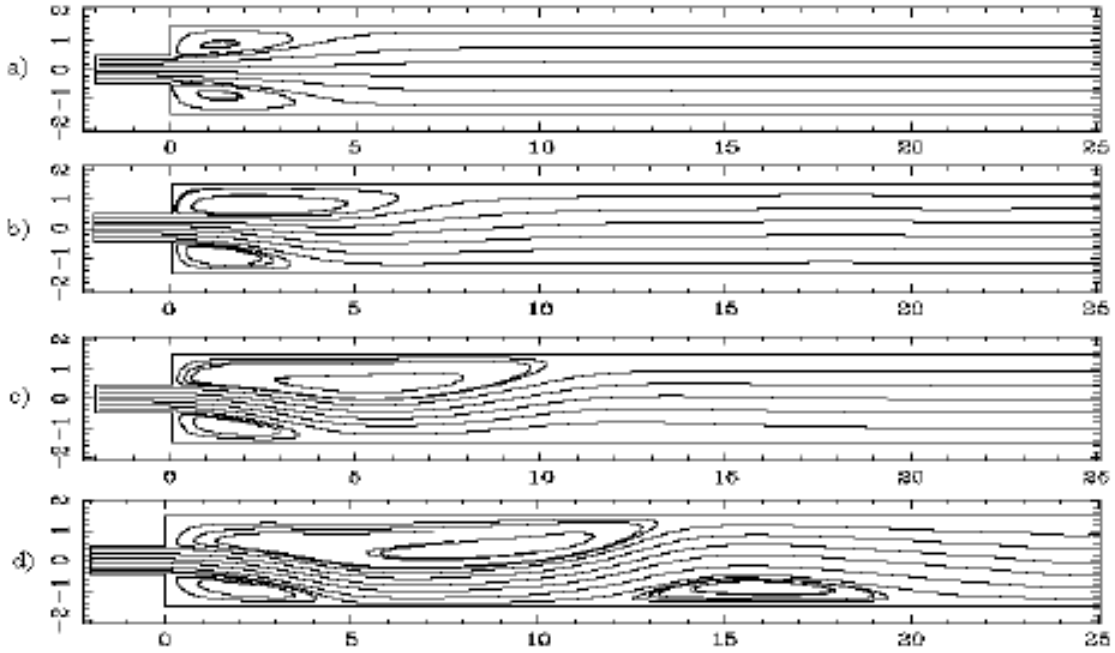

Figure 2.1 Streamlines computed for flow in a 1:3 symmetric sudden expansion. The Reynolds number Re is: (a) 40, (b) 50, (c) 80, and (d) 140. The flow patterns are symmetric when Re = 40 in (a) and asymmetric when $\mathrm{Re} \geq 50$ in (b-d) (from Manica and de Bortoli, 2003).

Nashta and Garde (1988) presented the results of analytical and experimental investigations in channels with a sudden expansion with expansion ratios of 1.5 to 3 for subcritical flow. The theoretical analysis assumed that the optimum shape for the transition is the shape in which the total energy loss, defined as the sum of the friction loss at the bed and loss due to expansion, is minimum. The functional relationship for the total loss is the objective function to be minimized for obtaining the optimum transition profile. To solve this problem, the

boundary condition at one end is relaxed and the solution is forced to satisfy the relaxed condition.

For $\frac{B_2}{B_1}$ ratios equal to or greater than 1.5, the flow is asymmetric (where B_1 is the width of the main channel and B_2 is the width of expanded channel). In such a case, the centerline of the jet does not coincide with the axis of expansion and the angle between the two lines, called the deflection angle, dependents on $\frac{B_2}{B_1}$. Nashta and Garde (1988) observed that velocity distributions tend to be more uniform as $\frac{x}{b}$ increases (b is equal to $\frac{(B_2 - B_1)}{2}$). The reason for this uniformity is the diffusion of turbulence generated at high shear zone, which has influence on velocity distribution. Nashta and Garde (1988) derived the mean velocity profile and separating streamline in the expansion and found that discharge and hence the Reynolds number have no effect on mean velocity and streamline.

Nashta and Garde (1988) concluded that the transition Lebedev's equation with n_b around 0.6 is preferable for determining the transition shapes because of the smaller separation zones and smaller head loss, where $n_b + 1$ is the highest degree in the normalized distance. The lengths of longer and shorter eddy can be predicted by Abbott and Kline's curve (Abbott and Kline, 1962). An expression for energy loss in a sudden expansion was obtained from the continuity, momentum and energy equations. The length scales for velocity and shear distributions are functions of $\frac{x}{B_1}$ and $\frac{B_2}{B_1}$, where x is the distance from the entrance of the transition.

Foumeny *et al.* (1996) carried out experiments and showed that the asymmetric behaviour of the flow is related to the Reynolds number. Also, Mehta (1981) showed that the flow patterns become more asymmetric and unsteady with increasing expansion ratios. Smith and Yu (1966) observed in a rapid expansion that the fluid flowing from upstream follow one sidewall and large turbulent eddies exist between the flowing jet and the other sidewall.

2.3.2 Flow characteristics in expansions

Mehta (1979, 1981) showed that flow separation can take place on both sides of the expansion with the maximum velocity line deviating from the centerline of the expansion. Mehta (1979) investigated flow separation in two-dimensional, sudden rectangular channel with width ratios ranging from 1.25 to 3.0, using numerical model and experiments.

The experimental investigations covered both symmetric and asymmetric flow patterns. Mehta (1979) reported that flows in two-dimensional sudden expansions are asymmetric and unstable, with three-dimensional character when the expansion ratio is larger than 1.25; Reynolds number in the range of 0.5 to 1.0×10^5 has no influence on the asymmetric behaviour of the flow. Also, unequal pressure occurs in eddy pockets on both sides of the axis of symmetry. All the important parameters of flow are influenced by the expansion ratio.

Mehta (1981) conducted an experimental study of the behaviour of the mean flow pattern and the turbulent characteristics for two-dimensional flow through large, sudden expansions. The flow patterns become more asymmetric and unsteady with increasing expansion ratios, whereas the degree of turbulence does not change except the peak values develop earlier and decay faster compared to cases of low expansion ratio.

Seetharamiah and Ramamurthy (1968) presented the idea of using a triangular sill in a channel expansion to decrease separation and eddy formation downstream of the expansion. The sill increases the transition length, and therefore reduces the sharpness of deceleration. They assumed that the amount of energy losses over the sill is negligible and showed two stages of deceleration of subcritical flow in the specific energy diagram. Seetharamiah and Ramamurthy (1968) also pointed out that the geometry of the sill can be chosen such that the theoretical retardation is nearly uniform along the sill, although it can be chosen to accelerate the flow up to the crest of the sill in canals where to reducing silting resulting from deceleration in the transition is very important.

Swamee and Basak (1991) presented a design method for subcritical expansions for rectangular channels, in order to achieve a minimum head loss. By analysing a large number of profiles, they obtained an equation for the design of rectangular expansion, producing the optimal bed-width profile.

Swamee and Basak (1992) discussed an analytical method for the design of expansions that connect a rectangular channel section with a trapezoidal channel section for subcritical flow. They suggested that flow separation in the expansion and the associated energy losses were considerably reduced through the optimal design of bed-width as well as side-slope profiles, on the basis of the momentum and energy equations. They claimed that the optimal profiles represent an improvement from the design of Vittal and Chiranjeevi (1983) in terms of reducing flow head losses. Swamee and Basak (1993) used the optimal control theory for the design of rectangular-to-trapezoidal expansions for gradually varied subcritical flow. They obtained equations for bed-width, side-slope and bed profiles based on the minimization of the transition head losses

Escudier *et al.* (2002) conducted an experimental study of turbulent flow in a sudden expansion with an expansion ratio of 4 and an aspect ratio of 5.33. A laser Doppler anemometer was used to measure mean flow velocity fluctuations and the Reynolds shear stress. They reported that the flow downstream of the expansion is asymmetric. They concluded that the effect of inlet of expansion is the reason for asymmetrical behaviour of flow.

2.4 The effect of solid surface friction

Babarrutsi *et al.* (1989) experimentally investigated re-circulating flows in a sudden open-channel expansion, considering the frictional effects of the channel bed. Their measurements showed that the re-circulating flow rate and length decrease due to friction. They recommended the use of materials with insignificant roughness height when studying flow separation in expansions.

2.5 Geometric shape of expansions

As shown in Figure 2.2, channel expansions can be classified into five categories, namely, straight line expansions, square end expansions, cylindrical quadrant expansions, warped expansions, and wedge expansions.

Hinds (1927) considered different empirical design methods for various geometries of flumes and siphons. The design criterion was to minimize the transition length and energy losses. To achieve this objective, Hinds (1927) assumed a water-surface profile as two reversed parabolas with equal length, merging tangentially with the upstream and downstream water surface. The energy principle was used to expresses the expanding width as a function of the

distance from the inlet of the expansion, with an assumed energy loss coefficient. Hinds (1927) concluded that an S-curved warped wall expansion is the most suitable one.

Smith and Yu (1966) examined the results of Hinds (1927) and found that the S-curved warped wall expansion is inefficient results, and causes flow separation. Smith and Yu (1966) recommended a straight walled diverging expansion (Figure 2.2, “straight line” type).

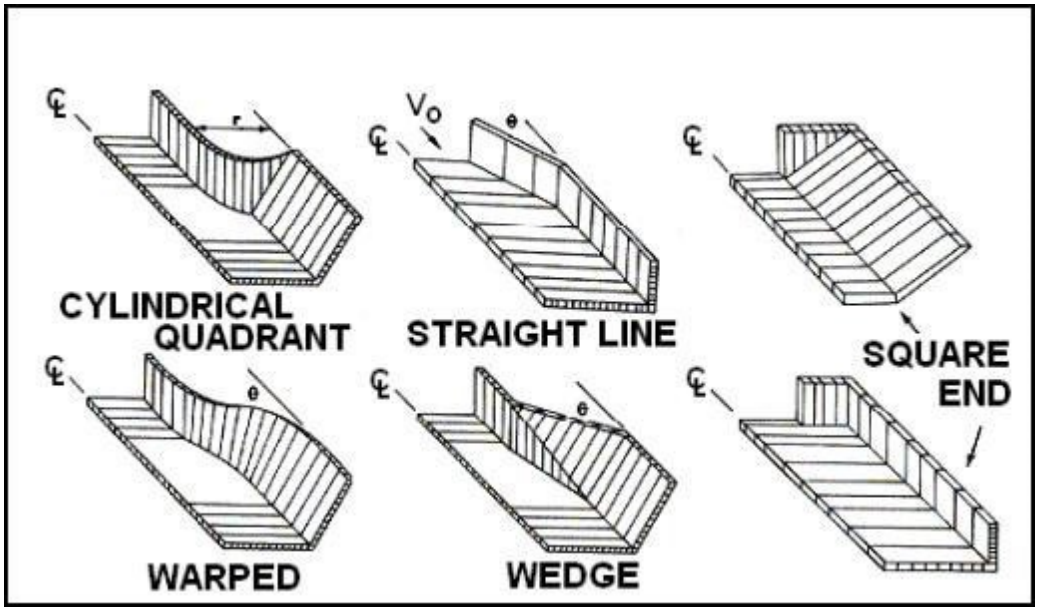

Figure 2.2 Channel expansion types (from U.S. Department of Transportation 1983, Chapter 4). All the expansions have geometry symmetric about the centerline.

2.6 Energy loss analyse for expansions

Using a rational method based on the concept of specific energy, Vittal and Chiranjeevi (1983) attempted to determine the boundary shape of expansions and flow conditions, with minimum head losses. Through experiments, they derived functions for the geometric features of expansions such as the bed width, bed elevation and sidewall slope. Their method was for designing a trapezoidal expansion.

When subcritical flow passes through an expansion, there is a decrease in velocity and an increase in pressure. Without any change in bed level, the water surface will rise by a vertical distance that is equal to the amount of drop of velocity head between the entrance and exit of the expansion. This means a conversion from kinetic to potential energy. However, this conversion is accompanied by energy losses. Mathematic analyses of energy losses in expansions of arbitrary geometry are difficult to perform. Therefore, it is a good alternative to find the energy losses for specific expansions and then extend the results by careful interpolations. Kalinske (1944) found that the rate of loss of energy in a 30° expansion is more than that in a sudden expansion. He found a major portion of the energy in the expansions is lost by direct conversion into heat at the high shear region in the fluid, and the total loss of energy is much higher than the turbulence energy.

Using the energy principle, Skogerboe *et al.* (1971) expressed the head loss in an expansion as a function of the velocity head at the entrance of the expansion. However, there was a small head loss correction which will varied for each expansion. The head loss coefficient was expressed as a function of the inlet Froude number as well as the expansion ratio, instead of a function of the specific energy ratio, as suggested by other researchers.

Skogerboe *et al.* (1971) argued that since a unique relationship exists between the head loss coefficient and specific energy ratio for any particular geometry of open channel expansion, and since a unique relationship between the specific energy ratio and the inlet Froude number, a unique relationship exists between the inlet Froude number and head loss coefficient for any particular expansion geometry. This means that the Froude number is a factor to consider.

As stated in Morris and Wiggert (1972, p. 185), the efficiency of energy conversion requires the flow profile to be continuous and as smooth as possible. Also, the profile should be

tangent to the water-surface curves in the upstream and downstream sections of the expansion. In summary, for the design of expansions, the water-surface profile is computed using the energy principle. The accuracy of computations relies on more or less guessed energy losses.

2.7 Hydraulic behaviour of channel expansions

An expansion with a large amount of change of the differential kinetic energy to potential energy is considered to be hydraulically efficient. In fact, the rise of the water surface or the recovery of energy head is less than the theoretical vertical distance (Hinds 1927). Smith and Yu (1966) considered expansions as gradual if the total central angle between sidewalls, α, is smaller than 28°10'. Separation can occur when α reaches 19°, except at the expansion ratio less than 2. Note that α = 28°10' corresponds to a 1:4 ratio of flare; this is a rapid expansion. Except when the expansion ratio is between 1 and 2, separation cannot be avoided. However, reducing α to avoid flow separation in an expansion is not practical because the length of the expansion will increase and the cost to build such an expansion is high.

According to Smith and Yu (1966), in a rapid expansion, flow from contracted section leans toward one of the sidewalls and a large turbulent eddy forms between the jet and the other sidewall. A straight wall flare is better than curved wall flare of equal length (Smith and Yu, 1966), because when the curved wall flare is used, the central angle between wall tangents continuously increases, and the flow may separate on one side of the expansion when the central angle becomes too large. They concluded that the same benefit could be obtained at less cost by using a shorter gradual expansion so that there is no justification for using the rapid expansion.

Kalinske (1944) found that the rate of loss of energy in a 30° expansion is more than the sudden expansion. The author indicated that a major portion of the energy in the expansion is

lost by a direct conversion into heat at the high shear region in the fluid, and the total loss of energy is much higher than the turbulence energy.

Chapter Three Modelling Methodologies

This study aims to model subcritical turbulent flow in the expansion section of an open channel. CFX software (ANSYS 2010a, 2010b) was used to create an appropriate model channel of different geometric configurations and to predict the three orthogonal components of water velocity along with the depth of flow in the model channel. This chapter begins with a description of the model domain. Then, the hydrodynamics equations and turbulence closure schemes are presented. This is followed by specifications of boundary and initial conditions. Next, strategies for the generation of finite volume meshes for flow computation are discussed.

3.1 Model domain

The model domain for flow computations consists of an upstream channel section, an expansion and a downstream channel section, with or without a hump fitted at the channel bottom of the expansion section (Figure 3.1). In some cases, the model domain allows for an additional extension channel section at downstream. The length of the expansion section matches that of an existent physical model in the Hydraulics Lab at Concordia University; experimental data from the physical model are available for comparison.

The velocity and pressure fields of steady state are computed for given conditions of inflow at the upstream end and outflow at the downstream end of the model channel. Inclusion of an upstream channel section of efficient length allows the development of realistic flow profiles or vertically distributed flow velocities that approach the expansion, whereas inclusion of a downstream channel section is helpful for removing possible end effects, which are artificial, on the computed flow field in the expansion.

(a) Elevation

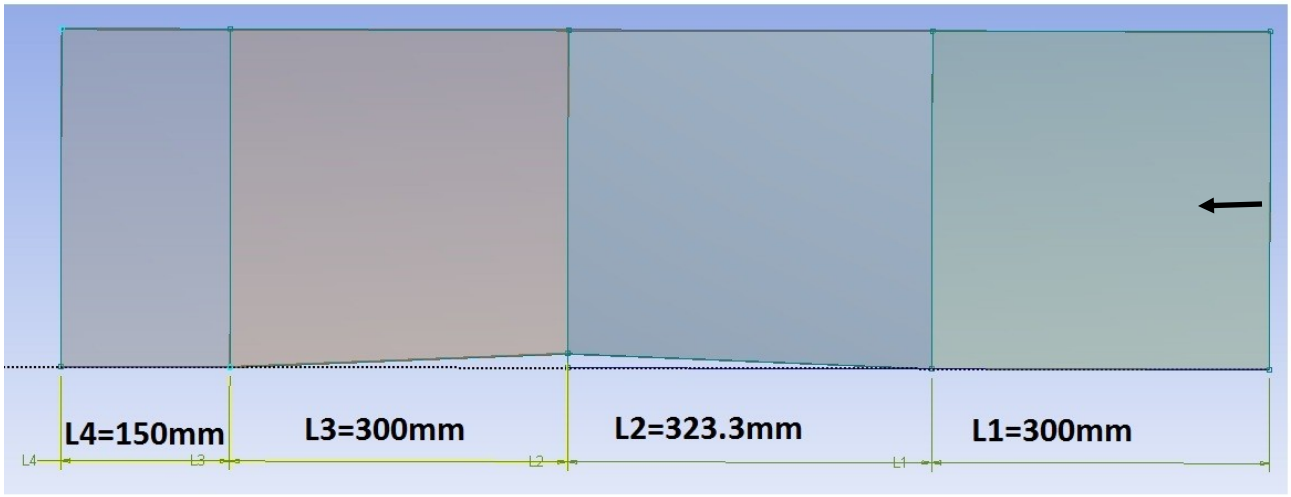

(b) Plan view

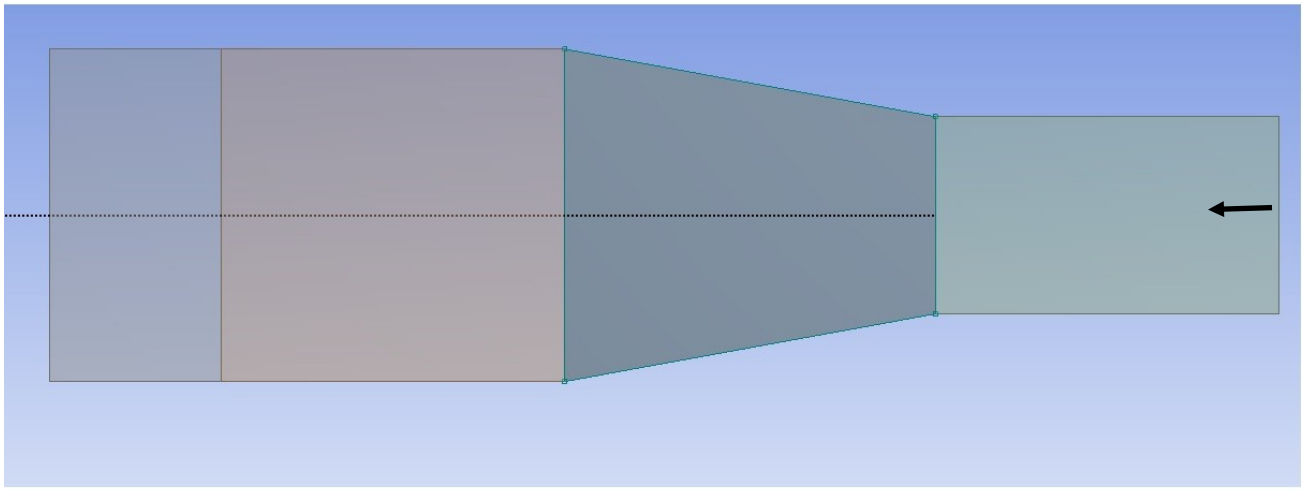

Figure 3.1 Geometry of the model channel, showing dimensions of various channel sections and bottom configurations. Uniform water flow enters (arrow) the model channel from the relatively narrow channel section.

3.2 Reynolds-averaged continuity and momentum equations

3.2.1 Continuity equation

Let (u, v, w) denote the three orthogonal components of the instantaneous velocity field in the Cartesian coordinates (x, y, z). The positive direction of the z-axis points upward. For an incompressible fluid, the equation of continuity is given by

$$\frac{\partial u}{\partial x}+\frac{\partial v}{\partial y}+\frac{\partial w}{\partial z}=0 \tag{3.1}$$

Open channel flows are always fluctuating or turbulent; practically it is extremely difficult to resolve the instantaneous flow field. One way to deal with turbulent flow is to split the instantaneous velocity into mean components (U, V, W) and fluctuations (u′, v′, w′) through the so-called Reynolds decomposition, expressed as

$$u=U+u' \tag{3.2}$$

$$v=V+v' \tag{3.3}$$

$$w=W+w' \tag{3.4}$$

Substitutions of Eqs. (3.2)-(3.4) into Eq. (3.1) give:

$$\frac{\partial\overline{(U+u')}}{\partial x}+\frac{\partial\overline{(V+v')}}{\partial y}+\frac{\partial\overline{(W+w')}}{\partial z}=0 \tag{3.5}$$

The operation of the Reynolds time average gives rise to

$$\frac{\partial U}{\partial x}+\frac{\partial V}{\partial y}+\frac{\partial W}{\partial z}+\frac{\partial\overline{u'}}{\partial x}+\frac{\partial\overline{v'}}{\partial y}+\frac{\partial\overline{w'}}{\partial z}=0 \tag{3.6}$$

Since the averages of velocity fluctuations are zero, resultant equation become the Reynolds-averaged equation of continuity

$$\frac{\partial U}{\partial x}+\frac{\partial V}{\partial y}+\frac{\partial W}{\partial z}=0 \tag{3.7}$$

The three Reynolds-averaged velocity components (U, V, W) are unknowns.

3.2.2 Momentum equations

Let ρ denote the density of water, t denote the time, μ denote the dynamic viscosity of water, and p denote the instantaneous pressure field. The momentum equations for open channel flow can be written as

$$\rho\left[\frac{\partial u}{\partial t}+\frac{\partial}{\partial x}(uu)+\frac{\partial}{\partial y}(vu)+\frac{\partial}{\partial z}(wu)\right]=-\frac{\partial p}{\partial x}+\mu\left(\frac{\partial^2 u}{\partial x^2}+\frac{\partial^2 u}{\partial y^2}+\frac{\partial^2 u}{\partial z^2}\right) \tag{3.8}$$

$$\rho\left[\frac{\partial v}{\partial t}+\frac{\partial}{\partial x}(uv)+\frac{\partial}{\partial y}(vv)+\frac{\partial}{\partial z}(wv)\right]=-\frac{\partial p}{\partial y}+\mu\left(\frac{\partial^2 v}{\partial x^2}+\frac{\partial^2 v}{\partial y^2}+\frac{\partial^2 v}{\partial z^2}\right) \tag{3.9}$$

$$\rho\left[\frac{\partial w}{\partial t}+\frac{\partial}{\partial x}(uw)+\frac{\partial}{\partial y}(vw)+\frac{\partial}{\partial z}(ww)\right]=-\frac{\partial p}{\partial w}+\mu\left(\frac{\partial^2 w}{\partial x^2}+\frac{\partial^2 w}{\partial y^2}+\frac{\partial^2 w}{\partial z^2}\right) \tag{3.10}$$

On the left hand side of the above equations, the first term is a transient term that describes the local rate of change of the velocity, and the remaining three terms are convection terms. On the right side of the equations, there are a pressure gradient term, and three molecular diffusion terms. It is assumed that the fluid is incompressible, and therefore, the density of water is constant with respect to time and space.

Because of the difficulty in dealing with the instantaneous velocity field, the Reynolds decomposition is applied to Eqs. (3.8)-(3.10). Similar to the instantaneous velocity components decomposed in Eqs. (3.2)- (3.4), the instantaneous pressure p is split into a mean value P and a fluctuation p′, i.e.

$$p = P + p' \tag{3.11}$$

Substituting Eqs. (3.2)-(3.4) and (3.11) into (3.8)-(3.10) and taking the Reynolds average yield

$$\rho\left[\frac{\partial U}{\partial t}+\frac{\partial}{\partial x}(UU)+\frac{\partial}{\partial y}(UV)+\frac{\partial}{\partial z}(UW)\right]=-\frac{\partial P}{\partial x}+\mu\left(\frac{\partial^2 U}{\partial x^2}+\frac{\partial^2 U}{\partial y^2}+\frac{\partial^2 U}{\partial z^2}\right)-\rho\left[\frac{\partial}{\partial x}\left(\overline{u'u'}\right)+\frac{\partial}{\partial y}\left(\overline{u'v'}\right)+\frac{\partial}{\partial z}\left(\overline{u'w'}\right)\right] \tag{3.12}$$

$$\rho\left[\frac{\partial V}{\partial t}+\frac{\partial}{\partial x}(UV)+\frac{\partial}{\partial y}(VV)+\frac{\partial}{\partial z}(WV)\right]=-\frac{\partial P}{\partial y}+\mu\left(\frac{\partial^2 V}{\partial x^2}+\frac{\partial^2 V}{\partial y^2}+\frac{\partial^2 V}{\partial z^2}\right)-\rho\left[\frac{\partial}{\partial x}\left(\overline{u'v'}\right)+\frac{\partial}{\partial y}\left(\overline{v'v'}\right)+\frac{\partial}{\partial z}\left(\overline{w'v'}\right)\right] \tag{3.13}$$

$$\rho\left[\frac{\partial W}{\partial t}+\frac{\partial}{\partial x}(WU)+\frac{\partial}{\partial y}(WV)+\frac{\partial}{\partial z}(WW)\right]=-\frac{\partial P}{\partial z}-\rho g+\mu\left(\frac{\partial^2 W}{\partial x^2}+\frac{\partial^2 W}{\partial y^2}+\frac{\partial^2 W}{\partial z^2}\right)-\rho\left[\frac{\partial}{\partial x}\left(\overline{u'w'}\right)+\frac{\partial}{\partial y}\left(\overline{v'w'}\right)+\frac{\partial}{\partial z}\left(\overline{w'w'}\right)\right] \tag{3.14}$$

In these equations, there are four unknowns: the Reynolds-averaged pressure field P and the three unknown Reynolds-averaged velocity components (U, V, W).

In addition, the Reynolds average operation produces six extra unknown quantities involving velocity component fluctuations. These quantities are the so-called specific Reynolds shear stresses: $\tau_{xx}=-\overline{u'u'}$, $\tau_{xy}=-\overline{u'v'}$, $\tau_{xz}=-\overline{u'w'}$, $\tau_{yx}=-\overline{v'u'}$, $\tau_{yy}=-\overline{v'v'}$, $\tau_{yz}=-\overline{v'w'}$, $\tau_{zx}=-\overline{w'u'}$, $\tau_{zy}=-\overline{w'v'}$ and $\tau_{zz}=-\overline{w'w'}$, some of which are identical. These unknown shear stresses must be modelled, giving rise to a turbulence closure problem.

3.3 Turbulence models

3.3.1 The concept of turbulent eddy viscosity

In this study, turbulence closure makes use of the concept of turbulent eddy viscosity ν_t. The specific Reynolds shear stresses are related to the mean flow strain rates using the Boussinesq approximation:

$$\tau_{xx} = 2\nu_t S_{xx}, \qquad \tau_{xy} = 2\nu_t S_{xy}, \qquad \tau_{xz} = 2\nu_t S_{xz} \tag{3.15a,b,c}$$

$$\tau_{yx} = 2\nu_t S_{yx}, \qquad \tau_{yy} = 2\nu_t S_{yy}, \qquad \tau_{yz} = 2\nu_t S_{yz} \tag{3.16a,b,c}$$

$$\tau_{zx} = 2\nu_t S_{zx}, \qquad \tau_{zy} = 2\nu_t S_{zy}, \qquad \tau_{zz} = 2\nu_t S_{zz} \tag{3.17a,b,c}$$

The mean flow strain rates are given below

$$S_{xx} = \frac{1}{2}\left(\frac{\partial U}{\partial x} + \frac{\partial U}{\partial x}\right), \quad S_{xy} = \frac{1}{2}\left(\frac{\partial U}{\partial y} + \frac{\partial V}{\partial x}\right), \quad S_{xz} = \frac{1}{2}\left(\frac{\partial U}{\partial z} + \frac{\partial W}{\partial x}\right) \tag{3.18a,b,c}$$

$$S_{yx} = S_{xy}, \quad S_{yy} = \frac{1}{2}\left(\frac{\partial V}{\partial y} + \frac{\partial V}{\partial y}\right), \qquad S_{yz} = \frac{1}{2}\left(\frac{\partial V}{\partial z} + \frac{\partial W}{\partial y}\right) \tag{3.19a,b,c}$$

$$S_{zx} = S_{xz}, \qquad S_{zy} = S_{yz}, \qquad S_{zz} = \frac{1}{2}\left(\frac{\partial W}{\partial z} + \frac{\partial W}{\partial z}\right) \tag{3.20a,b,c}$$

These terms can readily be evaluated once the Reynolds-averaged velocity components. The eddy viscosity is obtained from the k-ω turbulence model.

3.3.2 The standard k-ω model

For open channel flow applications, a variety of turbulence models have been developed, each with certain advantages and disadvantages. The choice of a specific turbulence model depends on the type and nature of the flow field to be simulated and the desired accuracy of results. The k-ω model is one of the most commonly used turbulence models.

This model is the first two-equation model of turbulence proposed by Kolmogorov (1942). It is a two equation model; i.e. it includes two extra transport equations to represent the turbulent properties of the flow. This allows a two equation model to account for history effects like convection and diffusion of turbulent energy. Kolmogorov (1942) chose the kinetic energy of turbulence, *k*, as one of his turbulence parameters, and modeled the partial differential equation that governs the behaviour of k. His second parameter was the dissipation per unit

turbulence kinetic energy i.e. $\frac{\varepsilon}{k}$. This is the so-called ω. In his k-ω model, ω satisfies a partial differential equation similar to the equation for *k*. Kolmogorov's justifications for introducing the k-ω model are:

- Because k already appears in $\tau_{ij} = 2\nu_t S_{ij} - \frac{2}{3}k\delta_{ij}$, it is conceivable that $\nu_t \propto k$.
- The dimensions of eddy viscosity are $\frac{m^2}{s}$, whereas the dimensions of k are $\frac{m^2}{s^2}$.
- Therefore, $\frac{\nu_t}{k}$ has the dimension of time.
- Turbulence dissipation, ε, has dimension of $\frac{m^2}{s^3}$.
- Consequently $\frac{\varepsilon}{k}$ has a dimension of $\frac{1}{s}$.
- Thus, we can close $\tau_{ij} = 2\nu_t S_{ij} - \frac{2}{3}k\delta_{ij}$ and the transport equation for k by introducing a variable with dimension *s* or $\frac{1}{s}$.

Given that the most common processes in fluid motion are unsteadiness, convection, diffusion, dissipation, dispersion and production, Kolmogorov (1942) combined the physical processes with dimensional arguments and proposed a transport equation for ω as below

$$\frac{\partial \omega}{\partial t} + \left(U\frac{\partial \omega}{\partial x} + V\frac{\partial \omega}{\partial y} + W\frac{\partial \omega}{\partial z} \right) = -\beta\omega^2 + \left[\frac{\partial}{\partial x}\left(\sigma\nu_t \frac{\partial \omega}{\partial x} \right) + \frac{\partial}{\partial y}\left(\sigma\nu_t \frac{\partial \omega}{\partial y} \right) + \frac{\partial}{\partial z}\left(\sigma\nu_t \frac{\partial \omega}{\partial z} \right) \right] \tag{3.21}$$

where β and σ are two new closure coefficients. This equation is not written in terms of ω^2. In fact, ω^2 is the mean square vorticity of the "energy containing" eddies and *k* is the kinetic energy

of the motion induced by this vorticity. Therefore, it is better to write the equation in terms of ω^2. A production term was added to the equations later by other researchers. The k-ω model equations, closure coefficients and relationships are as follows:

Kinematic eddy viscosity is given by

$$\nu_T = \frac{k}{\tilde{\omega}} \tag{3.22}$$

where $\tilde{\omega} = \max\left\{\omega, C_{\lim}\sqrt{\frac{2(S_{xx}{}^2 + S_{xy}{}^2 + S_{xz}{}^2 + S_{yx}{}^2 + S_{yy}{}^2 + S_{yz}{}^2 + S_{zx}{}^2 + S_{zy}{}^2 + S_{zz}{}^2)}{\beta^*}}\right\}$,

$C_{\lim} = \frac{7}{8}$

It means that the eddy viscosity depends on $\tilde{\omega}$ rather than ω and this makes the eddy viscosity a function of k and ω and effectively, the ratio of the turbulence-energy production to the turbulence-energy dissipation.

The two model equations are given by

$$\begin{aligned}&\frac{\partial k}{\partial t} + U\frac{\partial k}{\partial x} + V\frac{\partial k}{\partial y} + W\frac{\partial k}{\partial z} = P_r - \beta^* k\omega + \\ &\frac{\partial}{\partial x}\left[\left(\nu + \sigma^*\frac{k}{\omega}\right)\frac{\partial k}{\partial x}\right] + \frac{\partial}{\partial y}\left[\left(\nu + \sigma^*\frac{k}{\omega}\right)\frac{\partial k}{\partial y}\right] + \frac{\partial}{\partial z}\left[\left(\nu + \sigma^*\frac{k}{\omega}\right)\frac{\partial k}{\partial z}\right]\end{aligned} \tag{3.23}$$

$$\begin{aligned}&\frac{\partial \omega}{\partial t} + U\frac{\partial \omega}{\partial x} + V\frac{\partial \omega}{\partial y} + W\frac{\partial \omega}{\partial z} = \alpha\frac{\omega}{k}P_r - \beta\omega^2 + \\ &\frac{\partial}{\partial x}\left[\left(\nu + \sigma\frac{k}{\omega}\right)\frac{\partial \omega}{\partial x}\right] + \frac{\partial}{\partial y}\left[\left(\nu + \sigma\frac{k}{\omega}\right)\frac{\partial \omega}{\partial y}\right] + \frac{\partial}{\partial z}\left[\left(\nu + \sigma\frac{k}{\omega}\right)\frac{\partial \omega}{\partial z}\right] + \\ &\left[\left(\frac{\sigma_d}{\omega}\frac{\partial k}{\partial x}\frac{\partial \omega}{\partial x}\right) + \left(\frac{\sigma_d}{\omega}\frac{\partial k}{\partial y}\frac{\partial \omega}{\partial y}\right) + \left(\frac{\sigma_d}{\omega}\frac{\partial k}{\partial z}\frac{\partial \omega}{\partial z}\right)\right]\end{aligned} \tag{3.24}$$

where P_r is the turbulence production term, given by

$$P_r = 2\nu_t\left(S_{xx}\frac{\partial U}{\partial x} + S_{xy}\frac{\partial U}{\partial y} + S_{xz}\frac{\partial U}{\partial z} + S_{yx}\frac{\partial V}{\partial x} + S_{yy}\frac{\partial V}{\partial y} + S_{yz}\frac{\partial V}{\partial z}\right) + 2\nu_t\left(S_{zx}\frac{\partial W}{\partial x} + S_{zy}\frac{\partial W}{\partial y} + S_{zz}\frac{\partial W}{\partial z}\right) \quad (3.25)$$

Closure coefficients and auxiliary relations are as below

- $\alpha = \frac{13}{25},\ \beta = \beta_0 f_\beta\ ,\ \beta^* = \frac{9}{100},\ \sigma = \frac{1}{2},\ \sigma^* = \frac{3}{5},\ \sigma_{d0} = \frac{1}{8}$ (3.26)

- $\sigma_d = \begin{cases} 0, & \frac{\partial k}{\partial x}\frac{\partial \omega}{\partial x} + \frac{\partial k}{\partial y}\frac{\partial \omega}{\partial y} + \frac{\partial k}{\partial z}\frac{\partial \omega}{\partial z} \le 0 \\ \sigma_{d0}, & \frac{\partial k}{\partial x}\frac{\partial \omega}{\partial x} + \frac{\partial k}{\partial y}\frac{\partial \omega}{\partial y} + \frac{\partial k}{\partial z}\frac{\partial \omega}{\partial z} \succ 0 \end{cases}$ (3.27)

- $\beta_0 = 0.0708\ \ ,\ f_\beta = \frac{1+85\chi_\omega}{1+100\chi_\omega}\ \ ,\ \chi_\omega \equiv \left|\frac{\Omega_{ij}\Omega_{jk}S_{ki}}{(\beta^*\omega)^3}\right|$ (3.28)

- $\varepsilon = \beta^*\omega k$ and $l = k^{1/2}/\omega$ (3.29)

The two tensors in Equation (3.28) are the mean rotation (vorticity) and mean-strain-rate tensors.

In Equation (3.24), the cross diffusion term, $\frac{\sigma_d}{\omega}\frac{\partial k}{\partial x_j}\frac{\partial \omega}{\partial x_j}$, is added to the equation to remove the original model's sensitivity to the free stream value of ω, and to remove the sensitivity to the imposed boundary condition. This is good for applications to wall-bounded flows. The reciprocal of ω is the time scale on which dissipation of turbulence energy occurs. While the actual process of dissipation takes place in the smallest eddies, the rate of dissipation is the transfer rate of turbulence kinetic energy to the smallest eddies. Therefore, the dissipation rate is set by the properties of the large eddies (scales with k and l). Therefore, ω is indirectly associated with the dissipative process.

3.4 The volume of fluid method

The interface between the gas and liquid, where the difference in density between these two phases is quite large, is considered as a free surface. The inertia of the gas could usually be neglected due to a low density. Therefore, the only influence of the gas is the pressure acted on the interface and it is not necessary to model details of the gas phase. Hence, the free surface is simply modelled as a boundary with constant pressure.

The volume of fluid method is used to determine the shape and location of free surface based on the concept of a fractional volume of fluid. A unity value of the volume fraction corresponds to a full element occupied by the fluid (or liquid), and a zero value indicates an empty element containing no fluid (or gas). A value of volume fraction between zero and one means that the corresponding element is the surface (or partial) element. The equation of the volume of fluid method for determining the shape of the free surface is given by

$$\frac{\partial F}{\partial t} + U\frac{\partial F}{\partial x} + V\frac{\partial F}{\partial y} + W\frac{\partial F}{\partial z} = 0 \tag{3.30}$$

where F is the volume fraction.

3.5 Boundary conditions

The appropriate use of boundary conditions is required to fully define the fluid flow problem. The external boundaries of the model domain are the inlet, outlet, sidewalls and channel-bed.

3.5.1 Inlet condition

Inlets are used mostly for regions where inflow is expected. At the inlet where the fluid flows into the domain (Fig. 3.1), the imposed mass and momentum conditions is the normal speed v_n. The magnitude of the inlet velocity is specified and the direction is taken to be normal to the

boundary. The normal speed is steady and uniform. For instance, v_n equals 0.78 m/s for some simulations. Also, the relative pressure at the inlet is specified

$$P = (\rho_w - \rho_a) g F_w (\eta_1 - z) \tag{3.31}$$

where the subscripts w and a indicate water and the air, respectively, g is gravity, η_1 is the elevation (above the channel bed) of the free surface at the inlet, and z changes from zero at the channel bed to η_1 at the free surface. A value for η_1 is given (e.g. η_1 = 0.25 m for some simulations).

At the inlet, the turbulence intensity and turbulence length scale are specified. The turbulence intensity is given in terms of a fractional intensity (5%), and the turbulence length scale is taken to be equal to η_1.

3.5.2 Outlet condition

At the outlet where the fluid leaves the model domain (Fig. 3.1), the appropriate condition to impose is the relative static pressure, given by

$$P = (\rho_w - \rho_a) g F_w (\eta_2 - z) \tag{3.32}$$

where η_2 is the elevation (above the channel bed) of the free surface at the outlet, and z changes from zero at the channel bed to η_2 at the free surface. Usually, η_2 must be known as part of the problem definition. For the case of flows in expansions, the elevation is not known in advance. However, it is sufficient to provide an estimate of η_2 using the energy principle (Henderson 1966) for the purpose of determining the distribution of the relative static pressure with depth below the free surface.

3.5.3 Solid surface condition

Channel sidewalls and the channel bed (Fig. 3.1) are solid surfaces where conditions to be imposed can be a no-slip wall, a free slip wall or specified shear. In this study, the no-slip wall condition is applied. The flow near to the no-slip wall is modelled using wall function approach. Based on the wall function approach , the near wall tangential velocity in the log-law region is related to the wall-shear-stress , τ_w, by means of a logarithmic relation. The logarithmic relation for the near wall velocity is given by

$$u^+ = \frac{U_t}{u_\tau} = \frac{1}{\kappa}\ln\left(y^+\right) + C \tag{3.33}$$

where

$$y^+ = \frac{\rho \Delta y u_\tau}{\mu}, \tag{3.34}$$

$$u_\tau = \left(\frac{\tau_w}{\rho}\right)^{1/2} \tag{3.35}$$

u^+ is the near wall velocity , U_t is the known velocity tangent to the wall at a distance of Δy from the wall, u_τ is the friction velocity, y^+ is the dimensionless distance from the wall, τ_w is the shear stress of the wall, κ is the von Karman constant, and C is the log-layer constant that depends on the wall roughness.

3.6 Initial conditions

Let h_w denote the initial depth of water. Initially, the volume of fraction for air is given by a step function $f_a = \chi\left(z - h_w\right)$, where z is the vertical coordinates pointing upward with z = 0 at the channel bed. The step function χ gives $f_a = 1$ for $z - h_w \succ 0$, and $f_a = 0$ for $z - h_w \le 0$. The

initial volume of fluid for water is $f_w = 1 - f_a$. Initially, the relative pressure field, P, in water is hydrostatic or $P = \rho_w g(h_w - z)$ and is uniformly zero in the air (the pressure in the air is set to zero). Thus, the initial conditions for the pressure field and the volume fraction are consistent.

3.7 Finite volume meshes

It is desirable to use fine meshes for flow computations in order to capture detailed flow features such as eddies and velocity shears. Meshes were generated on the basis of a number of criteria: First, meshes are fine enough in order to resolve rapid spatial variations in the velocity fields, especially near wall boundaries. This requirement is satisfied by performing inflation on meshes adjacent to solid walls where eddies and velocity shear are expected to appear (Fig. 3.2).

Second, the structure of meshes used for flow computations must not affect the computational results. In other words, the model results produced should be independent of the configurations of the meshes used. The strategies used to satisfy this requirement were to several mesh systems of progressive fine sizes (e.g. $10*10^{-3}$ m, $7*10^{-3}$ m, $5*10^{-3}$ m and $4*10^{-3}$ m) and to carry out model runs using the different meshes under identical flow conditions. The independence of the computed flow field for these runs was verified through comparisons of the results among these runs.

Third, the total number mesh points must not be excessively larger, resulting in prohibitively high computation cost. An excessively large number of mesh points will also create difficulties in the post processing of model output.

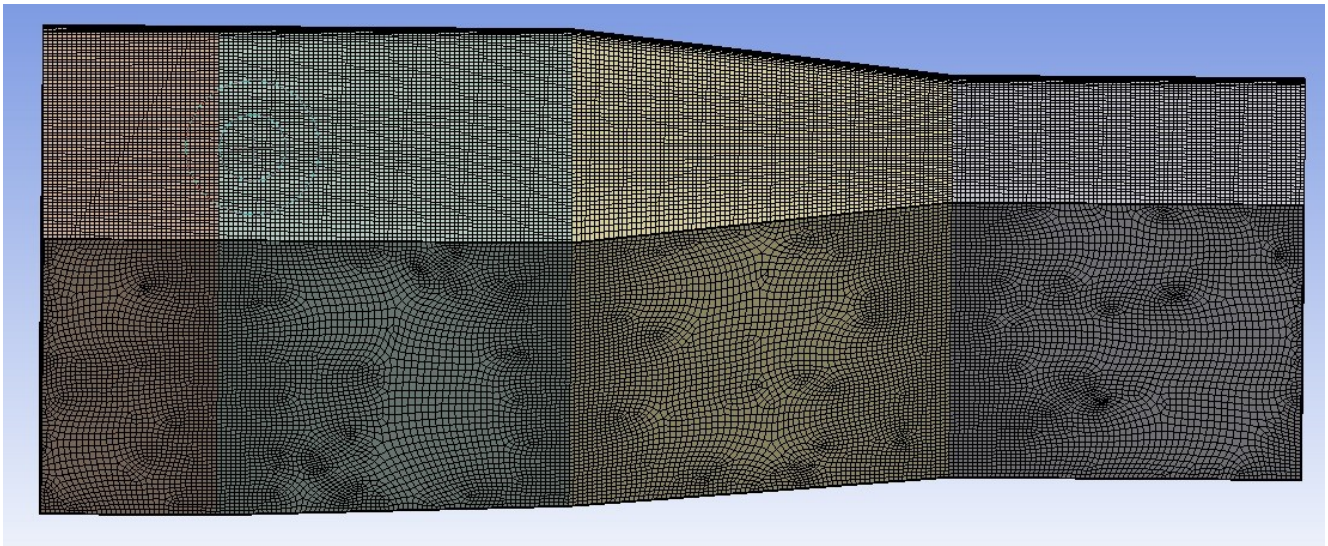

Figure 3.2 A sample finite volume mesh system used for flow computations, showing the inflation of meshes near all solid walls. The solid surface on the top is set to be slippery.

3.7.1 Determination of the near-wall mesh spacing

As described in ANSYS (2010b), for fluid flow of characteristic velocity U_o over a flat surface of characteristic length L, the Reynolds number can be defined as:

$$\mathrm{Re}_L = \frac{U_\infty L}{\nu} \tag{3.36}$$

An empirical correlation between the wall shear stress coefficient c_f and the Reynolds number is given by

$$c_f = 0.027\,\mathrm{Re}_x^{-1/7} \tag{3.37}$$

where x is the distance along the plate from the leading edge, and the Reynolds number is based on x, i.e.

$$\mathrm{Re}_x = \frac{U_\infty x}{\nu} \tag{3.38}$$

For near-wall spacing estimate, the definition of the dimensionless wall distance Δy^+ is given by

$$\Delta y^+ = \frac{u_\tau \Delta y}{\nu} \tag{3.39}$$

where u_τ is the friction velocity, which is unknown, Δy is the mesh spacing between the wall and the first mesh point away from the wall. If we can eliminate the unknown friction velocity, for target values of Δy^+, we will be able to determine Δy. Using the definition

$$c_f = 2\frac{\rho u_\tau^{\,2}}{\rho U_\infty^{\,2}} = 2\left(\frac{u_\tau}{U_\infty}\right)^2 \tag{3.40}$$

we can eliminate the friction velocity in Eq. (3.39) to yield

$$\Delta y = \Delta y^+ \sqrt{\frac{2}{c_f}}\,\frac{\nu}{U_\infty} \tag{3.41}$$

The wall shear stress coefficient c_f in equation (3.41) can be eliminated using the empirical correlation given in Eq. (3.37), to give

$$\Delta y = \Delta y^+ \sqrt{\frac{2}{0.027}\mathrm{Re}_x^{1/7}}\,\frac{\nu}{U_\infty} \tag{3.42}$$

Using the definition in Eq. (3.36), we may rewrite Eq. (3.42) as

$$\Delta y = L\Delta y^+ \sqrt{74}\,\mathrm{Re}_x^{1/14}\,\frac{1}{\mathrm{Re}_L} \tag{3.43}$$

Assume that $\mathrm{Re}_x = C\,\mathrm{Re}_L$, where C is some fraction. If C is assumed to be 0.5 with $C^{1/14} \approx 0.952$, Eq. (3.43) is reduced to

$$\Delta y \approx 7.9141 L\Delta y^+ \,\mathrm{Re}_L^{-13/14} \tag{3.44}$$

Except for very small Re_x (very close to the leading edge of the flat surface), Eq. (3.44) is suitable for estimates of the near wall mesh spacing.

For target values of Δy^+, the mesh spacing Δy can be determined. Some sample calculations are shown in Table 3.1. Values for the characteristic quantities used in these calculations are: L = 0.30 m (the approximate length of the expansion in question) and U_o = 0.70 m/s (the approximate normal speed of water flow at the inlet). The viscosity of water is taken as $\nu = 10^{-6}$ m^2/s. The Reynolds number [Eq. (3.36)] is $Re_L = 2.1\times10^5$.

Table 3.1 Mesh spacing (Δy) for various target values of the dimensionless wall distance (y^+).

y+	1	10	20	30	40	50	60	70	80	90	100	110	120
Δy (mm)	0.03	0.3	0.6	0.8	1.1	1.4	1.7	2.0	2.2	2.5	2.8	3.1	3.4
y+	130	140	150	160	180	200	220	240	260	280	300	320	340
Δy (mm)	3.6	3.9	4.2	4.5	5.1	5.6	6.2	6.7	7.3	7.9	8.4	9.0	9.5

The calculations shown in Table 3.1 provide some guidelines for generating appropriate meshes. It is well established that the wall function of the form

$$\frac{U}{u_\tau} = \frac{1}{\kappa}\ln\left(y^+\right) + C \tag{3.45}$$

is valid for the wall distance y^+ in the range of $30 < y^+ < 400$. In the equation, U denotes the tangential velocity parallel to the solid wall; κ (= 5.5) is the von Karman constant; the wall distance is defined as $y^+ = yu_\tau/\nu$, where y measures the normal distance of a point in question from the solid wall. From Table 3.1, we make several observations: First, if the wall function [Eq. (3.45)] is to be used as the condition at the solid wall, it would be acceptable to place the first mesh point at a normal distance of about $1*10^{-3}$ m from the solid wall. This is because the corresponding y+ value is between 30 and 40, and the first mesh point is within the logarithmic layer where Eq. (3.45) is valid. Note that if the first mesh point is placed at a normal distance of

less than $0.3*10^{-3}$ m, the corresponding y+ value is less than 11, meaning that the first mesh point is in the viscous sublayer.

Second, if meshes are created using $10*10^{-3}$ m as the size, there is a great uncertainty whether or not the first mesh point away from the wall is inside the logarithmic layer, since the corresponding y+ value is larger than 340. The first mesh point is at best in the outer edge of the logarithmic layer, and there will not be enough mesh points inside the logarithmic layer for the k-ε model to work accurately. Meshes created using $7*10^{-3}$ m as the size give a slight improvement from $10*10^{-3}$ m meshes; the corresponding y^+ value of the first mesh point is still too high, being about 250.

Third, if meshes are created using 5 or $4*10^{-3}$ m or smaller as the size and if subsequent inflation is performed on the meshes adjacent to the solid wall, the locally refined meshes for flow computations should contain several mesh points inside the logarithmic layer due to the presence of the wall. Also, the first mesh point from the solid wall of the refined meshes is about $1*10^{-3}$ m away from the wall, and the corresponding y^+ value is between 30 and 50. This makes it ideal to apply the wall function [Eq. (3.45)] as the boundary condition at the solid wall. The independence of model results on the meshes ($4*10^{-3}$ m, $5*10^{-3}$ m, $7*10^{-3}$ m and $10*10^{-3}$ m) will be verified.

3.7.2 Estimates of boundary layer thickness

Although we do not intend to resolve the boundary layer due to the presence of a solid wall, it would be constructive to obtain estimates of the boundary layer thickness δ. On the basis of the correlation $\mathrm{Re}_\delta = 0.14\,\mathrm{Re}_x^{6/7}$, with $\mathrm{Re}_\delta = \dfrac{U_\infty \delta}{\nu}$, δ can be estimated as

$$\delta = 0.14L\left(\frac{U_\infty x}{\nu}\right)^{6/7}\frac{\nu}{U_\infty L} \qquad \text{or} \qquad \delta = 0.14L\,\mathrm{Re}_x^{\,6/7}\frac{1}{\mathrm{Re}_L} \tag{3.46a,b}$$

As in the calculations of near-wall mesh spacing [Eq. (3.43)], the Reynolds number Re_x is some fraction of Re_L. If we assume that the fraction is 50%, Eq. (3.46b) will be simplified to

$$\delta = 0.0773L\,\mathrm{Re}_L^{\,-1/7} \tag{3.47}$$

which gives an estimate of $\delta = 4*10^{-3}$ m, for $L = 30*10^{-2}$ m (the approximate length of the expansion), $U_o = 0.70$ m/s (the appropriate normal speed at the inlet), and $\nu = 10^{-6}$ m^2/s (the viscosity of water).

If Δy is set to $4*10^{-3}$ m in Eq. (3.44), the corresponding y+ value is between 140 and 150. Eq. (3.47) appears to give conservative estimates or underestimates of δ based on $\mathrm{Re}_\delta = 0.14\,\mathrm{Re}_x^{6/7}$. Importantly, meshes created using $4*10^{-3}$ m as the size with subsequent inflation are expected to satisfy the requirement that the several mesh points are inside the logarithmic layer; this not only justifies the use of the wall function as the condition at the wall but also provides the condition for the turbulence model to work properly.

Chapter Four The Energy Principle

4.1 Energy balance for flow in expansions

In this study the expansion connects a cross section of rectangular shape with a smaller width to a cross section of rectangular shape with a larger width. Figure 4.1 shows the plan view of the channel expansion. The width of the expansion changes from b_2 at its upstream end (CS2) to b_3 at its downstream end (CS3) .With the assumption of hydrostatic pressure, an energy equation could be written between sections CS2 and CS3, as below:

$$z_2 + \frac{v_2^2}{2g} + y_2 = z_3 + \frac{v_3^2}{2g} + y_3 + h_L \tag{4.1}$$

where g is the gravity; y_2 and y_3 are the depth of flow ; v_2 and v_3 are the cross sectional mean flow velocity; z_2 and z_3 are the height of the bed above datum ; h_L is the energy loss in the expansion; the subscripts 2 and 3 refer to CS2 and CS3 , respectively.

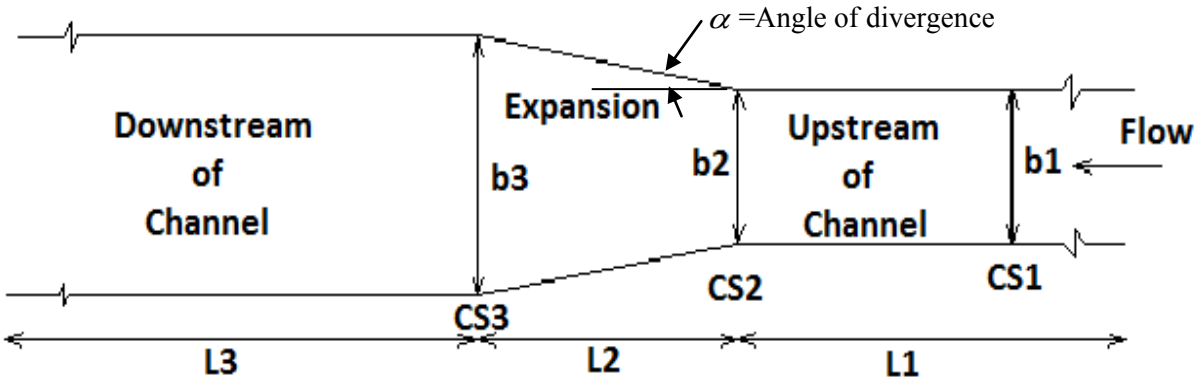

Figure 4.1 Plan view of a channel expansion.

If the channel bed is at the same level, z_2 and z_3 are the same. Also if h_L is neglected, Equation (4.1) will be simplified

$$y_2 + \frac{v_2^2}{2g} = y_3 + \frac{v_3^2}{2g} \tag{4.2}$$

Equation (4.2) shows that the flow at the two cross sections has the same specific energy. The term h_L in equation (4.1) is the energy loss in the expansion, including the energy loss h_f due to friction at the channel bed and on the sidewalls, and the energy loss h_e due to flow separation and eddy motions. h_e is expected to be much larger than h_f .Therefore, h_f can be neglected.

$$h_L \approx h_e \tag{4.3}$$

The energy loss, h_e , can be evaluated from

$$h_e = \left(y_2 + \frac{v_2^2}{2g} \right) - \left(y_3 + \frac{v_3^2}{2g} \right) \tag{4.4}$$

For the special case where the channel is rectangular, the discharge per unit width of channel; *q*, is related to the depth of flow, *y*, and flow velocity, *v*, through the equation of continuity,

$$v_2 = \frac{q_2}{y_2}, \tag{4.5}$$

$$v_3 = \frac{q_3}{y_3} \tag{4.6}$$

Equation (4.4) can be rewritten as

$$h_e = \left(y_2 + \frac{q_2^2}{2gy_2^2} \right) - \left(y_3 + \frac{q_3^2}{2gy_3^2} \right) \tag{4.7}$$

This equation is used for obtaining energy loss in the expansion due to flow separation and eddy motions. An energy loss coefficient can be defined as

$$k_E = \frac{h_e}{g_2^2 / \left(2gy_2^2\right)} \tag{4.8}$$

4.2 The concept of specific energy

The concept of specific energy is very important in the study of open-channel flows. Using the channel bed as datum, the specific energy, E, is defined as

$$E = y + \frac{v^2}{2g} \tag{4.9}$$

For the special case where the channel is rectangular, the equation of continuity is given by

$$q = \frac{Q}{b} = vy \tag{4.10}$$

where Q is the total discharge ; b is the width of the channel. The specific energy equation (4.9) can be rewritten as

$$E = y + \frac{q^2}{2gy^2} \tag{4.11}$$

Thus, for a given value of q, we have

$$(E - y)y^2 = \frac{q^2}{2g} = \text{constant} \tag{4.12}$$

4. 3 E-y curve

Consider water flow at two cross sections (CS2 and CS3) in an expansion, the corresponding per-unit-width discharges are $q_2 = Q/b_2$ and $q_3 = Q/b_3$. Since $b_3 > b_2$, we have $q_3 < q_2$. The state of

flow at cross sections 2 and 3 is represented by the two E-y curves (marked by q_2 and q_3, respectively).

The so-called E-y curve (Figure 4.2) shows how E will vary with y for a given value of q in a horizontal channel. More interestingly, as water flows through a channel expansion, the state of flow will change; this is equivalent to moving from one specific energy curve to another.

If there is no energy loss between cross sections 2 and 3, i.e. when the specific energy at cross sections 2 and 3 is the same (represented by the vertical line). The depth of flow, y, (dashed, horizontal lines) will increase from upstream (the E-y curve marked by q_2) to downstream (the E-y curve marked by q_3).

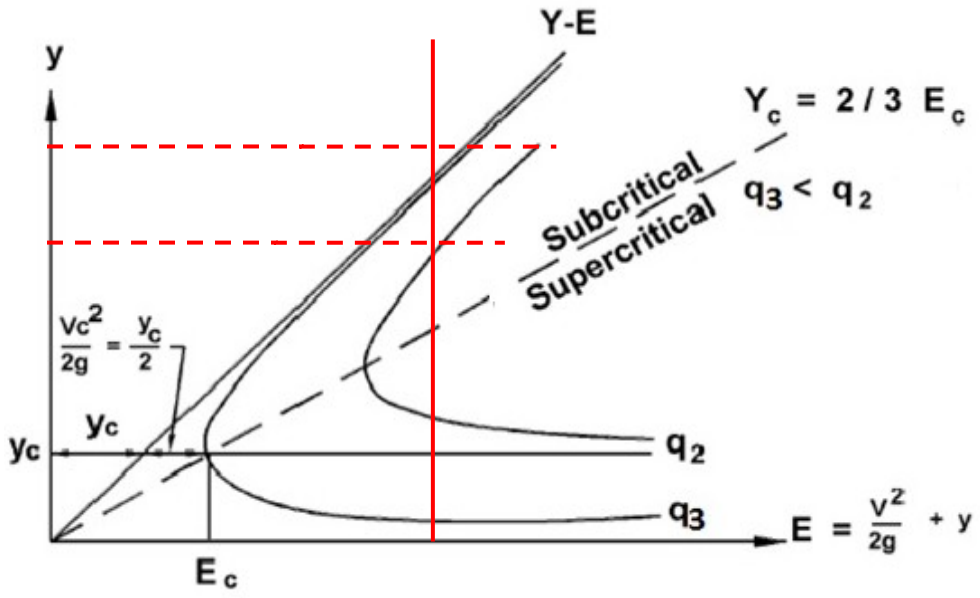

Figure 4.2 The specific energy curve and its application in the expansion problem.

4.4 Critical flow and the concept of the Froude number

The concept of critical flow is graphically illustrated in the E-y curve (Figure 4.2). For a given per-unit-width discharge, the flow is critical when the specific energy of flow is at a minimum

level. In a channel expansion when flow at high velocity discharges into a zone of lower velocity, a rather abrupt rise occurs in the flow surface. The rapidly flowing flow is abruptly slowed and increases in height, converting some of the flow's initial kinetic energy into an increase in potential energy (Henderson, 1966).

The specific energy equation (4.9) is valid only for small slopes (< 10%), where the flow has negligible acceleration in the vertical and hence the pressure distribution is hydrostatic. The velocity coefficient is usually quite high, between 0.95 and 0.99 for the rivers. Since the effects of the velocity variations across the flow section are neglected, the velocity coefficient, α, is assumed to be equal 1.0 in this study. This assumption implies that surface waves with high amplitudes are not generated and propagate during the expansion. This could be ensured when the Froude number is less than one at upstream, however, for large Froude numbers, the presence of such surface waves is inevitable.

The Froude number, F_r, is defined as the ratio of actual water velocity, *v*, to surface wave celerity, $\sqrt{gy}$ .The Froude number at cross section CS1(Figure 4.1) is defined as

$$Fr_1 = \frac{v_1}{\sqrt{gy_1}} \tag{4.13}$$

The Froude number is only defined for channel sections that have a free surface. When $Fr < 1$, the flow is said to be subcritical; when $Fr > 1$, the flow is said to be supercritical; when $Fr = 1$, the flow is said to be critical.

On the specific energy diagram (Figure 4.2), the parts corresponding to subcritical and supercritical flows are divided by the line $Y_c = \frac{2}{3} E_C$ (the crest point C), below which we have supercritical flow (the lower limb), whereas above which we have subcritical flow (the upper

limb). For critical flow denoted by the subscript *c*, the depth of flow, flow velocity and the specific energy are interrelated as

$$v_c = \sqrt{g y_c} \tag{4.14}$$

$$y_c = \frac{2}{3} E_c \tag{4.15}$$

4. 5 Flow over a step in the vertical (hump)

Consider an open channel of constant width but with a change in the bed level such as an upward step and divergence angle α, shown in Figure 4.1. If α is zero, the per-unit-width discharge will not change (Figure 4.3) .In Figure 4.3, CS2 and CS3 are cross sections, upstream of the vertical step and at the vertical step, respectively.

The behaviour of flow over a step in the vertical can be analyzed using the energy principle, written between cross sections CS2 and CS3

$$z_2 + E_2 = z_3 + E_3 \tag{4.16}$$

where z_2 and z_3 are the bottom elevations at the two cross sections, respectively. The maximum permissible height of step, $\Delta z = z_3 - z_1$, is equal to the difference energy, E_2, and the minimum possible specific energy $(E_3)_{\min} = E_c$ for the given per-unit-width discharge, *q*. Consider subcritical flow, represented by point A on the upper limb of the specific energy curve (Figure 4.4). Subcritical flow approaches the vertical step (hump).

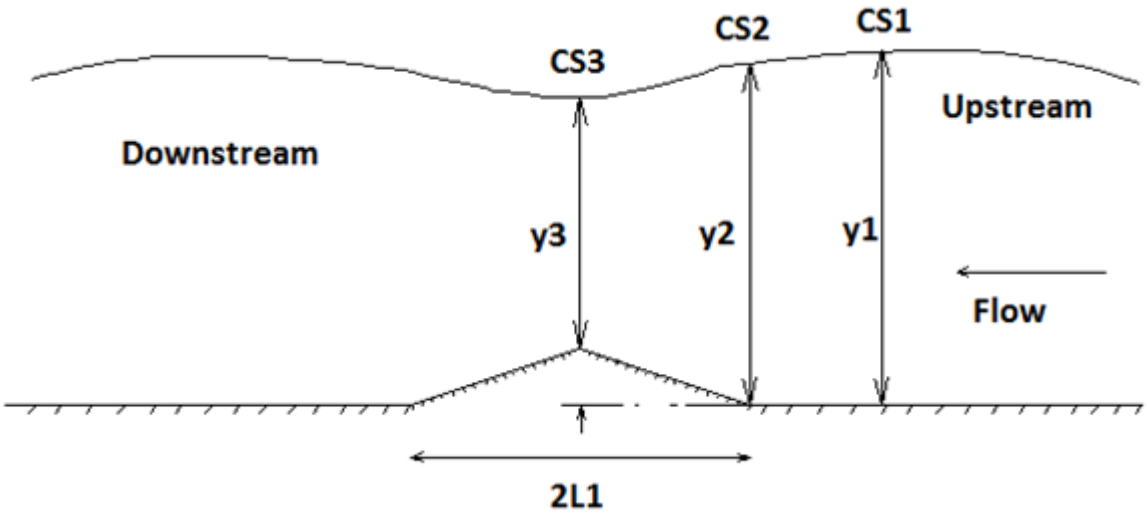

Figure 4.3 Water surface profile for flow over a vertical step (hump) fitted on the bottom of a uniform channel. The depth of flow decreases over the hump on the basis of the energy Principle. From cross section CS 2 to cross section CS 3, the bed level rises and the water pressure decreases; from cross section CS 3 toward downstream, the water pressure increases while the bed level drops.

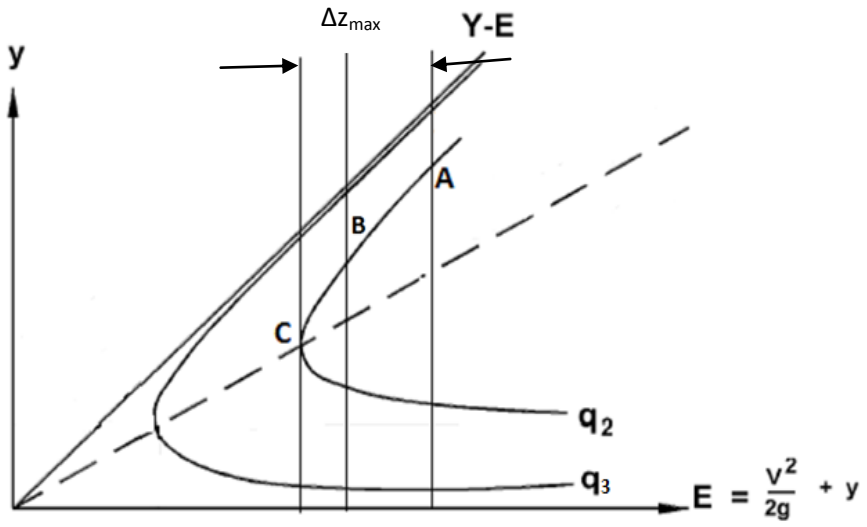

Figure 4.4 Specific energy diagram for a channel expansion.

Point C represents critical flow with the minimum specific energy for the given per- unit -width discharge. Δz_{max} is the maximum permissible difference between the two elevations or the distance between two vertical lines that passes from point A and point C (Figure 4.4) .

We assume a point B on the upper limb of the same E-y curve on which point A is. The distance between the vertical lines that passes through points A and B shows the elevation difference, Δz, being smaller than the maximum permissible value Δz_{max}. Point B represents the flow over the hump and the ordinate of this point shows the depth of flow over the hump. The depth of flow decreases over the hump.

4. 6 Flow in a combination of a horizontal expansion and a vertical step

A vertical step (Figure 4.3) causes the depth of the flow to decrease, whereas an expansion (Figure 4.1) causes the depth of flow to increase. The effects of a hump and expansion have been discussed separately. Now, we consider the effects of an expansion fitted with a hump.

The expanding width and rising bottom (hump) work against each other. A channel expansion causes the flow to decelerate and the depth of flow to increase, whereas a hump causes the flow to accelerate and the depth of flow to decrease. With a combination of two geometric factors, at high Froude numbers, the former is more influential, whereas at low Froude numbers, the latter has dominant effects.

4.7 Limitations on the use of the energy principle

There is a limitation on the use of the energy principle in short channel expansions. First of all, the assumption of zero energy head losses along the length of expansions is questionable. There

are energy losses not only due to friction on the sidewalls and at the channel bottom, but also due to eddy motions associated with flow separation.

Second, the depth of flow as well as flow velocity are never uniform across the section immediately following the expanding section, although, after reaching a certain point at some distance downstream, uniform flow conditions can be established again. The second limitation is less problematic if one is interested mainly in the cross-sectionally averaged flow velocity and the depth of flow. However, it is necessary to pay a great attention to this limitation when one deals with flow in boundary layers very close to the sidewalls and the bottom.

Chapter Five Results

In this chapter we present and compare results for flat bottom channels and channels with a hump. Different flow quantities including the velocity field, vorticity contours at different depths, and u-velocity contours at different cross-sections in the expansion length are compared. We consider channel expansions with different angles of divergence, different Froude numbers, and different hump crest heights. Table 5.1 shows the geometric properties of all channel expansions. We examine regions of flow and eddy motions in flat bottom channels, and the effect of humps on reducing the separation region and on the velocity field in the expansion and further down. We further examine the effects of the Froude number varying between 0.3 and 0.7. In all cases, subcritical flows, i.e. flows with Froude numbers less than unity are considered.

5.1 The model channel

The most important section of the channel is the expansion, without or with bottom variation (hump). The specifications of the expansion for different runs and the specifications of the hump fitted in the expansion are listed in Table 5.1. The expanding width and rising bottom (the hump) work against each other. The expanding width causes the flow to decelerate and the depth of flow to increase; whereas the rising bottom causes the flow to accelerate and the depth of flow to decrease. At low Froude numbers, the rising bottom is dominant; whereas at high Froude numbers the expanding width is dominant parameter. Therefore, we expect that humps will be more effective for flows with lower Froude numbers.

Table5.1 Geometric properties of channel expansions used in 13 model runs, for which the Froude number is equal to 0.5.These parameters, include upstream channel width (B1), downstream channel width (B2), upstream channel length (L1), expansion length (L2), downstream channel length (L3), expansion angle (α), downstream extension length (L4), hump crest height (H), and mesh resolution(Δx).

Run	B1 (m)	B2 (m)	L1 (m)	L2 (m)	L3 (m)	α (˚)	L4 (m)	H (m)	Δx (m)
FB1	0.172	0.290	0.300	0.3233	0.300	10.34	0	0	0.010
FB2	0.172	0.290	0.300	0.3233	0.300	10.34	0	0	0.007
FB8	0.172	0.290	0.300	0.3233	0.300	10.34	0	0	0.005
FB3	0.172	0.290	0.300	0.3233	0.300	10.34	0	0	0.004
FB4	0.172	0.290	0.300	0.3233	0.300	10.34	0.150	0	0.004
FB5	0.1996	0.2852	0.300	0.3233	0.300	7.54	0.150	0	0.004
FB6	0.2282	0.2852	0.300	0.3233	0.300	5.04	0.150	0	0.004
HQ1	0.172	0.290	0.300	0.3233	0.300	10.34	0.150	0.00635	0.004
HH1	0.172	0.290	0.300	0.3233	0.300	10.34	0.150	0.0127	0.004
HQ2	0.1996	0.2852	0.300	0.3233	0.300	7.54	0.150	0.00635	0.004
HH2	0.1996	0.2852	0.300	0.3233	0.300	7.54	0.150	0.0127	0.004
HQ3	0.2282	0.2852	0.300	0.3233	0.300	5.04	0.150	0.00635	0.004
HH3	0.2282	0.2852	0.300	0.3233	0.300	5.04	0.150	0.0127	0.004

Mehta (1979) reported that in pipe flow experiments, flows in a two-dimensional sudden expansion are asymmetric and unstable, with three-dimensional character, when the expansion ratio is larger than 1.25. In this study, the ratios for different angles are shown in Table 5.2. The expansion with $\alpha = 10.34°$ is considered as a gradual expansion because it satisfies the condition

$0.5(B_3 - B_1)/L_2 < 0.25$ (see Chapter 4, Figure 4.1). Nevertheless, since for the angle of divergence of $10.34°$, we have $B_3 / B_1 = 1.68 > 1.5$, the expansion is expected to be more influential to flow energy losses than the condition (the Froude number) of the upstream flow, as is the case for an abrupt expansion. However, for smaller angles of divergence, i.e. $\alpha = 7.54°$ and $\alpha = 5.04°$, the gradual expansion condition as expressed above is satisfied and therefore these expansions are considered as gradual expansions.

Table 5.2 The width ratio for different divergence angles.

α (°)	Width ratio ($\frac{B_3}{B_1}$)
10.34°	1.68
7.54°	1.42
5.04°	1.25

In order to make comparisons between channel expansions without and with a hump, simulations were carried out for channel expansions with a flat bottom and for expansions fitted with humps with a crest height of 1/4" (or 0.00635 m, with $\Delta z / y = 2.54\%$, where $\Delta z / y$ is the ratio of the crest height of hump to the height of water at the entrance of the channel) and 1/2" (or 0.0127 m, with $\Delta z / y = 5.08\%$). An upstream flow depth of 0.250 m is considered for all the runs listed in Table 5.1.

The channel expansion of 0.3233 m in length is short, relative to its width (ranging from 0.2852 to 0.290 m) at the downstream end. For short expansions frictional losses of energy head are not significant, compared to those caused by potential flow separation. According to laboratory experiments (Najafi-Nejad-Nasser, 2011), a 10% energy loss is assumed. Based on this assumed energy loss, elevations at the downstream end of the expansion are found and listed in Table 5.3 for the Froude number of 0.5. Table 5.3 also contains other parameters and boundary specifications of the simulated channels.

The flow simulations consider two fluids: air (at 25º C) and water (with density of 997 kg/m^3). The air interacts with water at the free surface where proper boundary conditions are given in terms of pressure and volume fraction. The volume fraction of air is 1 above the free surface and 0 below, whereas the volume fraction of water is 0 above the free surface and 1 below. At the free surface, the pressure is equal to the atmospheric pressure. Below the free surface, hydrostatic pressure is assumed.

The solution procedures in all the model runs allow a minimum of 100 iterations and a maximum of 200 iterations, with a convergence criterion set to10^{-5}.

We study two types of hump, with a crest height of 1/4” (or 0.00635 m, with $\Delta z / y = 2.54\%$), and 1/2" (or 0.0127 m, with $\Delta z / y = 5.08\%$), respectively, for different angles of divergence. Figure 3.1 shows the position of the hump fitted on the channel bottom. The design of the hump is as follows:

The hump begins from the entrance to the expansion. The bottom of the channel expansion has a slope of slightly less than 2% and 4% for 1/4" (or 0.00635 m, with $\Delta z / y = 2.54\%$), and 1/2" (or 0.0127 m, with $\Delta z / y = 5.08\%$) humps, respectively, which is steep

Table 5.3 Parameters and boundary specifications for nine model runs with the Froude number of 0.5. Solid walls are taken as non-slippery. Turbulence model used is k-ω.

Parameter	FB4	HQ1	HH1	FB5	HQ2	HH2	FB6	HQ3	HH3
Upstream flow depth (m)	0.250	0.250	0.250	0.250	0.250	0.250	0.250	0.250	0.250
Downstream flow depth (m)	0.270	0.270	0.270	0.265	0.265	0.265	0.260	0.260	0.260
Water density (kg/m3)	997	997	997	997	997	997	997	997	997
Normal flow speed at inlet (m/s)	0.78	0.78	0.78	0.78	0.78	0.78	0.78	0.78	0.78
Turbulence fractional intensity at inlet	0.05	0.05	0.05	0.05	0.05	0.05	0.05	0.05	0.05
Eddy length scale at inlet (m)	0.25	0.25	0.25	0.25	0.25	0.25	0.25	0.25	0.25
Physical timescale (s)	0.01	0.01	0.01	0.01	0.01	0.01	0.01	0.01	0.01

compared to typical slopes in natural river channels. The channel bottom is raised linearly, reaching its crest height at the exit of the expansion, and then drops linearly with a favourable slope equal to 2% and 4%, down to the bottom level at the downstream end of the model channel. Variations in the channel bottom are almost symmetric above the downstream end of the channel expansion.

The effects of a longitudinal slope are not important in this study, where the expansions considered are short. Long expansions are expensive to build, although they have smaller angles of divergence and are less likely to trigger flow separation. In short expansions, flow mainly changes in response to changes in channel width at different cross-sections and therefore varying channel width is a more influential parameter than the longitudinal slope. Therefore, we focus on the effects of different angles of divergence.

It is possible to scale up the model expansions discussed in this thesis, because scaling up will not change the angle of divergence, which is the most influential factor. The other influential factor is the dimensionless Froude number. It is possible to keep the same Froude numbers when scaling up.

5.2 Considerations of mesh resolution and downstream channel extension

To ensure that model results are independent of meshes used, water surface profiles for model runs FB1, FB2, FB8 and FB3, where mesh sizes are about 10, 7, 5and 4 mm, respectively, were compared. It was observed that water surface profiles for FB8 and FB3 are close to each other, meaning that a mesh resolution of 5 or 4 mm is sufficiently accurate. To have the best accuracy, 4mm mesh is used for the rest of model runs.

Also we compared the water surface profiles for FB3 and FB4, where FB4 has an extra downstream section of 0.150 m long (see Table 5.1). The water surface profiles were close to each other. However, changes to flow field (including flow depth and flow velocity) in the extended channel may persist over a long distance downstream of the expansion, even though the expansion itself is short. Therefore, for more realistic flow simulations, the model channel with a longer downstream length, i.e. FB4, is used for the rest of simulations.

In summary, the 4 mm mesh resolution and the model channel with the extended downstream length, i.e., extended by 0.150 m, is used for simulations.

5.3 Velocity field and flow separation for $\alpha = 10.34°$ and $F_r = 0.5$

In this section we examine the results of velocity for the channel expansion with $\alpha = 10.34°$ (profiles for runs FB4, HQ1, and HH1 in Table 5.1). Figures 5.1a and 5.1b show the velocity

field for FB4 (flat-bottom channel). The velocity field is plotted in the xy-plane, at an elevation of 0.230 m above the channel bed. We observe non-uniform water velocities, starting from the entrance to the expansion and continuing until about one-third of the expansion. The velocities decrease in the longitudinal direction as a result of the widening of the channel. The average velocity is 0.804 m/s before the entrance to the expansion and 0.496 m/s in the expansion. The minimum velocity is 0.203 m/s before the entrance to the expansion and 0.005 m/s in the expansion. These small velocities are an indicator of the formation of turbulent eddies.

Regions of eddies (Figures 5.1a and 5.1b) are displayed as the dark blue areas next to the right (to an observer facing downstream) sidewall as well as next to the left sidewall of the expansion. These turbulent eddies result from flow separation from the diverging sidewalls and cause energy losses. In a given xy-plane (i.e. a given elevation above the channel bed), the region of eddy motions is assumed as the flow area where velocities are below 20% of the average velocity for the upstream channel section. This velocity range is consistent with the eddy regions (dark blue area) as shown in Figures 5.1a and 5.1b. For Run FB4, the average velocity is 0.804 m/s, and the corresponding threshold velocity for eddy motion delineation is 0.16 m/s. According to this criterion, eddies in the expansion occupy 10.6 % of the flow area, and eddies occupy 4.5% of the flow area between the downstream end of the expansion and the downstream end of the model channel.

From Figures 5.1a and 5.1b, it is observed that the distribution of eddies is asymmetric. Eddies to the right side are larger than those to the left. The percentages of area, occupied by eddies near the right sidewall (to an observer facing downstream) and near the left sidewall of the channel expansion, are 15.1% and 5.1%, respectively. These values confirm that the eddies are more active near the right sidewall of the channel.

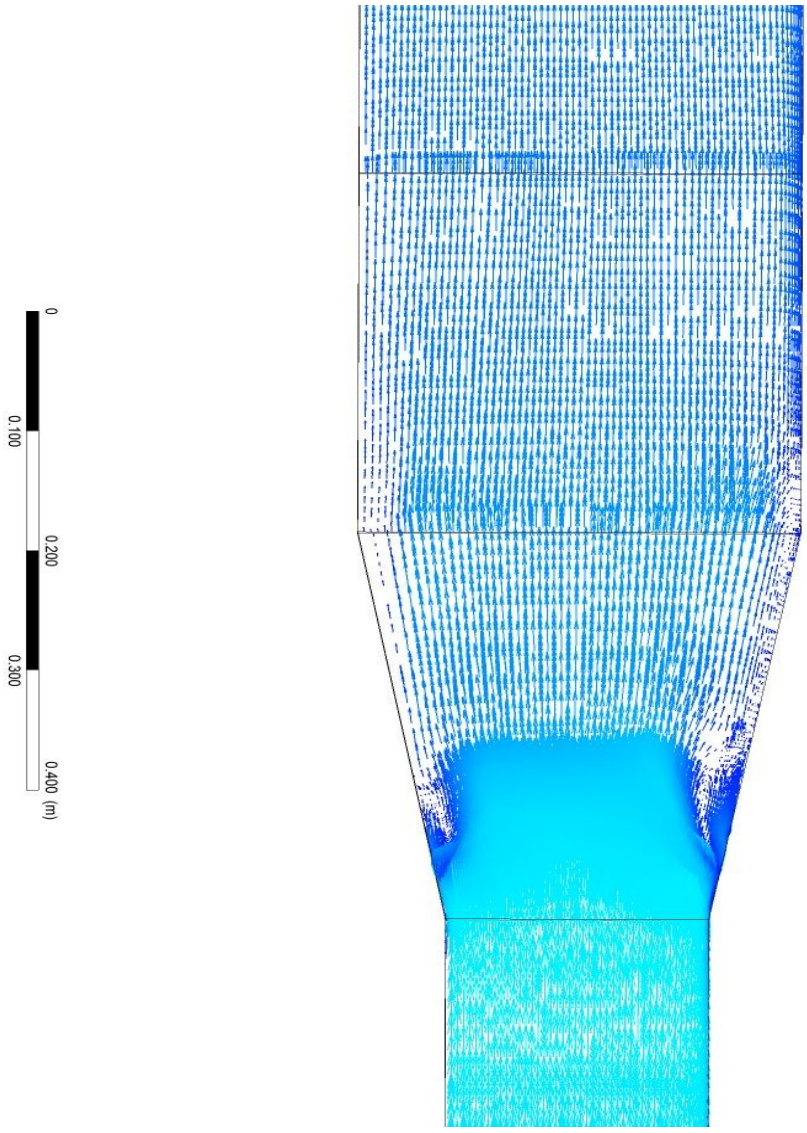

(a)

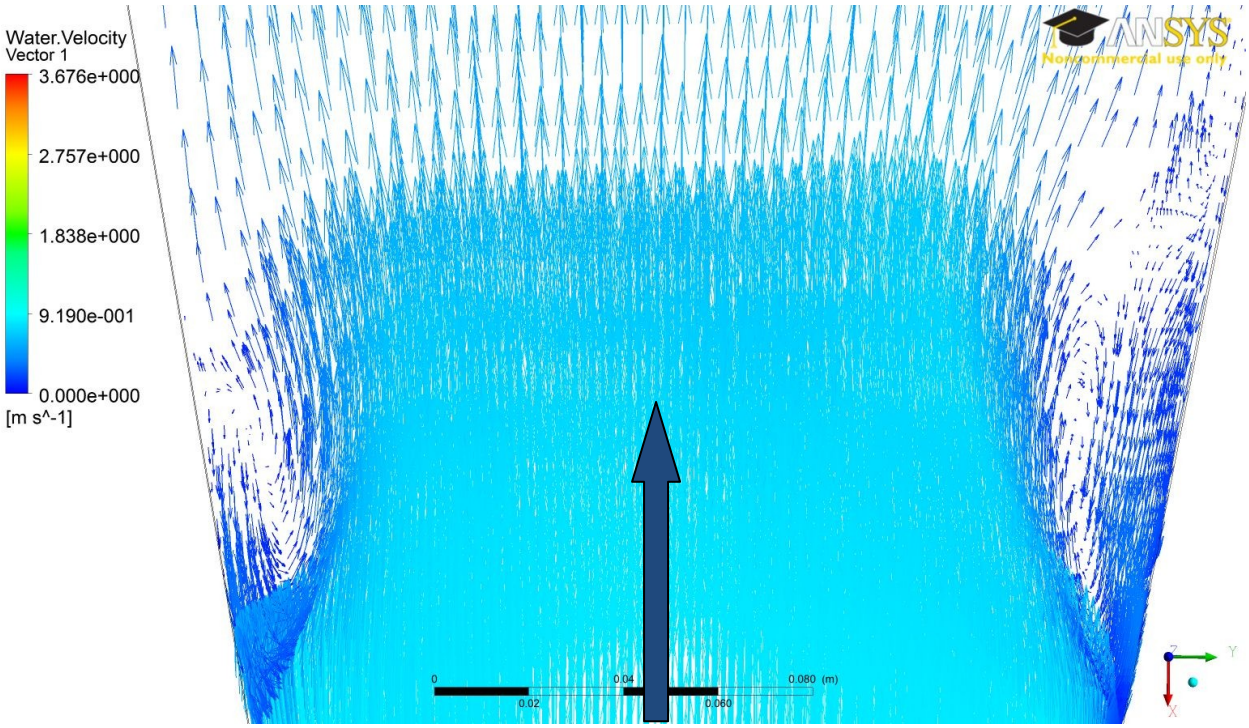

(b)

Figure 5.1 (a) Velocity vectors at an elevation of 0.230 m above the channel bed for Run FB4 for the Froude number of 0.5. The maximum velocity is 0.86 m/s. (b) The close up of velocity vectors in (a). Regions of eddies are observed near both sidewalls.

We found that the region of eddies near the right sidewall begins immediately after the entrance to the expansion and continues up to 4 mm before the exit of the expansion. However, on the left side, the region of eddies begins 0.030 m after the entrance of the expansion and extends up to 4 mm before the exit of the expansion. We observe a difference between the vertical ranges of eddies on the right and left sidewalls. On the right sidewall, eddies are located at a distance of up to 0.0774 m from the channel centerline, whereas on the left sidewall eddies are up to 81.8 mm from the centerline. It means that eddies to the left are closer to the wall or the region of eddies is narrower to the left. The presence of eddies to the right and the left and the

asymmetric behaviour are shown in Figure 5.2, where the flow separation (eddies) from both sidewalls are clearly illustrated by velocity streamlines.

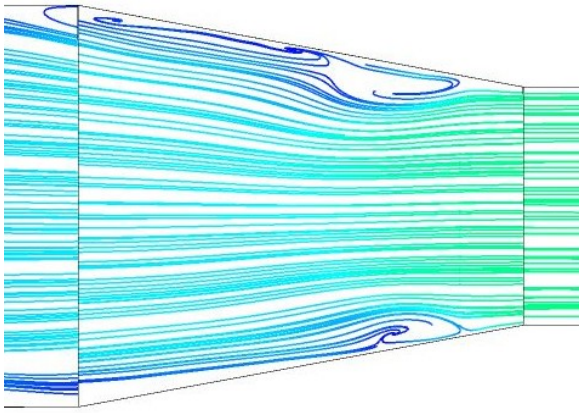

Figure 5.2 Flow streamlines at an elevation of 0.230 m above the channel bed in the expansion for Run FB4. The Froude number is 0.5.

At different elevations above the channel bed, the average velocities exhibit similar features. The average velocities decrease after the entrance to the expansion. The minimum velocities after the entrance to the expansion decrease to very small values. The average velocities are listed in Table 5.4, where h represents the elevation above the channel bed, $\overline{V_b}$ and $\overline{V}_a$ represent the average velocities before and after the entrance to the expansion, respectively. The minimum velocities before and after the entrance to the expansion are also listed in Table 5.5 ($V_{\min,b}$ represents the minimum velocity before the entrance to the expansion and $V_{\min,a}$ represents the minimum velocity after the entrance to the expansion). In all the cases, $V_{\min,a}$ is close to zero, which confirms the presence of eddies at all elevations down to 0.050 m above the channel bed.

The area occupied by eddies (E_{ex} in Table 5.6) in the expansion almost monotonically decreases with decreasing elevation (i.e. toward the channel bed). The area occupied by eddies between the downstream end of the expansion and the downstream end of the model channel ($E_{d/s}$ in Table 5.6) decreases at elevations below 0.230 m and will remain almost the same for different elevations.

The asymmetric behaviour of eddies at different elevations is persistent. The area occupied by eddies to the right is present at all elevations, however, its percentage in area at elevations closer to the surface is larger than its percentage at elevations close to the channel bed, as shown as E_r in Table 5.7. The area occupied by eddies to the left diminishes at elevations below 0.230 m, shown as E_l in Table 5.7. Eddies are more asymmetric close to the channel bed.

Table 5.4 Average velocities at different elevations above the channel bed, before and after the entrance to the expansion for Run FB4.

h(m)	0.230	0.200	0.150	0.100	0.050
$\overline{V}_b(m/s)$	0.804	0.806	0.791	0.782	0.780
$\overline{V}_a(m/s)$	0.496	0.555	0.596	0.580	0.565

Table 5.5 Minimum velocities at different elevations above the channel bed, before and after the entrance to the expansion for FB4.

h(m)	0.230	0.200	0.150	0.100	0.050
$V_{\min,b}(m/s)$	0.203	0.564	0.558	0.547	0.544
$V_{\min,a}(m/s)$	0.005	0.007	0.009	0.003	0.003

Table 5.6 Percentage in area of eddies at different elevations above the channel bed, in the expansion and downstream of the expansion for Run FB4.

h(m)	0.230	0.200	0.150	0.100	0.050
E_{ex} (%)	10.6	9.5	3.9	5.6	4.5
$E_{d/s}$ (%)	4.5	1.7	1.9	1.8	1.6

Table 5.7 Percentage in area of eddies near the right and left sidewalls in the expansion for Run FB4.

h(m)	0.230	0.200	0.150	0.100	0.050
E_r (%)	15.1	16.4	6.8	9.9	7.6
E_l (%)	5.1	2.5	0.2	0.2	0.08

Figure 5.3 shows the velocity vectors for Run FB4 at an elevation of 0.200 m above the channel bed. The area occupied by eddies to the left is negligible below 0.230 and the area to the right reduces at elevations below the surface.

5.3.1 The effects of a hump

The effects of a hump on flow velocity and eddies are revealed through Runs HQ1 and HH1. The presence of a hump tends to increase the flow velocity and reduce eddy motions. The simulation conditions with a hump for $\alpha = 10.34°$ are given in Table 5.1, where HQ1 refers to a 1/4″ (or 0.00635 m, with $\Delta z / y = 2.54\%$) hump, and HH1 refers to a 1/2″ (or 0.0127 m, with $\Delta z / y = 5.08\%$) hump At an elevation of *h=0.200 m,* we compare the velocity field and eddy

motion area for Runs FB4, HQ1and HH1.In Table 5.8 the average and minimum velocities before and after the entrance to the expansion for FB4, HQ1, and HH1are listed.

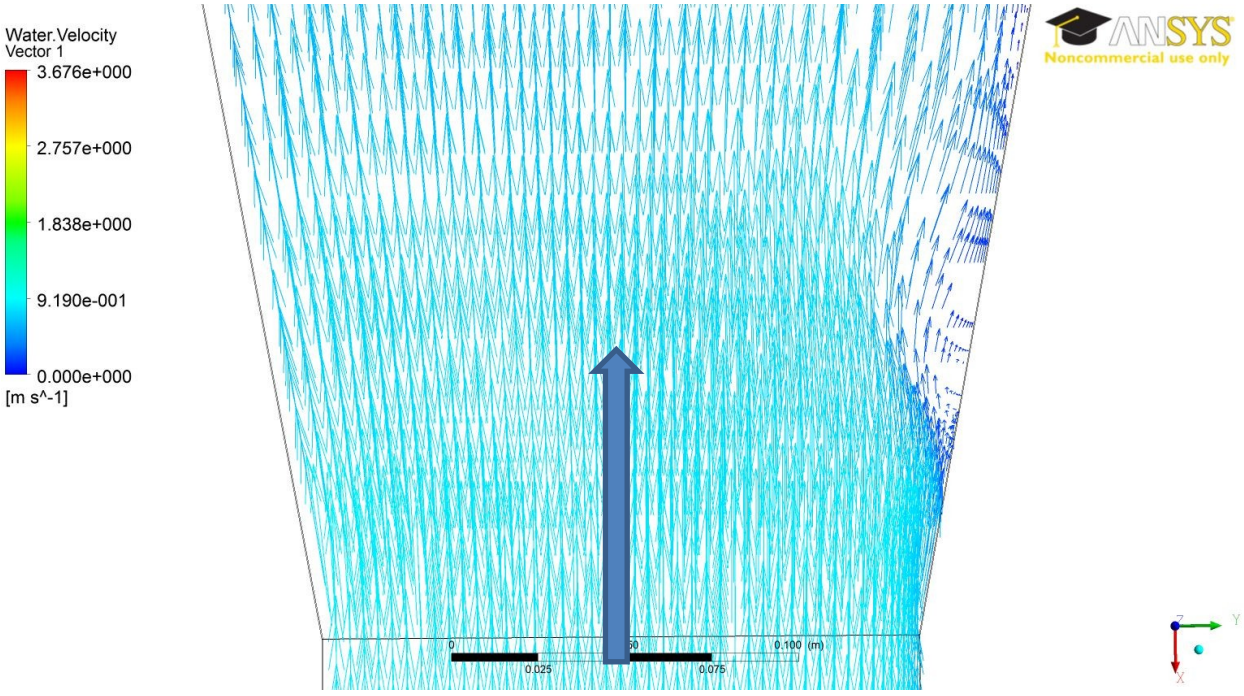

Figure 5.3 Velocity vectors in the expansion at an elevation of 0.200 m above the channel bed for Run FB4. The Froude number is 0.5. The maximum velocity is 0.89m/s.

Table 5.8 Average and minimum velocities before and after the entrance to the expansion for a flat-bottom expansion, and expansions with a hump. The elevation is 0.200 m above channel bed.

Runs	FB4	HQ1	HH1
$\overline{V}_b(m/s)$	0.805	0.772	0.807
$\overline{V}_a(m/s)$	0.555	0.530	0.571
$V_{\min,b}(m/s)$	0.564	0.132	0.390
$V_{\min,a}(m/s)$	0.007	0.001	0.088

It is observed that the use of a 1/4″ (or 0.00635 m, with $\Delta z / y = 2.54\%$) hump, (HQ1), does not have a considerable effect on the average and minimum velocities; however, the use of a1/2″ (or 0.0127 m, with $\Delta z / y = 5.08\%$) hump, (HH1), increases the average and minimum velocities after the entrance to the expansion.

In Table 5.9, we compare the percentage in area of eddies for a flat-bottom channel and channels with a hump at an elevation of 0.200 m above the channel bed. It is observed that the 1/4″ (or 0.00635 m, with $\Delta z / y = 2.54\%$) hump, has reduced the percentage of eddies in the expansion area from 9.5% to 7.8%. The use of the 1/2″ (or 0.0127 m, with $\Delta z / y = 5.08\%$) hump reduces the percentage to a negligible value of 0.5%. Similar trends are observed for percentages to the right sidewall of the channel expansion. The percentage of eddies in the downstream region is small and remains almost the same for channels without and with a hump.

In Figure 5.4 we show the velocity vectors for a flat bottom channel (panel a) and a channel with a 1/2" (or 0.0127 m) hump (panel b), around the exit of the expansion. The region of

Table 5.9 Percentage in area of eddies in the expansion and between the downstream end of the expansion and downstream of the model channel for a flat-bottom expansion, and expansions with a hump. The elevation from channel bed is 0.200 m.

Runs	FB4	HQ1	HH1
E_{ex} (%)	9.5	7.8	0.5
E_r (%)	16.4	12.2	0.5
E_l (%)	2.5	3.4	0.4
$E_{d/s}$ (%)	1.7	2.0	1.8

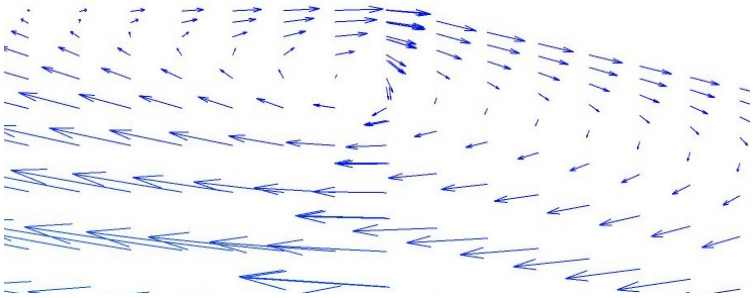

(a)

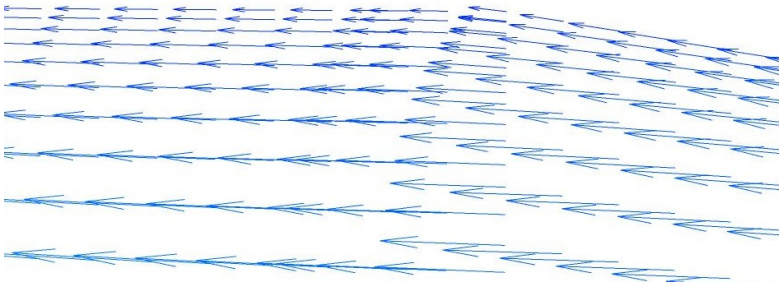

(b)

Figure 5.4 A comparison of velocity vector around the exit of the expansion between a flat bottom channel (a) and a channel with a 1/2" (0.0127 m) hump (b). The elevation is 0.200 m above the channel bed.

eddies (flow separation area) to the right is clearly present for Run FB4, and almost vanishes for Run HH1. Similar behaviours are observed at other elevations above the channel bed.

Figure 5.5 shows the velocity streamlines for Runs FB4 and HH1 at an elevation of 0.200 m above the channel bed. The presence of eddies (flow separation) to the right for Run FB4 (panel a) is clearly shown. The effect of the hump on reducing the eddy area is clearly observed in panel (b).

(a)

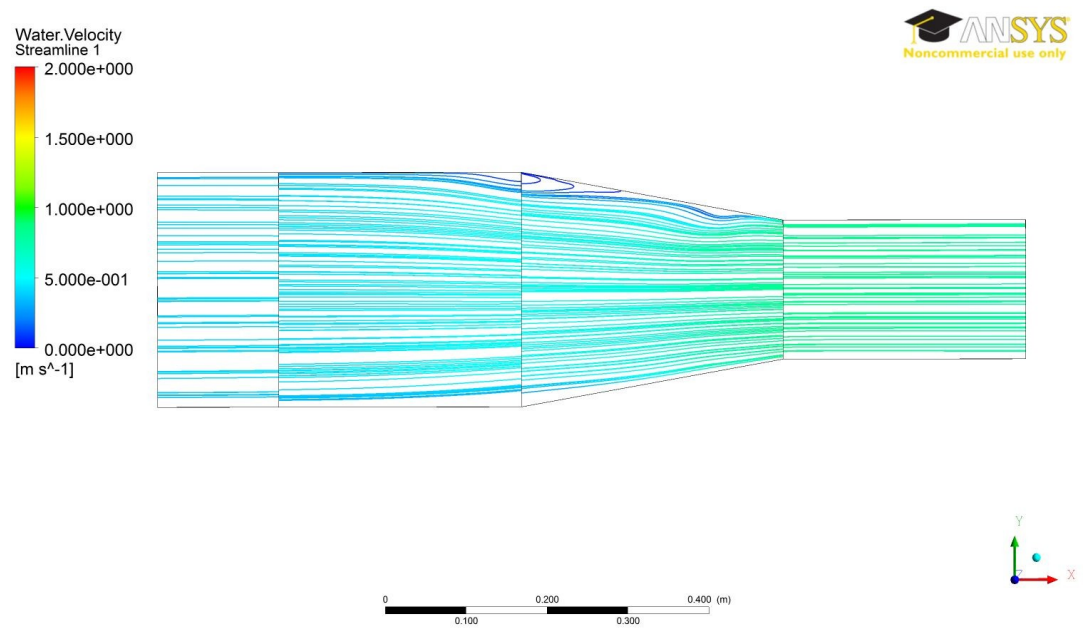

(b)

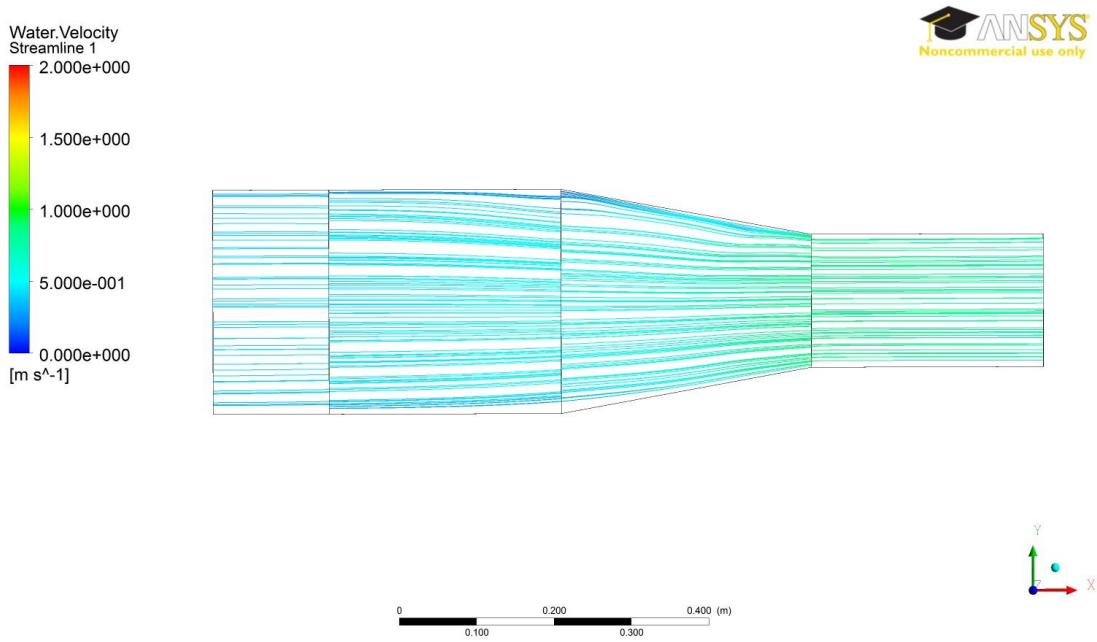

Figure 5.5 Velocity streamlines at an elevation of 0.200 m above the channel bed for Runs FB4 and HH1. The Froude number is 0.5.

5.4 Velocity field and flow separation for $\alpha = 7.54°$ and $F_r = 0.5$

In this section we compare results of the velocity field for expansions with a divergence angle of 7.54º (FB5, HQ2, and HH2 in Table 5.1). Using a smaller angle of divergence (FB5 in table 5.1), we carried out model runs for a flat bottom expansion and expansions with a hump. The angles and other parameters of the different expansions are given in Table 5.1. For $\alpha = 7.54°$, FB5 is for a flat bottom expansion and HQ2 and HH2 are for expansions with 1/4" (or 0.00635 m), and 1/2"(or 0.0127 m), respectively.

The results of Run FB5 show the same features as for Run FB4. However, due to the use of a smaller angle of divergence, eddies are reduced and the velocity vectors are more uniform, i.e. the difference between the average velocity before and after the entrance to the expansion decreases. Tables 5.10 and 5.11 show the average and minimum velocities for Run FB5. In Table 5.11, the minimum velocities after the entrance to the expansion are close to zero, which confirms the presence of eddies. To show the effects of the angle of divergence on velocity drop after the entrance to the expansion, we compare the velocity drops for Runs FB4 and FB5. The velocity drop is defined as the absolute value of the difference between the average velocities before and after the entrance to the expansion.

Table 5.10 Average velocities at different elevations above the channel bed, before and after the entrance to the expansion for Run FB5.

Elevation(m)	0.230	0.200	0.150	0.100	0.050
$\overline{V}_b(m/s)$	0.765	0.763	0.759	0.759	0.754
$\overline{V}_a(m/s)$	0.512	0.592	0.602	0.613	0.608

Table 5.11 Minimum velocities at different elevations above the channel bed, before and after the entrance to the expansion for Run FB5.

Elevation(m)	0.230	0.200	0.150	0.100	0.050
$V_{\min,b}(m/s)$	0.121	0.152	0.155	0.148	0.144
$V_{\min,a}(m/s)$	0.009	0.004	0.002	0.007	0.005

Table 5.12 shows the velocity drops for Runs FB4 and FB5 at different elevations above the channel bed. Smaller velocity drops are observed for Run FB5 which indicates more uniformity for water velocity before and after the entrance to the expansion.

Table 5.12 A comparison of velocity drops between Runs FB4 and FB5.

Elevation(m)	0.230	0.200	0.150	0.100	0.050
Velocity drop for FB4 (m/s)	0.308	0.250	0.195	0.202	0.216
Velocity drop for FB5 (m/s)	0.253	0.171	0.157	0.146	0.146

Table 5.13 shows the area occupied by eddies in the expansion region and the area occupied by eddies downstream of the expansion (i.e. between the exit of the expansion and the downstream end of the model channel). The area occupied by eddies increases with increasing elevation. As given in Table 5.13 and Table 5.6, the results for FB4 show that the area of eddy motions reduces for smaller angles of divergence. The region of eddies in downstream is similar between Runs FB4 and FB5. The results for Run FB5show less flow separation and hence less energy losses, however, the drawback of using small angles of divergence is the increase in length of the expansion, which is not an economic solution.

Table 5.14 shows the area of eddy motions to the right and the left, respectively. The asymmetric behaviour of eddy motions is clear; no eddy motions are observed to the left sidewall, whereas eddy motions are present to the right.

Table 5.13 Percentage in area of eddies at different elevations above the channel bed, in the expansion and downstream for Run FB5.

Elevation(m)	0.230	0.200	0.150	0.100	0.050
E_{ex} (%)	8.2	3.3	3.7	1.9	1.0
$E_{d/s}$ (%)	3.5	2.2	1.9	2.2	1.6

Table 5.14 Percentage in area of eddies near the right and left sidewalls in the expansion for Run FB5.

Elevation(m)	0.230	0.200	0.150	0.100	0.050
E_r (%)	16.5	6.6	7.4	3.6	2.0
E_l (%)	0.0	0.0	0.0	0.0	0.0

5.4.1 The effects of a hump

The effects of a hump on velocity vectors and eddies are evaluated through Runs HQ2 and HH2 at an elevation of 0.230 m above the channel bed. The average and minimum velocities before and after the entrance to the expansion are listed in Table 5.15. The use of a 1/4″(or 0.00635 m, with $\Delta z / y = 2.54\%$)hump,(HQ2), does not have a considerable effect on the average and minimum velocities, however, the use of a1/2″(or 0.0127 m, with $\Delta z / y = 5.08\%$) hump, (HH2), increases the average and minimum velocities after the entrance to the expansion. The minimum

velocity before the entrance to the expansion is considerably increased in Run HH2. This is a decrease in the eddy motions right before the entrance to the expansion.

In Table 5.16 the percentage in area of eddies for a flat-bottom channel and channels with a hump are compared .The elevation is 0.230 m above the channel bed. The 1/4″ (or 0.00635 m, with $\Delta z / y = 2.54\%$) hump, has reduced the percentage in area of eddies in the expansion from 8.2% to 4.3%. The 1/2″ (or 0.0127 m, with $\Delta z / y = 5.08\%$) hump reduces the percentage to a considerably smaller value of 1.4%. Similar trends are observed for percentages to the right of the channel expansion. Note that due to the use of a smaller angle of divergence, the expansion is more gradual. Thus, the asymmetric behaviour of eddies is more clear, where in Table 5.16 it is observed that the eddy percentage to the left is zero, even for a flat bottom expansion.

The eddy motions are persistent over a long distance downstream of the expansion. Therefore, the eddies are observed even after the expansion (the last row of Table 5.16). The percentage in area of eddies in the downstream region is small for expansions without and with a hump, however, the percentage in area occupied by eddies decreases when a hump is used.

Table 5.15 Average and minimum velocities before and after the entrance to the expansion for a flat-bottom channel (FB5) and channels with a hump. The elevation above the channel bed is 0.230 m.

Runs	FB5	HQ2	HH2
$\overline{V}_b(m/s)$	0.765	0.766	0.793
$\overline{V}_a(m/s)$	0.512	0.571	0.582
$V_{\min,b}(m/s)$	0.121	0.118	0.236
$V_{\min,a}(m/s)$	0.009	0.008	0.033

Table 5.16 Percentage in area of eddies in the expansion and between the downstream end of the expansion and downstream end of the model channel for flat-bottom channel (FB5) and channels with a hump. The elevation above the channel bed is 0.230 m.

Runs	FB5	HQ2	HH2
E_{ex} (%)	8.2	4.3	1.4
E_r (%)	16.5	8.8	2.6
E_l (%)	0.0	0.0	0.0
$E_{d/s}$ (%)	3.5	2.0	1.4

5.5 Velocity field and flow separation for $\alpha = 5.04°$ and $F_r = 0.5$

In this section we compare the results of the velocity field for expansions with a divergence angle of 5.04 º for Runs FB6, HQ3, and HH3 (See Table 5.1). For $\alpha = 5.04°$, the results for a flat-bottom expansion (FB6) and expansions with a hump (HQ3, and HH3) are similar to the results for previous Runs with larger angles. Due to the use of a small angle of divergence, compared to Runs FB4 and FB5, the percentage in area of eddies considerably drop in case of FB6. Tables 5.17 and 5.18 compare the velocity field and flow separation for Runs FB6, HQ3, and HH3.The elevation is 0.200 m above the channel bed. The results for all the expansions confirm that a hump, especially a 1/2″ (or 0.0127 m, with $\Delta z / y = 5.08\%$) hump have significant effects on reducing eddy motions and hence eddy areas and on increasing flow velocities after the entrance to the expansion. Although the area percentages are small even for the case of FB6, the use of a hump (especially a 1/2″ hump) will reduce these percentages to a negligible level.

Table 5.17 Average and minimum velocities before and after the entrance to the expansion for a flat-bottom expansion (FB6), and expansions with a hump (HQ3 and HH3). The elevation above the channel bed is 0.200 m.

Runs	FB6	HQ3	HH3
$\overline{V}_b(m/s)$	0.772	0.769	0.774
$\overline{V}_a(m/s)$	0.585	0.594	0.602
$V_{\min,b}(m/s)$	0.179	0.183	0.324
$V_{\min,a}(m/s)$	0.063	0.090	0.120

Table5.18 Percentage in area of eddies in the expansion and between the downstream end of the expansion and downstream of the model channel for a flat-bottom expansion (FB6), and expansions with a hump (HQ3and HH3). The elevation above the channel bed is 0.200 m.

Runs	FB6	HQ3	HH3
$E_{ex}(\%)$	1.1	0.7	0.2
$E_r(\%)$	2.0	1.4	0.4
$E_l(\%)$	0.0	0.0	0.0
$E_{d/s}(\%)$	0.1	0.7	0.3

5.6 Velocity field at different Froude numbers

The effects of an expansion on creating eddies and the effects of a hump on reducing eddy motions are the most profound for a large angle of divergence ($\alpha = 10.34°$), we use this angle in

Runs FB4, HQ1, and HH1 in order to study the effects of different Froude numbers. The purpose is to show how the percentage in area of eddies changes with the Froude number. We consider different humps at different Froude numbers, i.e. to what extent the humps will reduce the percentage in area of eddies.

For Runs FB4, HQ1and HH1 (Table 5.1), the Froude number ranges from Fr = 0.3 to 0.7. In addition to varying the Froude number, the downstream elevation of water above the channel bed has changed to 0.257 m for the Froude number $F_r = 0.3$ and 0.291 m for $F_r = 0.7$.

At the inlet, velocity is 0.47 m/s for Froude number $F_r = 0.3$, and 1.1 m/s in corresponded to the Froude number $F_r = 0.7$. At smaller inlet velocities, smaller regions of separating waves and eddies are expected. Therefore, we expect to observe less eddies at smaller Froude numbers. Tables 5.19 shows the percentage in area of eddies for a flat bottom channel (FB4) at the Froude number $F_r = 0.3$. A Comparison of the results given in Table 5.19 with the results in Table 5.6 (for FB4 at the Froude number $F_r = 0.5$) shows a considerable reduction in eddy motions in the expansion.

Table 5.19 Percentage in area of eddies at different elevations above the channel bed, in the expansion and downstream for Run FB4 at the Froude number $F_r = 0.3$.

Elevation(m)	0.230	0.200	0.150	0.100	0.050
E_{ex} (%)	3.8	4.9	4.0	5.4	3.0
$E_{d/s}$ (%)	3.3	2.5	2.7	2.6	5.0

The effects of a hump on decreasing the eddy area are summarised in Table 5.20. The use of a 1/4″ (or 0.00635 m, with $\Delta z / y = 2.54\%$) hump helps reduce the eddy motion area in the

expansion. The use of a 1/2″ (or 0.0127 m, with $\Delta z / y = 5.08\%$) hump has a considerably better effect, where the area of eddies in the expansion has reduced to a negligible value of 1.2%.

Figure 5.6 shows that, for large Froude numbers (i.e. $F_r = 0.7$), the eddies appear in almost all the regions of the expansion, beginning from the area before the entrance to the expansion. The percentage in area of eddies is larger at elevations closer to the water surface (Table 5.21). Therefore, the flow is more turbulent closer to the surface, with larger areas of eddies. A comparison among Table 5.21 with Tables 5.19 and 5.6, indicates that the area of eddies inside the expansion considerably increases at the Froude number $F_r = 0.7$.

Table 5.22 compares effect of 1/4" (or 0.00635 m), and 1/2" (or 0.0127 m) humps on the eddy motion areas for Froude number of 0.7, at elevation of 0.200 m above the channel bed. As observed, HQ1 does not have a constructive effect; however, the 1/2" (or 0.0127 m) hump, i.e. HH1, considerably reduces the area of eddy motions and completely vanishes this area in the left sidewall.

Table 5.20 Percentage in area of eddies in the expansion and between the downstream end of the expansion and downstream of the model channel for a flat-bottom expansion, and expansions with a hump. The Froude number is 0.3. The elevation above the channel bed is 0.200 m.

Runs	FB4	HQ1	HH1
E_{ex} (%)	3.8	3.0	1.2
E_r (%)	7.6	5.9	2.4
E_l (%)	0.0	0.0	0.0
$E_{d/s}$ (%)	3.3	2.9	1.7

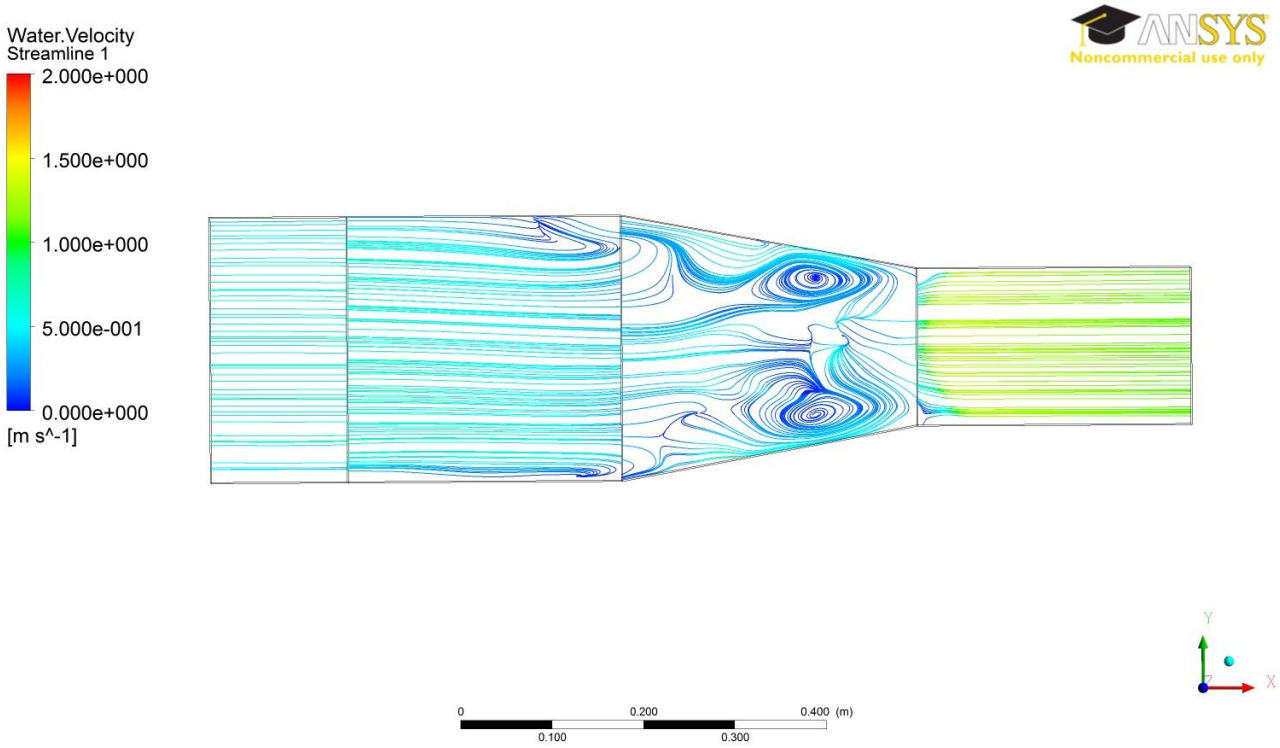

Figure 5.6 Velocity streamlines at an elevation of 0.230 m above the channel bed for Run FB4. The Froude number is 0.7.

Table5.21 Percentage in area of eddies at different elevations above the channel bed, in the expansion and downstream for Run FB4 .The Froude number is 0.7.

Elevation(m)	0.230	0.200	0.150	0.100	0.050
E_{ex}(%)	27.5	20.5	3.1	2.8	5.3
$E_{d/s}$ (%)	7.5	9.3	3.5	5.5	4.5

Table 5.22 Percentage in area of eddies in the expansion and between the downstream end of the expansion and downstream of the model channel for a flat-bottom expansion,

and expansions with a hump. The Froude number is 0.7. The elevation above the channel bed is 0.200 m.

Runs	FB4	HQ1	HH1
E_{ex}(%)	20.5	28.7	6.8
E_r(%)	28.3	32.0	12.6
E_l(%)	13.9	22.3	0.0
$E_{d/s}$ (%)	9.3	3.3	3.7

Figure 5.7 shows the effect of 1/2" (or 0.0127 m, with $\Delta z / y = 5.08\%$) hump in reducing eddies at elevation of 0.200 m above the channel bed. Also by comparing Figure 5.7 with Figure 5.6, it is obvious that the region of eddies becomes smaller at lower elevations.

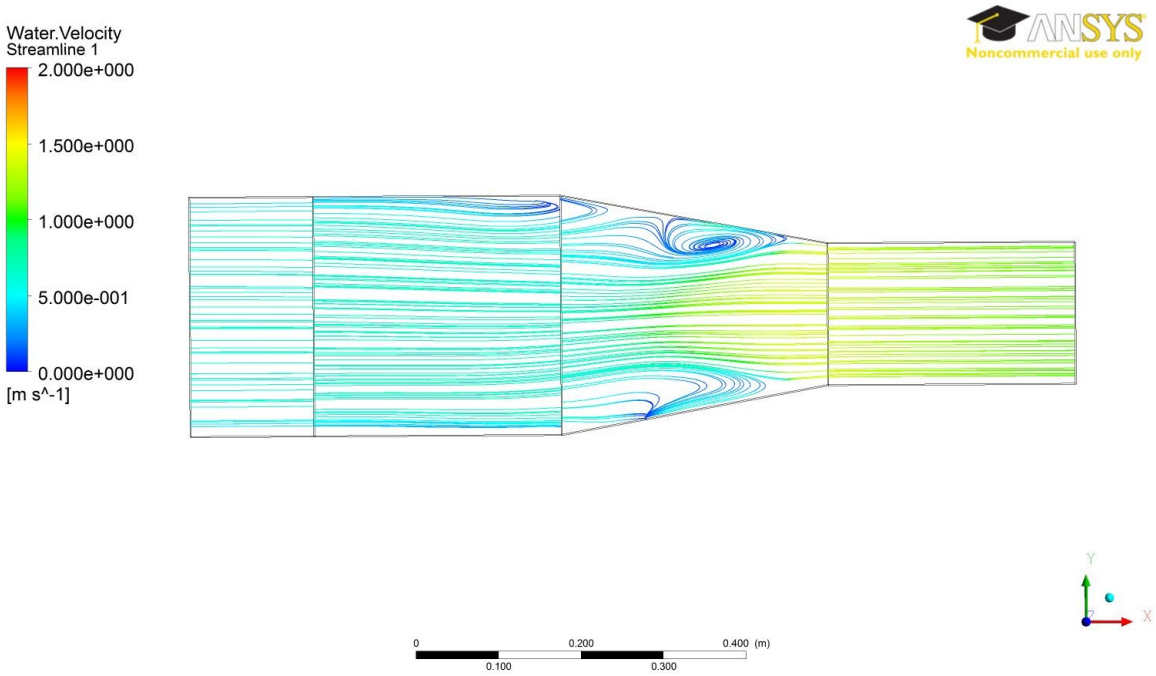

(a)

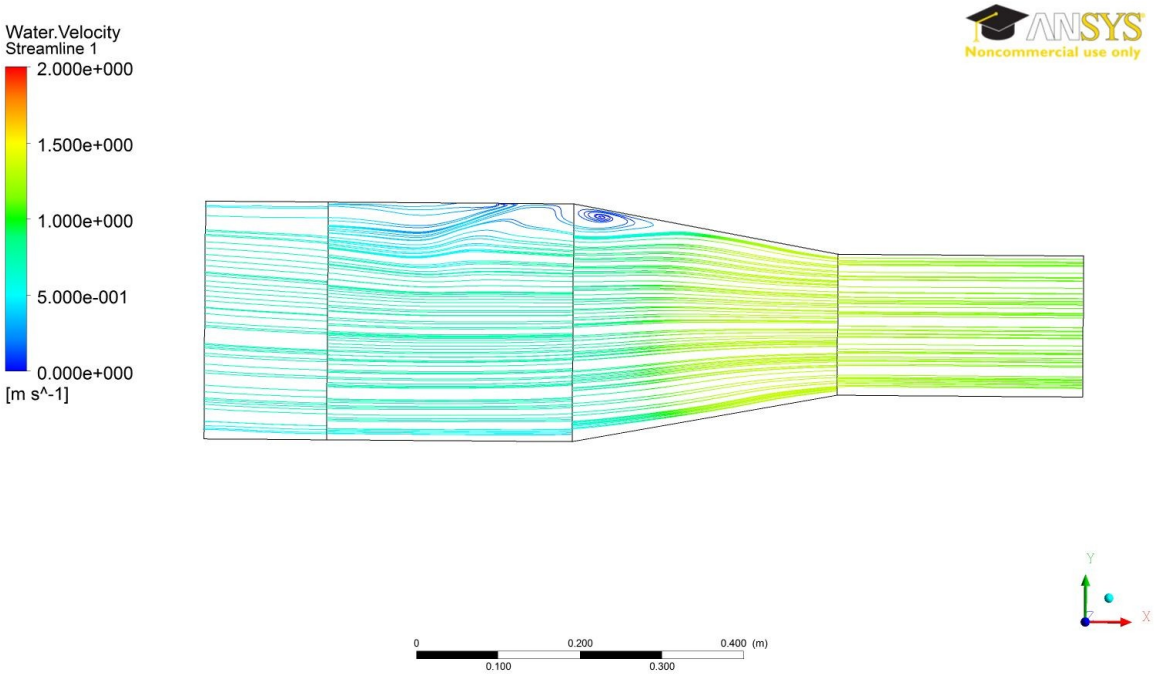

(b)

Figure 5.7 Velocity streamlines at an elevation of 0.200 m above the channel bed for Runs FB4 (panel a) and HH1 (panel b). The Froude number is 0.7.

5.7 Vorticity field

Vorticity is the curl of the fluid velocity. Vorticity can be considered as the circulation per unit area in a fluid flow field. For a two-dimensional flow, the vorticity vector is perpendicular to the two-dimensional plane. The components of vorticity in three-dimensional Cartesian coordinates are

$$\omega_x = \frac{\partial w}{\partial y} - \frac{\partial v}{\partial z} \tag{5.1}$$

$$\omega_y = \frac{\partial u}{\partial z} - \frac{\partial w}{\partial x} \tag{5.2}$$

$$\omega_z = \frac{\partial v}{\partial x} - \frac{\partial u}{\partial y} \tag{5.3}$$

Figure 5.8shows the velocity vectors (panel a) and associated vorticity (panel b) in the expansion. In the area near sidewalls where eddies are present, large vorticity are shown in red colour.

Figure 5.9 shows the vorticity contours for a flat-bottom expansion (FB4), at an elevation of 0.200 m above the channel bed. The red areas next to the sidewalls of the expansion are areas where flow has circulation and flow separation occurs. Therefore, areas with high vorticity (red area) are undesirable from the energy conservation perspective, and thus it is desired to reduce them by using a hump. Figure 5.10 shows the vorticity contours for an expansion with a 1/2"(or 0.0127 m, with $\Delta z / y = 5.08\%$) hump, (HH1), at an elevation of 0.200 m above the channel bed. A comparison between Figures 5.9 and 5.10 indicates that high-vorticity areas have decreased, especially near the exit of the expansion.

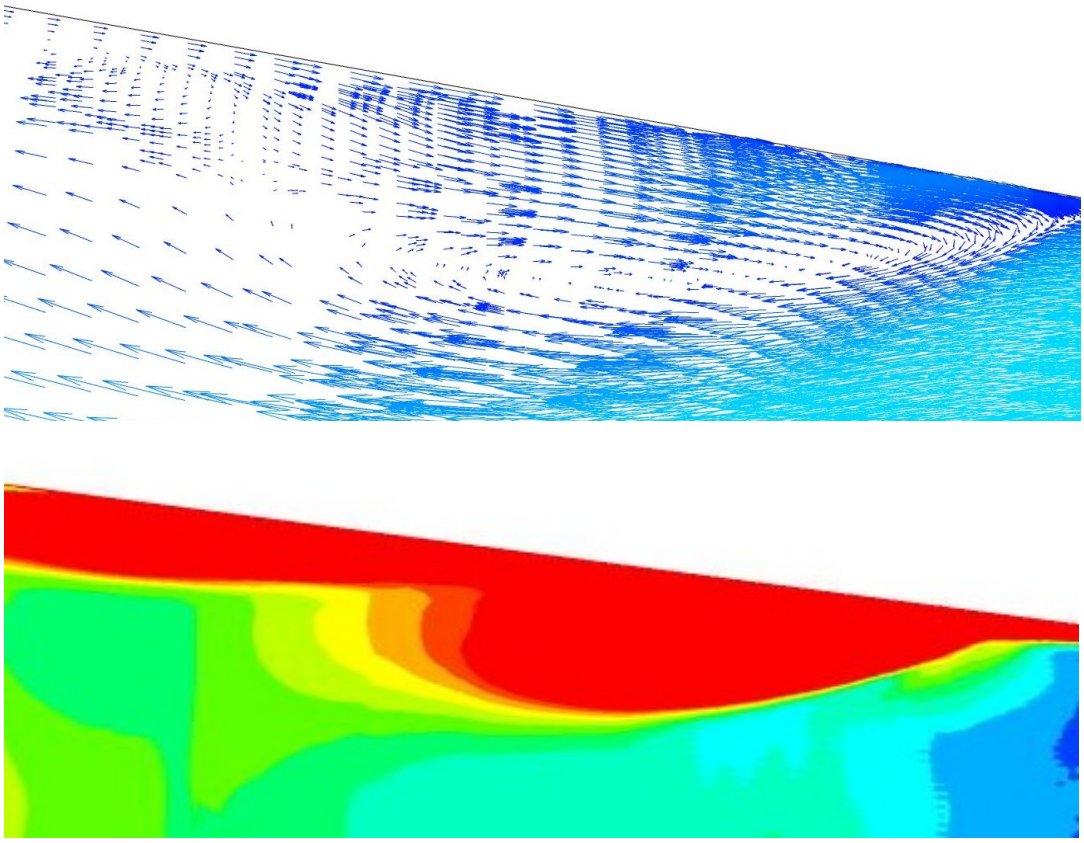

Figure 5.8 Velocity vectors and associated vorticity in the expansion. The area occupied by eddies is shown as high-vorticity region near the sidewall, in red color. The maximum velocity is 0.86 m/s. The results are for Run FB4.

To determine the high-vorticity area quantitatively, we calculate the ratio of area of high- vorticity to the whole area after the entrance to the expansion (i.e. from the entrance to the expansion to the downstream end of the model channel). Based on the color bar in Figure 5.9, we define the high-vorticity area as the area where vorticities are larger than 9.0(s^{-1}).

Table 5.23 shows the percentage in area of high-vorticity region, Vor_{high}, at different elevations above the channel bed (h), for Run FB4. It is observed that the area of high-vorticity area monotonically decreases toward the channel bed.

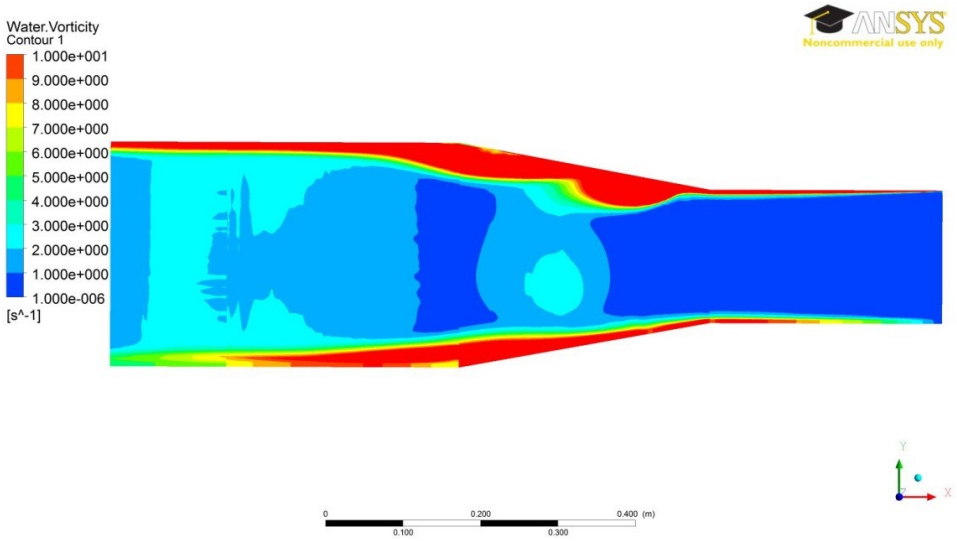

Figure 5.9 Vorticity contours at an elevation of 0.200 m above the channel bed for a flat-bottom expansion, (FB4).

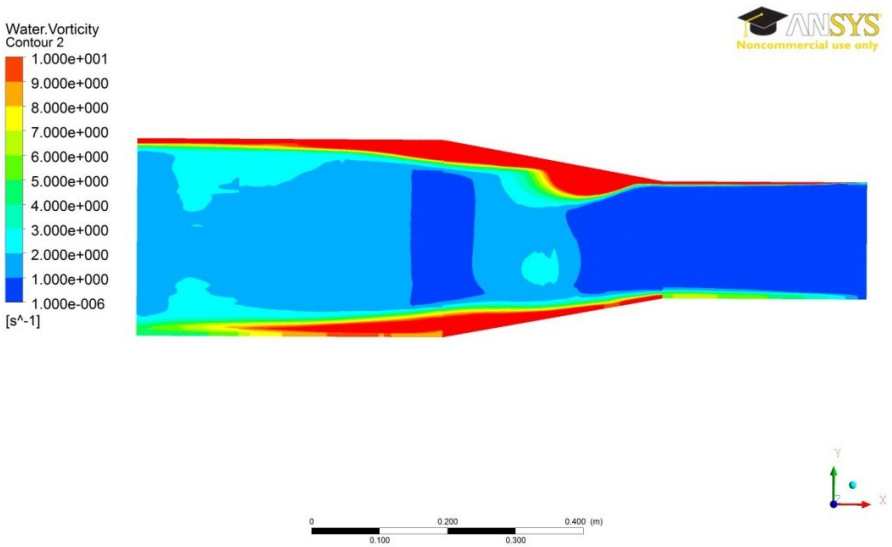

Figure 5.10 Vorticity contours at an elevation of 0.200 m above the channel bed, for the expansion with a 1/2"(or 0.0127 m) hump, (HH1).

Table 5.23 Percentage in area of high vorticity area, at different elevations above the channel bed for Run FB4.

h (m)	0.230	0.200	0.150	0.100	0.050
$Vor_{high}(\%)$	25.7	18.2	16.8	16.6	14.3
$Vor_{right}(\%)$	29.8	26.4	23.8	23.6	21.2
$Vor_{left}(\%)$	21.7	10.2	9.8	9.5	7.4

From Table 5.23 and Figures 5.9 and 5.10, it is clear that high-vorticity areas exist at all elevations to both the right and the left in the expansion; the asymmetric patterns of vorticity appear at all elevations (the high-vorticity region to the left sidewall is smaller).

Tables 5.24 and 5.25 also show the percentage in area of high-vorticity regions for Runs FB5and FB6 (flat-bottom expansions with the angle of divergence $\alpha = 7.54°$ and $5.04°$, respectively). Similar to Run FB4, the high-vorticity regions monotonically reduce toward the bottom. The high-vorticity regions for Runs FB5 and FB6 are smaller, compared to that for Run FB4. This is due to the fact that at smaller angles of divergence, less flow separation and hence lower vorticity are expected.

Table 5.24 Percentage in area of high vorticity at different elevations above the channel bed for Run FB5.

Elevation(m)	0.230	0.200	0.150	0.100	0.050
$Vor_{high}(\%)$	19.5	15.2	15.6	15.0	14.1

Table 5.25 Percentage in area of high vorticity at different elevations above the channel bed for Run FB6.

h (m)	0.230	0.200	0.150	0.100	0.050
$Vor_{high}(\%)$	15.3	14.6	13.5	12.0	11.1

5. 7. 1 Effects of a hump on vorticity

To reveal the effect of a hump on the vorticity field, in Table 5.26, we compare the high-vorticity areas for a flat-bottom expansion (FB), expansion with a 1/4" (or 0.00635 m) hump, (HQ), and expansion with a 1/2" (or 0.0127 m) hump, (HH), at an elevation of 0.200 m above the channel bed. The 1/2"(or 0.0127 m, with $\Delta z / y = 5.08\%$) hump, has a stronger effect on reducing the high-vorticity region. For example, at an angle of divergence of 7.54˚, the 1/4" (or 0.00635 m with $\Delta z / y = 2.54\%$) hump, has reduced the high-vorticity region from 15.8% to 12.8%. The 1/2" (or 0.0127 m, with $\Delta z / y = 5.08\%$) hump, has further reduced the area of this region to 10.5% of the whole area from the entrance to the expansion to the downstream end of the model channel.

Table 5.26 A comparison of percentages in area of high-vorticity between a flat-bottom expansion and expansion with a hump, at different angles of divergence at an elevation of 0.200 m above the channel bed. The Froude number is 0.5.

Angle of divergence α	Percentage in area of vorticity larger than 9.0 s^{-1}		
	Flat-bottom	1/4″ hump	1/2″ hump
10.34˚	18.2% (FB4)	17.2% (HQ1)	14.6% (HH1)
7.54˚	15.2% (FB5)	12.8% (HQ2)	10.5% (HH2)
5.04˚	14.6% (FB6)	11.1% (HQ3)	9.3% (HH3)

5.7.2 Vorticity at different Froude numbers

In this section, we focus on high-vorticity regions and flow separation for an angle of divergence equal to 10.34˚and Froude numbers from 0.3 to 0.7. The run parameters are discussed in Section 5.6. Figure 5.11 shows the vorticity contours for a flat-bottom expansion (FB4) at an elevation of 0.200 m above the channel bed. The Froude number is 0.3. A Comparison between Figures 5.11 and 5.9 (at the Froude number of 0.5) shows that the general shapes of high-vorticity areas are similar at the two values for the Froude number, however, the percentage in area of high-vorticity changes ,as shown in Table 5.27.

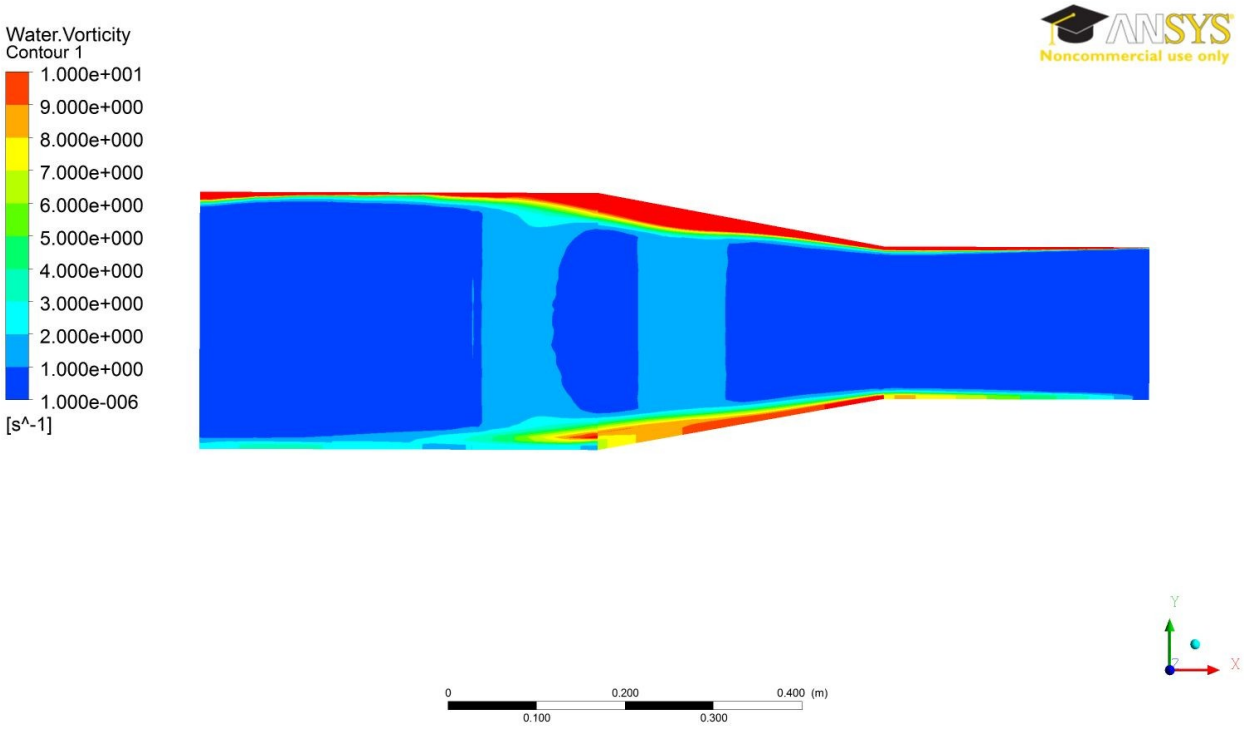

Figure 5.11 Vorticity contours at an elevation of 0.200 m above the channel bed for a flat bottom expansion (FB4) .The Froude number is 0.3.

Table 5.27 Percentage in area of high vorticity at different elevations above the channel bed for Run FB4. The Froude number is 0.3.

Elevation (m)	0.230	0.200	0.150	0.100	0.050
$Vor_{high}(\%)$	14.0	11.0	10.5	10.1	9.6
$Vor_{right}(\%)$	18.9	17.9	17.5	16.8	16.2
$Vor_{left}(\%)$	9.0	3.9	3.5	3.3	3.0

A comparison between Tables 5.27 and 5.23 (for the Froude number of 0.5) shows that when the Froude number drops from 0.5 to 0.3, the high-vorticity region has reduced at all elevations above the channel bed. Also, Table 5.27 shows that the high-vorticity region remains present at all elevations above the channel bed, however, it becomes smaller towards the bed. From Figure 5.11 and Table 5.27, it is obvious that the high-vorticity region is asymmetric; the region is smaller to the left. The region to the left considerably reduces at elevations lower than 0.230 m.

Figure 5.12 shows the vorticity contours for Run HH1. The Froude number is 0.3. The elevation is 0.200 m above the channel bed. A comparison between Figures 5.11 and 5.12 shows that the high-vorticity region reduces to the right and has almost vanished to the left.

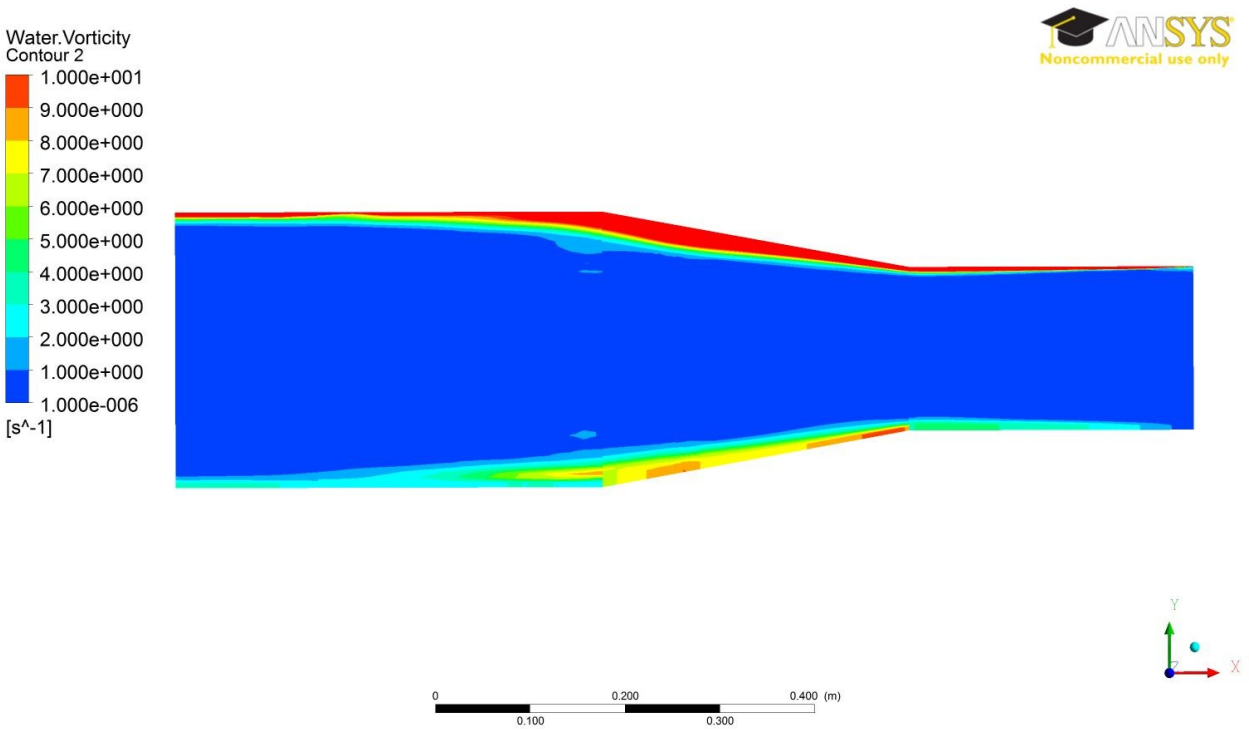

Figure 5.12 Vorticity contours for flow at an elevation of 0.200 m above the channel bed for a flat bottom expansion. The Froude number is 0.3(HH1).

Table 5.28 shows the effects of 1/4" (or 0.00635 m), and 1/2" (or 0.0127 m) humps on reducing the high-vorticity region. The 1/2" (or 0.0127 m, with $\Delta z / y = 5.08\%$) hump, is more effective.

Table5.28 Percentage in area of the high-vorticity for flat-bottom expansion and expansions with a hump. The Froude number is 0.3. The elevation is 0.200 m above the channel bed.

Runs	FB4	HQ1	HH1
$Vor_{high}(\%)$	11.0	9.4	7.0
$Vor_{right}(\%)$	17.9	15.3	12.9
$Vor_{left}(\%)$	2.1	1.5	1.1

Figure 5.13 shows the vorticity contours for a flat-bottom channel (FB4), at an elevation of 0.200 m above the channel bed. The Froude number is 0.7. The high-vorticity region has occupied most of the expansion and extends toward downstream to some extent. Despite the case of Froude numbers of 0.5 and 0.3 (see Figure 5.9, 5.11), where the high-vorticity regions were mainly next to right and left sidewalls, in case of Froude number of 0.7, the high-vorticity regions are present in almost all expansion area.

Figure 5.14 shows the vorticity contours for an expansion with 1/2" (or 0.0127 m, with $\Delta z / y = 5.08\%$) hump, (HH1).The Froude number is 0.7.The elevation is 0.200 m above the channel bed. A comparison between Figures 5.13 and 5.14 shows that the 1/2" (or 0.0127 m, with $\Delta z / y = 5.08\%$) hump has reduced the high-vorticity region, meaning that flow separation has been suppressed by using the 1/2"(or 0.0127 m, with $\Delta z / y = 5.08\%$) hump. In Figure 5.14 the high-vorticity regions are mostly limited to areas next to right and left sidewalls.

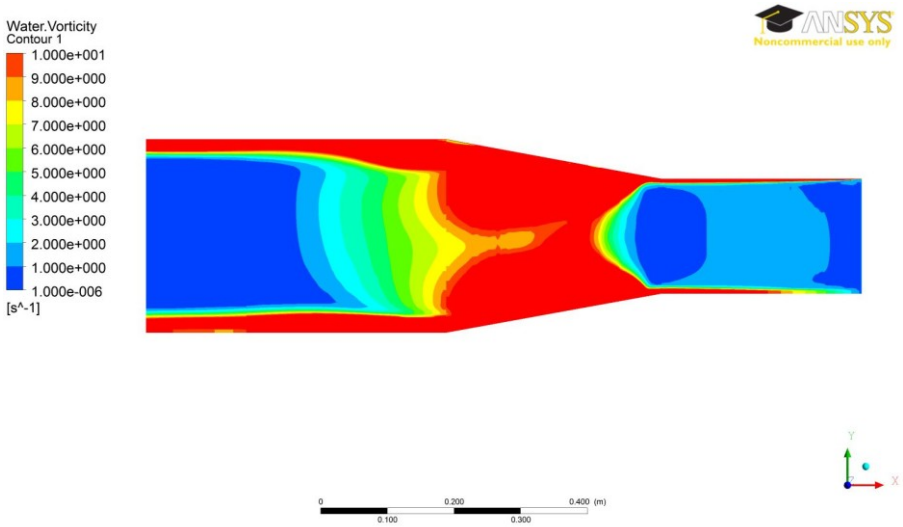

Figure 5.13 Vorticity contours at an elevation of 0.200 m above the channel bed for a flat bottom expansion. The Froude number is 0.7 (FB4).

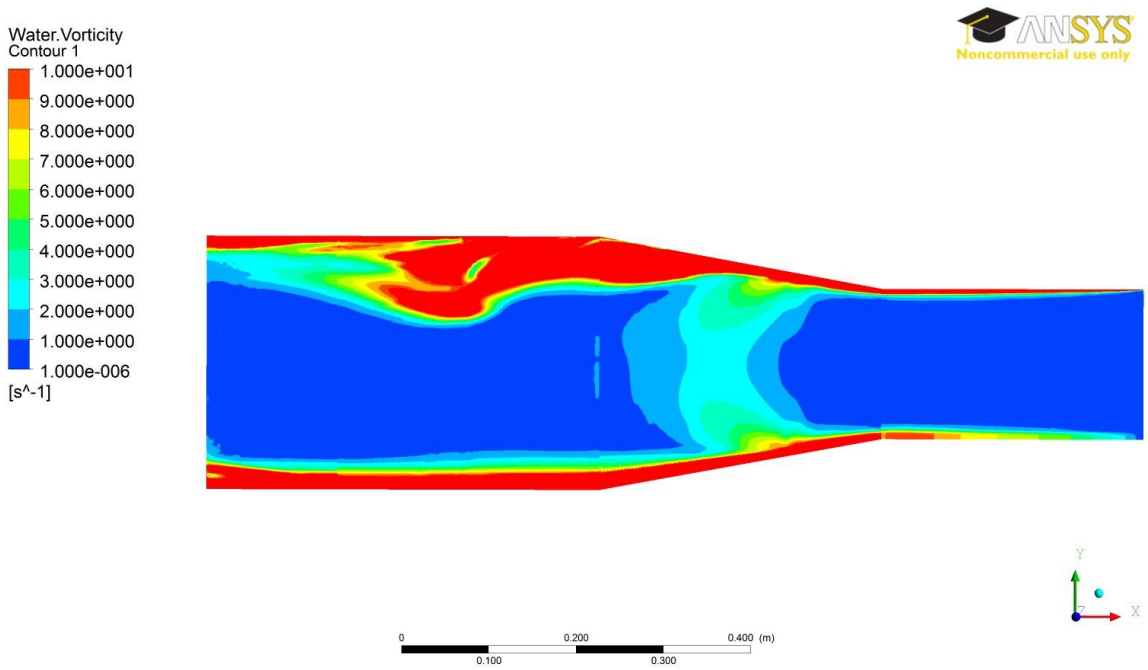

Figure 5.14 Vorticity contours at an elevation of 0.200 m above the channel bed for a flat bottom expansion. The Froude number is 0.7(HH1).

Table 5.29 shows the effects of a 1/2" (or 0.0127 m, with $\Delta z / y = 5.08\%$) hump on reducing the high-vorticity region at different elevations above the channel bed. The 1/4" (or 0.00635 m, with $\Delta z / y = 2.54\%$) hump, (HQ1), is not successful in reducing the high-vorticity region or flow separation.

5.8 u-velocity contours at different cross-sections

This section deals with u-velocity at selected cross-sections between the entrance to the expansion and the exit of the expansion. Eight cross-sections along the channel expansion are selected, labelled by cross-sections 1 to 8, where Cross-section 1 is located at the entrance to the expansion, Cross-section 8 is located at the exit of the expansion, and Cross-sections 2 to 7 are

Table 5.29 A comparison of percentage in area of high vorticity (> 9.0 s^{-1}) at different elevations above the channel bed for Runs FB4, HQ1and HH1. The angle of divergence is $\alpha = 10.34$. The Froude number is 0.7.

Elevation(m)	FB4	HQ1	HH1
0.230	50.2	50.5	24.1
0.200	35.1	37.0	24.4
0.150	21.0	19.1	12.2

equally-spaced between the entrance and the exit of the expansion.

Figure 5.16 shows the u-velocity contours for Run FB4 at Cross-section 7 (i.e. one cross-section before the exit of the expansion). Note that water flow direction is in the negative x-direction. Therefore, negative values in Figure 5.16 mean flow in the direction toward downstream, and positive u-velocity values show backward flow (i.e. flow separation or presence of eddies). As shown in Figure 5.16, backward flow appears in edges (sidewalls), and also appears in the corner of the channel bed.

Figure 5.15 shows the percentage in area of backward flow at different cross-sections. The percentages are compared among a flat-bottom expansion (FB4), expansion with a 1/4″ (or 0.00635 m, with $\Delta z / y = 2.54\%$) hump, (HQ1), and expansion with a 1/2″ (or 0.0127 m, with $\Delta z / y = 5.08\%$) hump, (HH1).The effects of a hump on reducing the percentage of backward flow is clear; HH1 is more successful in reducing the percentage. For example, at Cross-section 4 (at the middle of the expansion), the percentages of backward flow for Runs FB4, HQ1, and HH1 are 2.5, 1.9 and 1.0, respectively.

The effects of a hump on reducing the percentage of backward flow are also clear by comparing Figure 5.17, u-velocity contours for Run HH1 at Cross-section 7, to Figure 5.16, u-velocity contours for Run FB4 at Cross-section 7. The use of a 1/2″ (or 0.0127 m, with $\Delta z / y = 5.08\%$) hump has made the region of backward flow narrower. At some elevations, the backward flow is totally eliminated. Also, the backward flow that was present in Run FB4 at the corners of the channel bed has vanished in Run HH1 (with a 1/2″ hump).

Figures 5.18 and 5.19 show the u-velocity contours at Cross-section 4 (at the middle of the expansion), for Runs FB4 and HH1, respectively. The effects of a 1/2″ (or 0.0127 m, with $\Delta z / y = 5.08\%$) hump on removing the region of backward flow at the bottom corners are clear. The region of backward flow near the water surface shrinks due to the use of a 1/2″ (or 0.0127 m, with $\Delta z / y = 5.08\%$) hump.

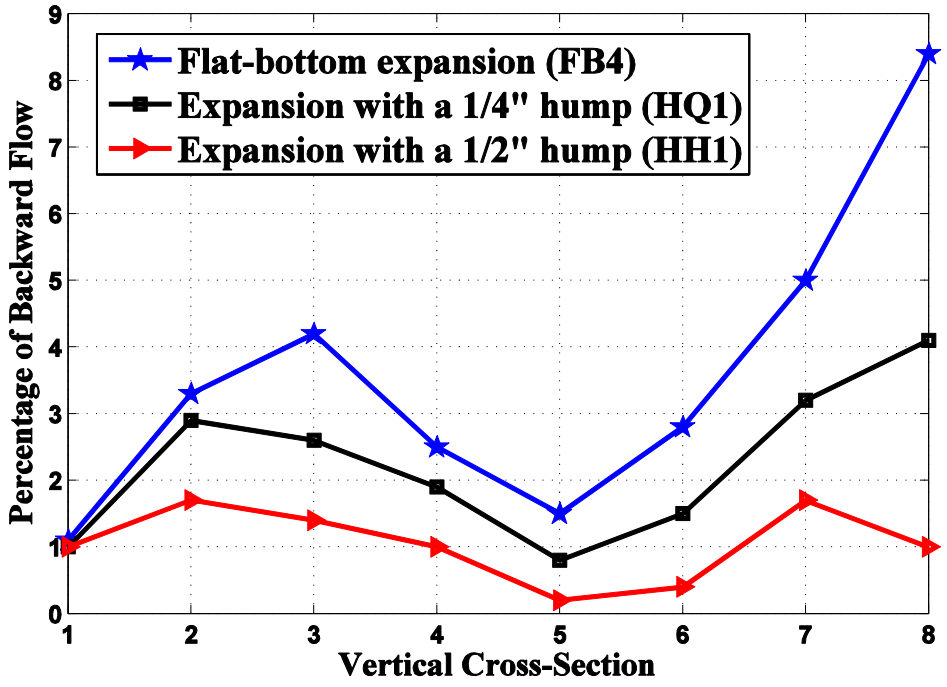

Figure 5.15 Percentage in area of backward flow in a flat-bottom expansion (FB4), and expansions with a hump (HQ1and HH1).

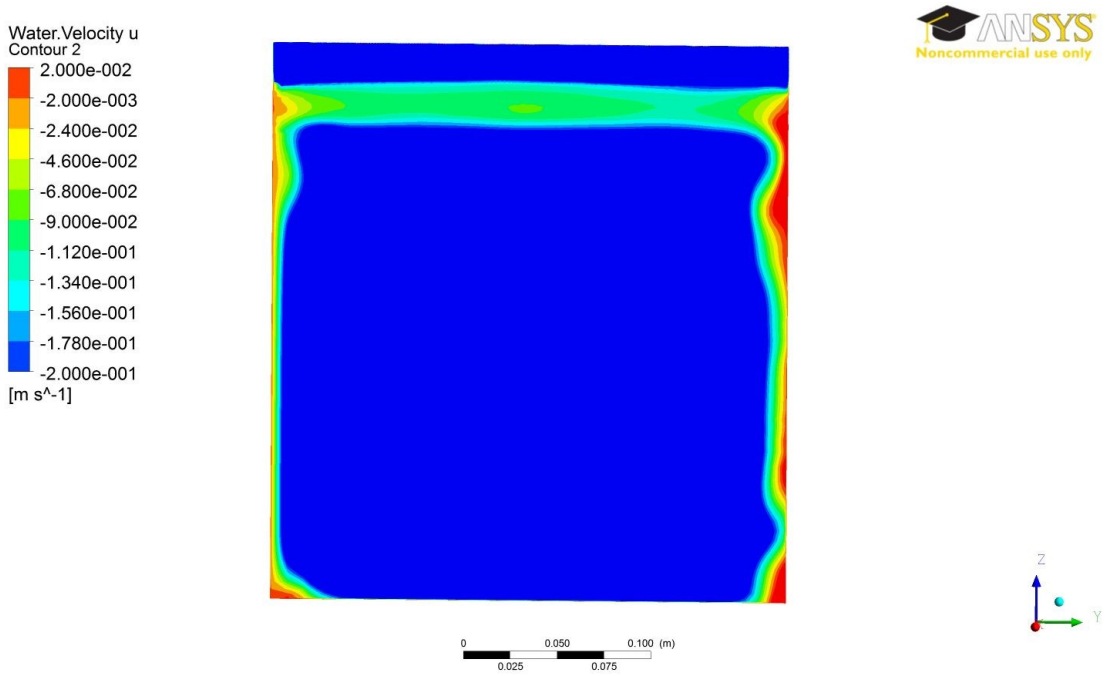

Figure 5.16 u-velocity contours for Run FB4 at Cross-section 7 (before the exit of the expansion).

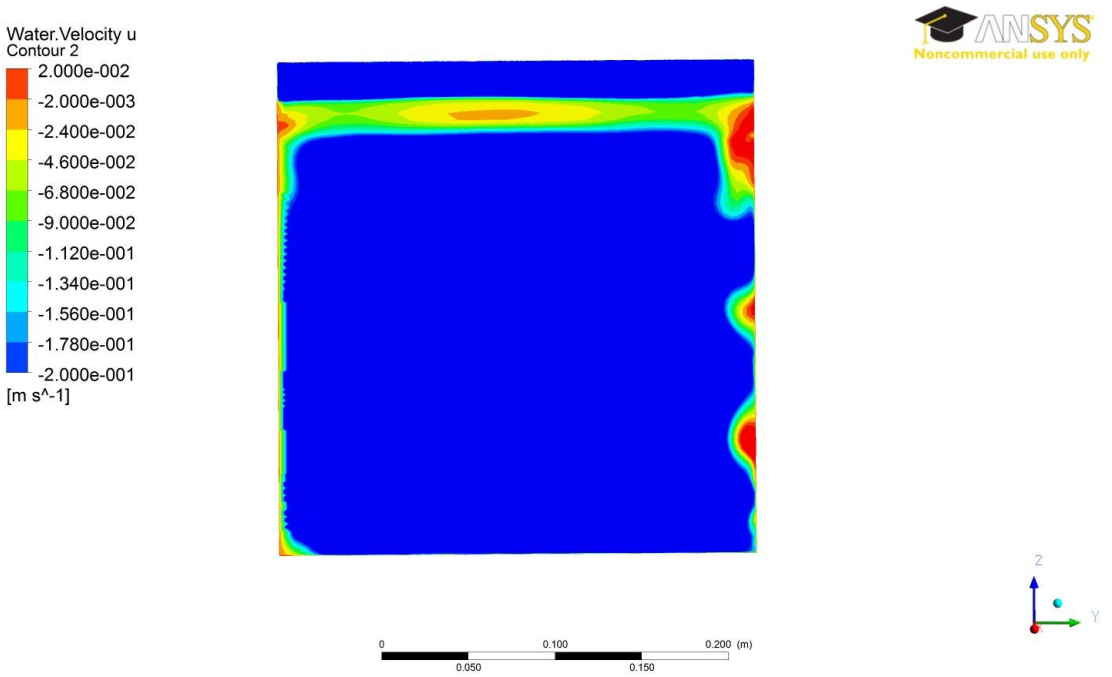

Fig. 5.17 u-velocity contours for Run HH1 at Cross-section 7 (before the exit of the expansion).

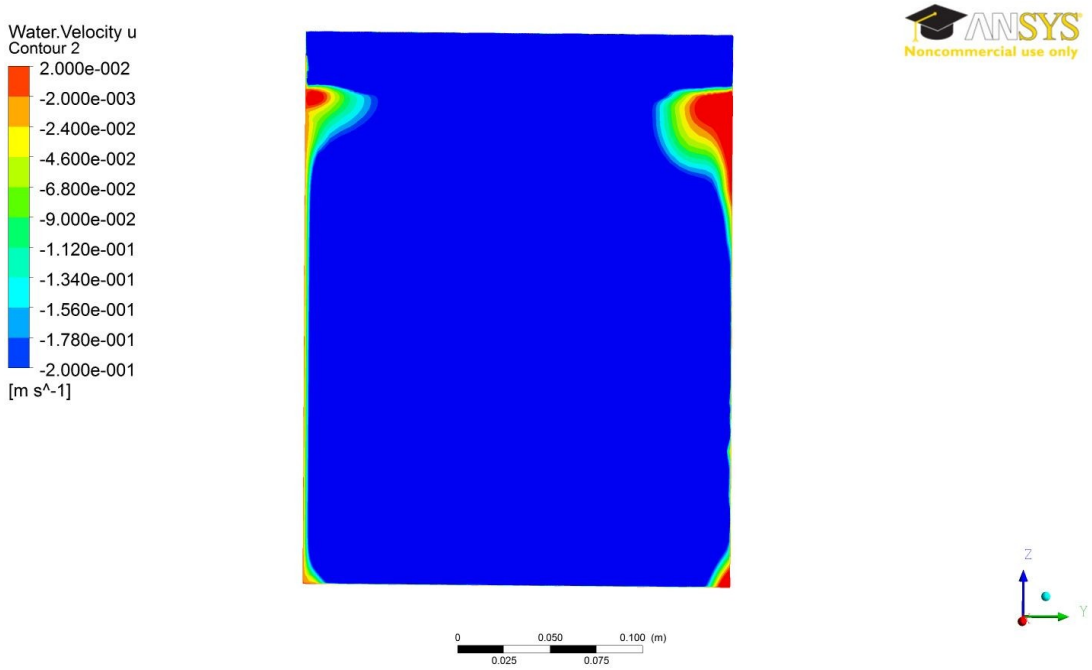

Figure5.18 u-velocity contours for Run FB4 at Cross-section 4 (at the middle of the expansion).

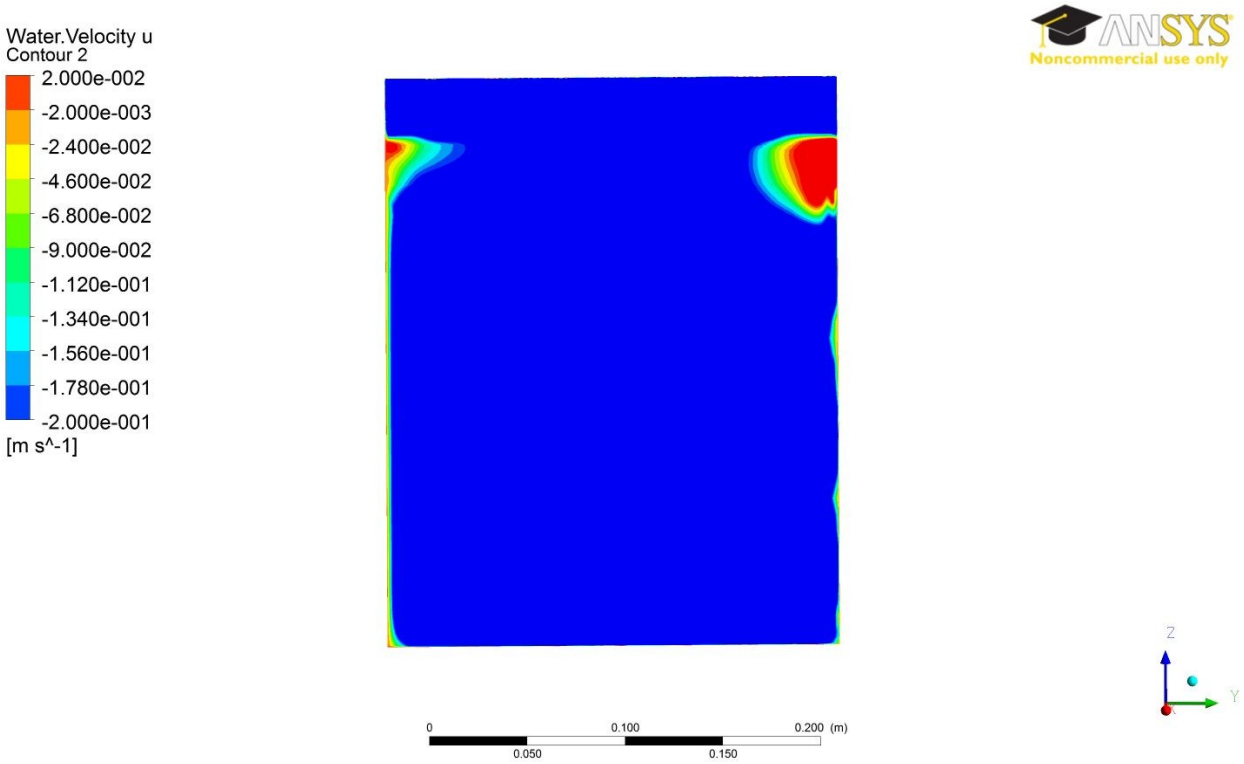

Figure5.19 u-velocity contours for Run HH1 at Cross-section 4 (at the middle of the expansion).

For expansions with smaller angles of divergence ($\alpha = 7.54°$ and 5.04°), due to a more gradual expansion, less eddies and lower percentages of backward flow are expected. Figure 5.20 shows the u-velocity contours for flat-bottom expansion (FB5, with an angle of divergence $\alpha = 7.54°$) at Cross-section 3. Compared to Run FB4, the region of backward flow has been reduced, at the corners of the channel bed. Figure 5.21 shows the u-velocity contours for an expansion with a 1/2″ (or 0.0127 m, with $\Delta z / y = 5.08\%$) hump at Cross-section 3.

By comparing Figures 5.20 and 5.21, the effects of a hump on removing the region of backward flow at the corners of the channel bed are revealed. Table 5.30 shows the percentage of backward flow for a flat-bottom expansion (FB5) and expansions with a 1/4″ (or 0.00635 m, with $\Delta z / y = 2.54\%$), and a 1/2″ (or 0.0127 m, with $\Delta z / y = 5.08\%$) hump, (HQ2), and HH2, respectively. The percentage of backward flow is low for all the expansions, however, expansions with a hump show smaller percentages of backward flow.

Table 5.30 Percentage in area of backward flow at different cross-sections for a flat-bottom expansion (FB5) and expansions with a hump (HQ2 and HH2).

Cross-Section	1	2	3	4	5	6	7	8
FB5	1.0	1.9	1.9	0.1	0.1	0.4	0.4	0.5
HQ2	0.1	0.2	0.3	0.0	0.0	0.0	0.0	0.0
HH2	0.1	0.2	0.2	0.0	0.0	0.0	0.0	0.0

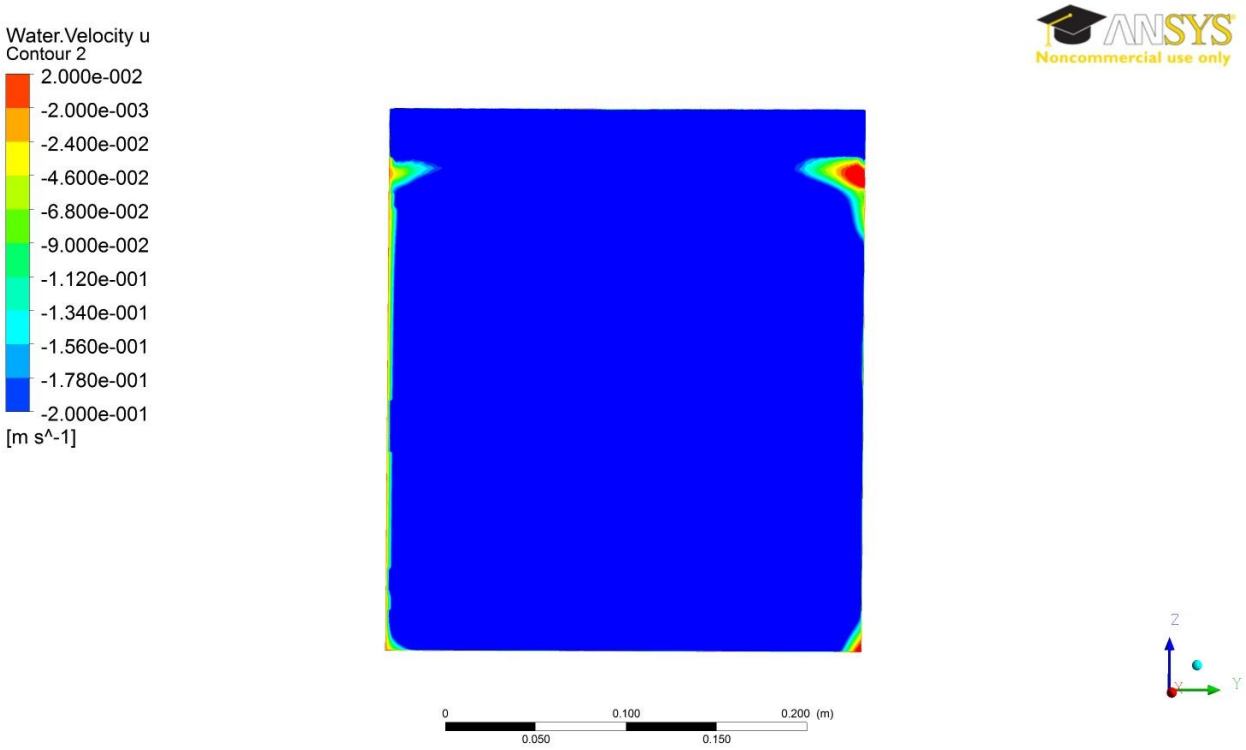

Figure5.20 u-velocity contours for Run FB5 at Cross-section 3 (before the middle of the expansion).

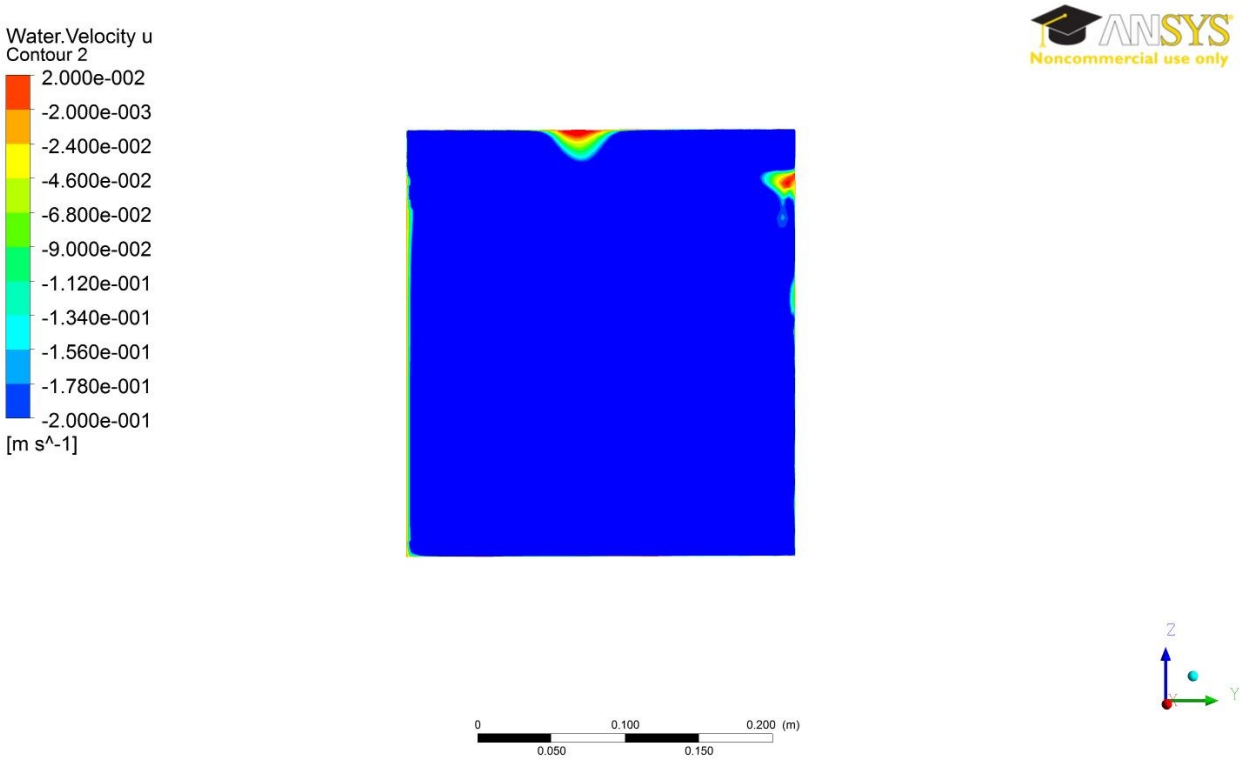

Figure 5.21 u-velocity contours for Run HH2 at Cross-section 3 (before the middle of the expansion).

At an angle of divergence $\alpha = 5.04°$, the percentage of backward flow is negligible, even without the aid of a hump. Figure 5.22 shows the u-velocity contours for Run FB6 at Cross-section 7 (before the exit of the expansion). Backward flow is negligible from this figure.

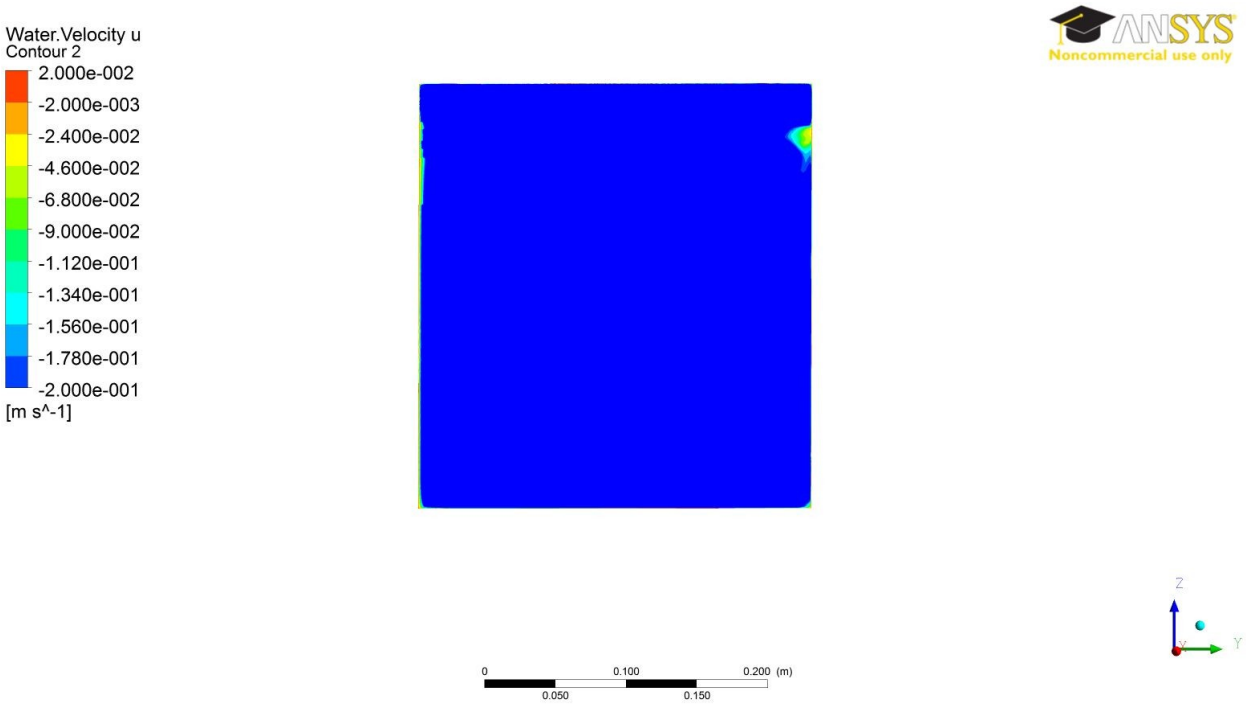

Figure5.22 u-velocity contours for Run FB6 at Cross-section 7 (before the exit of the expansion).

5.8.1 The effects of the Froude numbers

In this section we determine u-velocity contours at different cross-sections along the channel expansion, when the angle of divergence is $\alpha = 10.34°$ and the Froude number varies from 0.3 to 0.7.

Figure 5.23 shows the percentage in area of backward flow for a flat-bottom expansion (FB4) when the Froude number changes from 0.3 to 0.7. The percentage of backward flow increases at higher Froude numbers, as expected. At higher Froude numbers, the flow is stronger and flow separation in the expansion is more likely to occur.

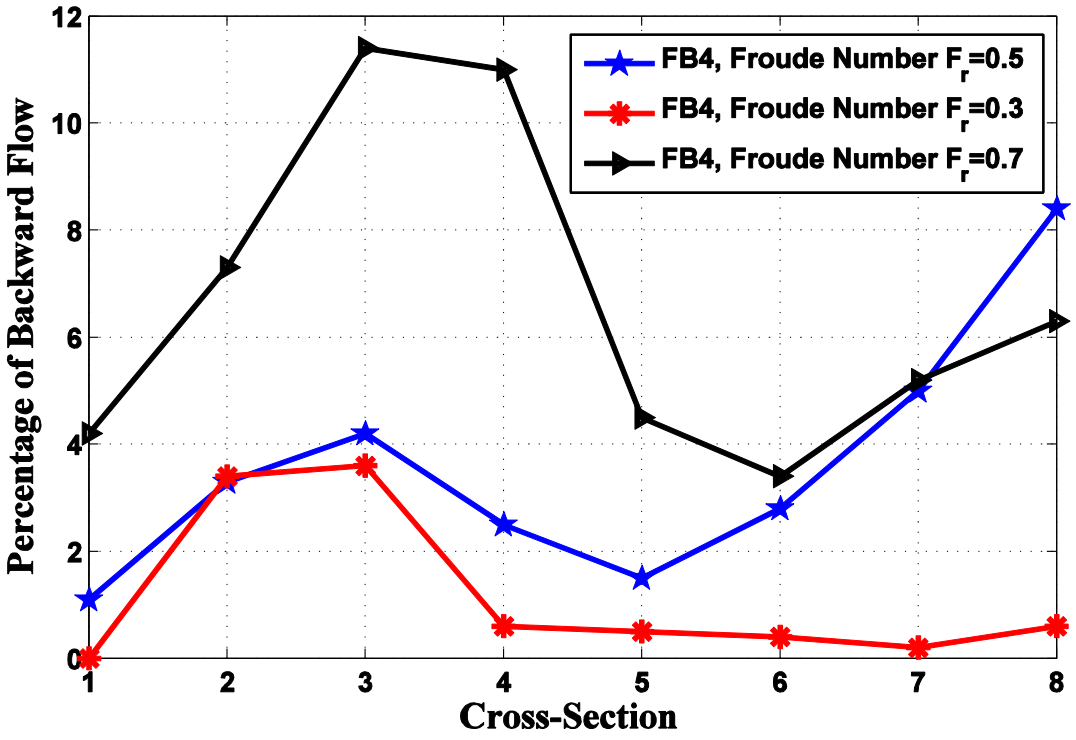

Figure 5.23 Percentage in area of backward flow at different cross sections for a flat-bottom expansion (FB4), at different Froude numbers.

Generally speaking, the percentage in area of backward flow at the Froude number $F_r = 0.3$ is small, even in a flat-bottom expansion (see Figure 5.23). Therefore, it is not expected to observe considerable changes in this percentage when using humps. However, based on our observations, humps help reduce the percentage of backward flow at some cross-sections.

The effects of a hump on changing the percentage of backward flow at the Froude number $F_r = 0.7$ are shown in Figure 5.24. The 1/4″ (or 0.00635 m, with $\Delta z / y = 2.54\%$) hump has maintained similar percentages for most cross-sections and has successfully reduced the percentage of backward flow in the middle of the expansion (Cross-section 4). The 1/2″ (or 0.0127 m, with $\Delta z / y = 5.08\%$) hump has reduced the percentage of backward flow from the beginning up to the middle of the expansion, however, it has increased the percentage at some cross-sections after the middle of the expansion. In general, based on Figure 5.24, we cannot recommend a 1/2″ (or 0.0127 m, with $\Delta z / y = 5.08\%$) hump as a solution to reduce the percentage of backward flow at the Froude number $F_r = 0.7$.

Cross-section 8, i.e. the exit of the expansion, is one of the cross-sections where the 1/4″ (or 0.00635 m, with $\Delta z / y = 2.54\%$) hump has reduced the percentage of backward flow, compared to a flat-bottom expansion (FB4). These effects are clearly shown by comparing Figure 5.25, u-velocity contour for Run FB4 at Cross-section 8, to Figure 5.26, u-velocity contours for Run HQ1 at Cross-section 8. The effects of a 1/4″ (or 0.00635 m, with $\Delta z / y = 2.54\%$) hump on reducing the backward flows (red region) are shown, especially next to the sidewalls, and next to the bottom corners.

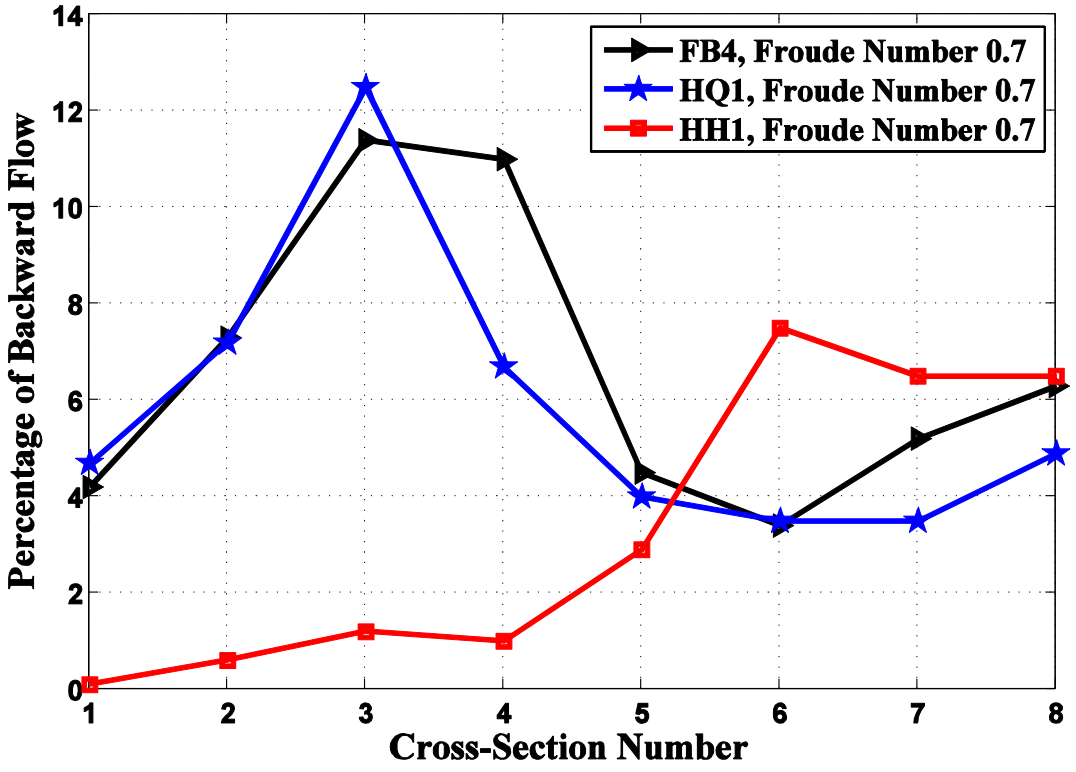

Figure 5.24 Percentage in area of backward flow at different cross-sections for a flat-bottom expansion (FB4), and expansions with a hump (HQ1 and HH1).

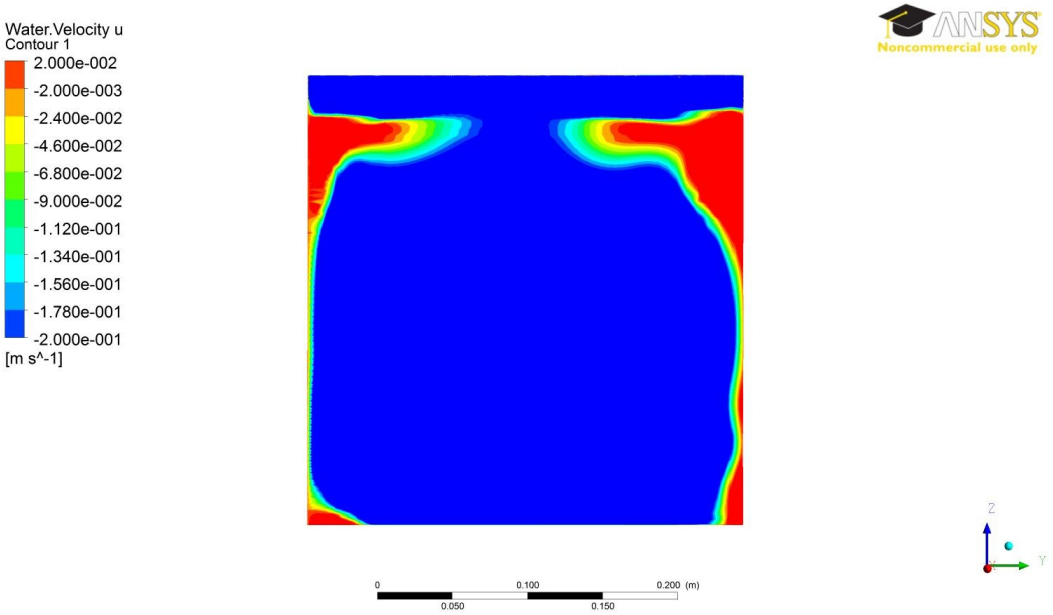

Figure 5.25 u-velocity contours for Run FB4 at Cross-section 8 (the exit of the expansion).The Froude number is 0.7.

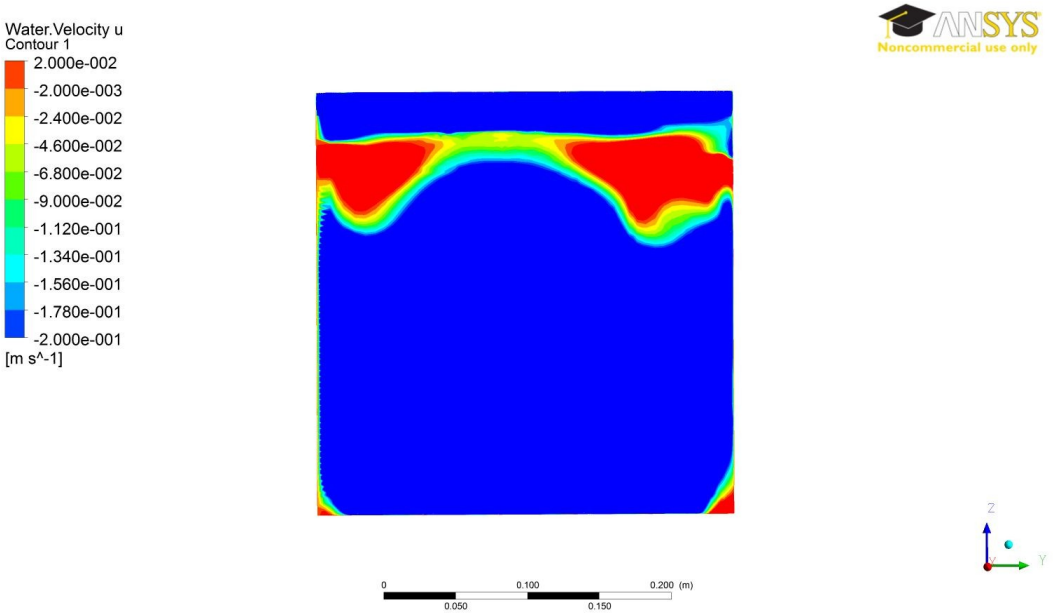

Figure 5.26 u-velocity contours for Run HQ1 at Cross-section 8 (the exit of the expansion).The Froude number is 0.7.

5.9 Comparison of model results with theoretical and experimental data

To validate the modelling methodologies, we make comparisons of the model results with existent analytical solutions under simplified conditions and available experimental data for a limited number of cases. The procedures are as follows. Energy losses in the expansion are calculated by subtracting the specific energy at the exit of the expansion from the specific energy at the entrance of the expansion [equation 4.7]. Then, the energy loss coefficient k_E is determined by dividing the energy loss by the velocity head at the entrance to the expansion [equation 4.8].

The energy loss coefficient is determined from the model results of velocity and flow depth found and compared with the average and standard deviation of the energy loss coefficient obtained from experimental data (Najafi-Nejad-Nasser, 2011). The experimental data is available for expansions FB4, HH1, and FB5 (See Table 5.1). Table 5.31 shows that the model results are very close to experimental data. Based on the agreement between our model results and experimental results, it is concluded that our channel model is a realistic model and the derived results are reliable.

Table 5.31 Comparison of energy loss coefficient k_E between numerical model and experiments.

Runs	k_E from model simulations	Average and standard deviation of k_E based on laboratory data
FB4	0.55	0.54 ± 0.058
HH1	0.38	0.31 ± 0.015
FB5	0.38	0.37 ± 0.095

Table 5.32 compares the energy loss coefficient from the numerical simulations to theoretical values for the coefficient (Henderson, 1966). The theoretical values appear to be higher than the corresponding numerical values. This is probably due to the assumption that the expansion is a sudden expansion, as made in the theoretical derivation of the coefficient.

Table 5.32 A comparison of the energy loss coefficient between this modelling study and the theoretical analysis by Henderson (1966). For all the listed runs, the angle of divergence is 10.34°, the mesh resolutions are 4 mm, and the downstream channel extension is 0.150 m.

Run	F_r	k_E from model simulations	Theoretical k_E
FB4	0.5	0.55	0.64
HQ1	0.5	0.52	0.71
HH1	0.5	0.38	0.35
FB5	0.5	0.38	0.55
HQ2	0.5	0.37	0.52
HH2	0.5	0.35	0.32
FB6	0.5	0.42	0.45
HQ3	0.5	0.26	0.29
HH3	0.5	0.09	0.16
FB4	0.3	0.44	0.89
HQ1	0.3	0.26	0.44
HH1	0.3	0.08	0.27
FB4	0.7	0.74	1.31
HQ1	0.7	0.55	1.11
HH1	0.7	0.53	0.98

Chapter Six Discussions and Conclusion

6.1 Discussions

This study deals with the issue of flow separation, energy losses and eddy motions in flows through open-channel expansions, which is important. In hydraulic engineering systems such as irrigation networks and hydropower structures, expansions are useful for providing a necessary cross-sectional increase in the direction of flow. However, energy losses in expansions are undesirable from the perspective of energy conservation and possibly expansion-induced turbulent eddy motions must be controlled to prevent the hydraulic engineering systems from damage. This modelling study has made a number of contributions, including

(1) an improved understanding of the behaviour of subcritical flows in expansions, e.g. variations in flow streamlines, velocities and eddy structures;

(2) a successful extension of experimental results to cover a wide range of conditions in terms of the angle of divergence, bottom geometry and the Froude number;

(3) quantitative evaluations of the effectiveness of altering the bottom geometry in the suppression of flow separation and eddy motions.

These contributions have been made through CFD simulations of three-dimensional subcritical turbulent flows in channel expansions with or without a hump fitted at the channel bed. These simulations have produced steady state solutions of the flow field for given hydraulic conditions and channel geometry. We have ensured that the model solutions are independent of mesh resolutions and configurations, and are not subject to artificial end effects. The k-ω turbulence model was used for turbulence closure in the simulations, which is known to handle anticipated anisotropic turbulence well.

Comparisons of the velocity field, vorticity structure and flow reversal in the expansion between the cases with and without a hump have clearly revealed the effects of using humps on the control of flow separation and eddy motions. Sudden expansions are easy and presumably less expensive to build, but they are known to cause flow separation and contribute to the formation of turbulent eddies. Therefore, they are not hydraulically efficient. Previously, research efforts have been made to improve the hydraulic efficiency; the focus has been on optimising expansion's shapes in the horizontal, but their research efforts have not produced consistent results (see e.g. Hinds, 1927; Smith and Yu, 1966; Swamee and Basak, 1992).

This modelling study represents an extension to the interesting idea of making modifications to the expansion geometry in the vertical, which arguably would be easier and less expensive, compared to modifications to the expansion sidewalls. It is possible to incorporate a simple hump at the channel bed to achieve smooth water surface and flow profiles in expansions and hence to reduce flow energy losses there and further downstream. Thus, the results from this study have important implications to the design of hydraulically efficient channel expansions. Within the regime of subcritical flow, the actual values for the Froude number should be taken into account in the design; this is among the new findings from this study.

The modelling strategies followed in this modelling study are appropriate, and the results are relevant, supported by reasonable comparisons with experimental data (for a limited number of cases) as well as with theoretical results (available for some simplified conditions). The comparisons are in terms of a dimensionless energy loss coefficient for channel expansions. The modelling strategies have allowed efficient and systematic explorations of combinations of different expansion geometry, flow conditions and hump configurations.

6.2 Conclusion

In total, 19 model runs were carried out in this study for predictions of the flow field in channel expansions with or without a hump fitted at the channel bed. These model runs covered conditions of the angle of divergence α = 5.04, 7.54 and 10.34, and the Froude numbers Fr = 0.3, 0.5 and 0.7. From the model results, we determined the percentage in area occupied by eddies, the percentage in area where the flow reverses direction, and the percentage in area where the vorticity is high. We have validated the modelling methodologies by achieving good comparisons with experimental data. Distributions of three-dimensional water velocities, vorticity contours, and along-channel velocity contours at selected vertical and horizontal planes for the cases of with and without a hump are presented. An analysis of the model results has leaded to the following conclusions:

(1) When the angle of divergence reaches α = 7.54°, flow separation from the expansion sidewalls occurs in the expansion and persistent eddy motions take place not only locally in the expansion but also cover a long distance further downstream. The flow patterns and eddy motions are asymmetric about the expansion's centreline, although the expansion geometry is symmetric about the centreline. Also, there are significant variations in the velocity field with height above the channel bed.

(2) When α reaches 10.34°, intensive flow separation and eddy motions occur. The resultant energy losses are significant, with the energy loss coefficient being as large as 0.42 (for *Fr* = 0.5, see Tables 5.1 and 5.32) and 0.74 (*Fr* = 0.7). An erosion problem is expected if the expansion is built with erodible materials.

(3) At moderate Froude numbers ($Fr \le 0.5$), the use of a 1/2″(or 0.0127 m, with $\Delta z / y = 5.08\%$)hump, which is about 5% of the depth of flow imposed at the entrance of

a gradual channel expansion, suffices to suppress flow separation from the expansion sidewalls and eliminates almost completely flow reversal and expansion-induced flow energy losses. The energy loss coefficient is reduced from 0.42 to 0.09. With respect to the elimination of flow reversal, both a 1/2″(or 0.0127 m, with $\Delta z / y = 5.08\%$) hump and a 1/4″(or 0.00635 m, with $\Delta z / y = 2.54\%$) hump are very effective.

(4) At high Froude numbers ($Fr = 0.7$), the use of a 1/2″ hump (with $\Delta z / y = 5.08\%$) has limited effects of on the control of flow separation and energy losses, with the energy loss coefficient dropped from 0.74 to 0.53. The significance of this finding is that the design of hydraulically efficient needs to consider the actual *Fr* values.

(5) The angle of divergence of the expansion in question is an influential factor in the hydraulic performance of humps. When the angle of divergence does not exceed 5.04°, there are no significant flow separation and eddy motions, and therefore the use of a hump may be redundant.

(6) When the angle of divergence and the Froude number are large (α = 10.34º and Fr = 0.7), the use of a 1/2″(or 0.0127 m, with $\Delta z / y = 5.08\%$) hump is shown to reduce the region in the expansion of high vorticity (defined as vorticity higher than 9.0 s^{-1}) by about 50%. In terms of flow reversal control, the use of a 1/2″(or 0.0127 m, with $\Delta z / y = 5.08\%$) hump or a 1/4″(or 0.00635 m, with $\Delta z / y = 2.54\%$) hump works at some vertical cross sections bur does not at others.

The use of a hump is shown to force flow to accelerate, and as a result, the otherwise adverse pressure gradient, which is known to be responsible for flow separation, diminishes. A hump in the vertical can easily be incorporated into the bed of existent channel expansions, and would be less expensive to construct than to modify the horizontal shape (or the sidewalls) of

existent expansions. The results presented in this study are of practical values for the optimal design of humps.

6.3 Suggestions for Future Research

This study has limited to the case of expansions of rectangular cross section. Future research on the topic should consider expansions of other shapes (e.g. trapezoidal shape). This study should be extended to include more cases where the Froude number is high (Fr > 0.5). We have considered humps with a triangle profile. It is worthy a while to investigate whether or not humps with a smooth profile will lead to a substantially better performance. The combined numerical and experimental approach would be interesting to take to tackle the problem. Future research should remove the assumption that the approach flow is uniform.

References

ANSYS (2010a) ANSYS CFX user's guide. Release 13.0, ANSYS, Inc., Canonsburg, PA 15317

ANSYS (2010b) ANSYS CF–Solver Theory Guide. Release 13.0, ANSYS, Inc., Canonsburg, PA 15317.

Abbott, D. E. and Kline, S. J. (1962) "Experimental investigation of subsonic turbulent flow over single and double backward facing steps." *Journal of Basic Engineering* 84: 317.

Alauddin, M. and Basak, B.C. (2006) "Development of an expansion transition in open channel sub-critical flow. "*Journal of Civil Engineering* 34(2): 91–101.

Babarrutsi, S., Ganoulis, J. and Chu, V. H. (1989) "Experimental investigation of shallow recirculating flows." *Journal of Hydraulic Engineering* 115(7): 906–924.

Chow, V. T. (1959) "Open-channel hydraulics." McGraw-Hill, N.Y., pp. 680.

Escudier, M. P., Oliveira, P. J. and Poole, R. J. (2002) "Turbulent flow through a plane sudden expansion of modest aspect ratio." *Journal of Physics of Fluids* – AIP 14(10): 3641–3654.

Filetti, E.G. and Kays, W. M. (1967) "Heat transfer in separated, reattached, and redevelopment regions behind a double step at entrance to a flat duct." *Journal of Heat transfer* 66-WA/HT-18:163–168.

Foumeny, E. A., Ingham, D. B. and Walker, A. J. (1996) "Bifurcations of incompressible flow through plane symmetric channel expansions." *Journal of Computers and Fluids* 25(3): 335–351.

Graber, S. D. (1982) "Asymmetric flow in symmetric expansions." *Journal of the Hydraulics Division* – ASCE 108(HY10): 1082–1101.

Henderson, F. M. (1966) "Open channel flow." Prentice-Hall, Upper Saddle River, NJ

07458.

Hinds, J. (1927) "The hydraulic design of flume and siphon transitions." *Proceedings of the American Society of Civil Engineers* Paper No.1690: 1423–1459.

Kalinske, A. A. (1944) "Conversion of kinetic to potential energy in flow expansions." *Transactions–American Society of Civil Engineers*, Paper No. 2273: 355–390.

Manica, R. and Bortoli, A.L. (2003) "Simulation of incompressible non-newtonian flows through channels with sudden expansion using the power-law model." *Uma Pulicacao da Sociedade Brasileire de Matematica Aplicade e Computacional* 3:333–340.

Mehta, P. R. (1979) "Flow characteristics in tow-dimensional expansions." *Journal of the Hydraulics Division* – ASCE 105(HY5): 501–516.

Mehta, P. R. (1981) "Separated flow through large sudden expansions." *Journal of the Hydraulics Division* – ASCE 107(HY4): 451–460.

Mohapatra, P. K. and Bhalamudi, S. M. (1994) "Bed-level variation in channel expansions with movable beds." *Journal of Irrigation and Drainage Engineering* – ASCE 120(6): 1114–1121.

Morris, H. M. and Wiggert, J. M. (1972) "Applied hydraulics in engineering." Second edition. The Ronald Press, N.Y.

Najafi-Nejad-Nasser, A. (2011) "An experimental investigation of flow energy losses in open-channel expansions." Thesis (Master of Applied Science), Department of Building, Civil and Environmental Engineering, Concordia University, Montreal.

Nashta, C. F. and Garde, R. J. (1988) "Subcritical flow in rigid-bed open channel expansions." *Journal of Hydraulic Research* 26(1): 49–65.

Papanicolaou, A. and Hilldale, R. (2002) "Turbulence characteristics in a gradual channel

transition." *Journal of Engineering Mechanics* 128(9): 948–960.

Ramamurthy, A. S., Basak, S. and Rao, P. R. (1970) "Open channel expansions fitted with local hump." *journal of Hydraulics Division* – ASCE 96(HY5): 1105–1113.

Seetharamiah, K. and Ramamurthy, A. S. (1968) "Triangular sills in open channel expansions." *Civil Engineering and Public Works Review 63*, March: 283.

Skogerboe, G. V., Austin, L. H. and Bennett, R. S. (1971) "Energy loss analysis for open channel expansions." *Journal of the Hydraulics Division*–ASCE 97(HY10): 1719–1735.

Smith, C. D. and Yu, J. N. G. (1966) "Use of baffles in open channel expansions." *Journal of the Hydraulics Division*–ASCE 92(HY2): 1–17.

Swamee, P. K. and Basak, B. C. (1991) "Design of rectangular open-channel expansion transitions." *Journal of Irrigation and Drainage Engineering* – ASCE 117(6): 827–838.

Swamee, P. K. and Basak, B. C. (1992) "Design of trapezoidal expansive transitions." *Journal of Irrigation and Drainage Engineering* – ASCE 118(1): 61–73.

Swamee, P. K. and Basak, B. C. (1993) "Comprehensive Open-Channel Expansion Transition Design." *Journal of Irrigation and Drainage Engineering* – ASCE 119(1): 1–17.

Taylor, E. H. (1944) "Flow characteristics at rectangular open-channel junctions." Transactions, ASCE, Vol.109: 893–902.

U.S. Department of Transportation (1983) "Hydraulic design of energy dissipaters for culverts and channels." *Hydraulic Engineering Circular* Number 14, Third Edition.

Vittal, N., and Chiranjeevi, V. V. (1983) "Open channel transitions: rational method of design." *Journal of Hydraulic Engineering* – ASCE 109 (1): 99–115.